Final Report for subcontract Sci-0201-99 (NASW-98007)
for the period: 03/01/98 - 02/28/01

Investigation of the Large Scale Evolution and Topology of Coronal Mass Ejections in the Solar Wind

Pete Riley
SAIC
10260 Campus Point Dr.
MS 1AP
San Diego, CA 92121

Abstract

This investigation (subcontract Sci-0201-99 of contract NASW-98007) is concerned with the large-scale evolution and topology of coronal mass ejections (CMEs) in the solar wind. During the course of this three-year investigation, we have undertaken a number of studies that are discussed in more detail in this report. For example, we conducted an analysis of all CMEs observed by the Ulysses spacecraft during its in-ecliptic phase between 1 and 5 AU. In addition to studying the properties of the ejecta, we also analyzed the shocks that could be unambiguously associated with the fast CMEs. We also analyzed a series of "density holes" observed in the solar wind that bear many similarities with CMEs. To complement this analysis, we conducted a series of 1-D and 2 1/2-D fluid, MHD, and hybrid simulations to address a number of specific issues related to CME evolution in the solar wind. For example, we used fluid simulations to address the interpretation of negative electron temperature-density relationships often observed within CME/cloud intervals. As part of this investigation, a number of fruitful international collaborations were forged. Finally, the results of this work were presented at 9 scientific meetings and communicated in 8 scientific, refereed papers.

1. Summary of Work

In this section we summarize the main topics of research undertaken during the 3-year span of this investigation. This work included: an analysis of CMEs observed by Ulysses; a study of different shock analysis techniques; numerical simulations of CME evolution; acceleration profiles of CMEs; an investigation of the relationship between electron density and temperature within CMEs; an analysis of so-called "density holes" observed in the solar wind; a survey of whether there exists two intrinsic classes of CMEs; and a study of multi-spacecraft observations of a CME.

Analysis of CMEs and their associated disturbances observed by Ulysses in the ecliptic plane

Our investigation began by assembling the relevant data sets necessary for the analysis of CMEs observed by Ulysses during its in-ecliptic passage to Jupiter. This data included (1) proton, alpha, and electron moments (e.g., density, velocity, temperature, pressure, and heat flux); (2) magnetic field vector measurements; and (3) electron spectrograms. We completed a preliminary survey of 25 CMEs with this data set, identifying CME boundaries, forward shocks, and intervals of counterstreaming electrons. This analysis highlighted the difficulty in locating the CME boundaries accurately. A table of the CMEs identified in the Ulysses in-ecliptic dataset, together with summaries of the important parameters associated with them, such as location, duration, plasma and field values and variations, and CME-driven shock parameters was produced. In addition to the plasma parameters usually considered when analyzing transient phenomena in the solar wind, we also included thermodynamic entropy, cross helicity and mass content (along the spacecraft trajectory) in our study. Where appropriate, the CMEs were analyzed within the context of magnetic clouds.

The results of our analysis have highlighted a number of interesting properties and trends with respect to CMEs in the ecliptic plane:

(1) The CMEs are generally expanding at all heliocentric distances (1-5.4 AU).
(2) The rate of expansion decreases away from the Sun.
(3) Eleven events (41%) are identified as magnetic clouds.
(4) These magnetic clouds exhibited predominantly north (N) to south (S) rotations in the magnetic field at the beginning of the interval and S to N rotations at the end of the interval.
(5) Eleven events (65%) map back to the vicinity of the source surface neutral line.
(6) Ten events (59%) occur within 2 days of a sector boundary; in 6 cases the sector boundary preceded the CME and in 4 cases it followed the CME.
(7) All events, by definition, contain some fraction of counterstreaming suprathermal electrons (ranging from 34% to 100% and averaging 70%), however no systematic trends

- either in the fraction of the interval occupied by CSEs or their relative position within the interval - were found with respect to heliocentric distance.

We also analyzed the 14 forward shocks that could be unambiguously associated with these CMEs. We computed shock strength, orientation, and speed (both in the inertial and upstream solar wind reference frames) for each of them. With respect to the shocks, we found the following:

(1) There is a clear tendency for the shock speed (in the upstream frame of reference) to decrease with increasing heliocentric distance as the CMEs transfer momentum to the ambient solar wind and slow down.
(2) Most of the shock fronts are oriented in the ecliptic plane such that their normals point westward (i.e., in the direction of planetary motion about the Sun).
(3) In 2/3 of the events, the shock is propagating toward the heliographic equator.
(4) No clear trend was found in the strength of the shocks versus heliocentric distance.

These results are discussed in more detail in appendix 2.

We also analyzed these CME intervals by comparing plasma parameters within the interval with ambient solar wind. Our results suggest that thermodynamic entropy (a property of the plasma that typically does not receive much attention) may provide a better indicator of CME intervals than proton temperature, which is usually used as a proxy discriminator of intervals of CME. Furthermore, we have derived several empirically-based functions of ion plasma-β, Helium abundance ratio, and thermodynamic entropy that may provide reliable discriminators of CME intervals. Such a discriminator is particularly important for future missions that hope to sample solar wind material and differentiate between various types of solar wind. We also began the development of an algorithm to automatically detect CME-related events in situ plasma and magnetic field data sets. So far, we have focused on identifying fast forward shocks preceding CMEs.

As part of this study, we maintained a regular schedule of viewing the Ulysses data set for CME-related events. In particular, we continued to monitor the latest measurements made by Ulysses and the Advanced Composition Explorer (ACE) spacecraft.

Shock analysis

There is a long standing debate on the most appropriate techniques for analyzing interplanetary shocks, and in particular, concerning the calculation of the orientation of shock fronts. Two approaches are most often used; magnetic coplanarity and velocity coplanarity. Magnetic coplanarity utilizes the upstream and downstream magnetic fields to calculate the local orientation of the shock. The approach is exact (at least within the

approximations of MHD) and the magnetic field is typically measured at much higher resolution than plasma parameters. However, fluctuations in the magnetic field components typically make its determination difficult. Velocity coplanarity, on the other hand, is only an approximate result, most valid for nearly perpendicular shocks and relies on velocity measurements, which are typically separated by several minutes.

Based on referee's comments to a paper we submitted during year 1 of this investigation, we re-analyzed the shocks observed by Ulysses during its in-ecliptic passage to Jupiter using magnetic coplanarity and compared the results with the previously applied velocity coplanarity approach. Significant quantitative differences were found between the two methods. Nevertheless, the conclusions reached in the paper were unchanged; that is, there is a preponderance of westward and northward tilts to the shock normals and the shock speed decreases with increasing heliocentric distance.

It is still not clear which approach is most appropriate for interplanetary shocks. If the goal is to determine other shock parameters (speed, strength, etc.), in addition to the orientation of the front, then the disparity in resolution is of secondary importance, since the plasma data must be utilized. We have previously shown that errors in neglecting the magnetic field can translate into as much as ~20% errors in the determination of the shock orientation. However, the contribution of waves and turbulence to the magnetic field and their effect on the coplanarity of the field cannot be easily determined. The consensus within the space physics community is that magnetic coplanarity is the better approach, and so we chose to include this method in our revised paper. This comparison, however, suggests that a detailed quantitative study of these two methods, including the analysis of realistic synthetic shocks, is necessary. The results of this analysis were included into a revised version of the manuscript, which was accepted and published in the *Journal of Geophysical Research.* It is included in appendix 2.

Numerical Simulations of CME Evolution and interpretation of in situ observations

This investigation was complemented by a number of numerical models. We began by comparing the results of our CME analysis with MHD simulations by D. Odstrcil and V. J. Pizzo at the Space Environment Center in Boulder, CO. Our results, which suggest that the shock fronts are almost exclusively propagating westward and that 2/3 are propagating toward the equatorial plane, are in general agreement with the results of the simulations. In particular, the simulations suggest a concave-outward shape for the shock plane in the meridional plane as the near-ecliptic portion of the CME is retarded by the slow wind and the higher latitude portion of the CME is accelerated by the coronal hole flow. Since Ulysses was slightly, but continually, in the southern hemisphere during its travel to Jupiter, we would predict a predominance of northward tilted shock fronts, as was observed. With regard to the westward tilt, the simulations show a variety of orientations in the azimuthal plane, depending on the launch site of the CME with respect to the streamer belt. This lead to an interesting proposal that the CMEs may be preferentially launched from the east side of the streamer belt. Using the constant speed

approximation, we mapped the CMEs back to the Sun and projected their inferred launch site onto source surface maps prepared from Wilcox Solar Observatory observations. Since there was no preferred bias in launch site with respect to the location of the neutral line, we concluded that this is an unlikely explanation for the westward tilts. However, care must be taken when applying the constant speed approximation to CMEs that are travelling at speeds substantially faster than the ambient solar wind. In such situations, it is likely that the significant deceleration has taken place, and thus the assumption of constant speed is not a good one. Another possibility is that the rotation of the Sun, which leads to the Parker spiral and the organization of corotating interaction regions is responsible for the westward tilts of the shocks. A significant approximation in the MHD model is the lack of small-scale inhomogeneities. These may turn out to provide the dominant 'steering' mechanism to orient the shock normals toward the west.

We also conducted a series of two-dimensional fluid simulations aimed at exploring the evolution of CME-driven disturbances in the meridional plane. These simple solutions are providing a useful catalogue of results and allow us to infer the probable initial conditions of the CMEs we observe at Ulysses. To complement these large-scale fluid simulations, we also conducted a series of hybrid simulations, modeling the formation, acceleration, and evolution of a flux rope disturbance at 1 AU. These simulations where the electrons are treated as a massless, charge-neutralizing fluid, allow us to probe the small-scale physics of discontinuities and shocks, explore reconnection processes on a kinetic level, while simultaneously model the global morphology and topology of CMEs and their interaction with the solar wind. Our initial simulation results suggest tentative answers to two unresolved aspects of CME observations in the solar wind. The first is a spike that is often observed in the sheath region between the flux rope and the forward shock. It has been suggested that this may just be the amplification of a pre-existing fluctuation due to compression of ambient solar wind ahead of the CME. On the other hand, our simulations show 'hot spot' regions just in front of the flux rope that display exactly the same profile as the observed spikes. Between these 'hot spots' are inverted spikes that are also occasionally observed. We have not yet identified the processes leading to the formation of these hot spots, but it is unlikely to be amplification of a pre-existing structure, since such structures were not present to begin with in the simulation. A second unresolved issue concerns radial field lines that are sometimes observed following CMEs. Several mechanisms for their formation have been suggested previously. Our initial results suggest is that field-line draping and reconnection behind the ejecta may reconfigure the field sufficiently to produce the radial field lines.

In collaboration with a team from the University of Mexico (led by J. Americo Gonzalez-Eparza), we obtained and compiled a fully three-dimensional MHD algorithm, known as ZEUS 3D, for the purpose of investigating the large-scale evolution of CMEs in the solar wind. The algorithm solves the 3-D time-dependent ideal (i.e. non-resistive, non-viscous, and adiabatic) non-relativistic MHD fluid equations. This code was developed at the Laboratory for Computational Astrophysics at the University of Illinois and contains

many recent enhancements in numerical techniques. Although the code is intended to run primarily on CRAY supercomputers, we have successfully compiled the algorithm on a workstation and anticipate that this will provide sufficient computing power to complete our proposed simulations. This effort, will continue beyond the duration of this investigation.

We have used a 2.5 dimensional MHD simulation of the eruption and subsequent evolution of a CME (containing a flux rope) to interpret a handful of in situ observations of magnetic clouds. The simulation combines two sophisticated MHD codes: At the sun, the SAIC solar MHD code simulates the eruption of a flux-rope CME by emerging magnetic flux below a sheared arcade. The resultant disturbance propagates away from the Sun to the outer boundary of the solar simulation at 20 solar radii. This output is then used to drive the inner boundary conditions of an interplanetary MHD code developed by D. Odstrcil at NOAA/SEC, Boulder, Colorado, which follows the evolution of the disturbance to 1 AU and beyond. At 1 AU, the simulation reproduces the essential large-scale plasma and magnetic field variations commonly seen in magnetic clouds – a subset of CMEs. In particular, the ejecta drives a shock ahead of it, which sweeps up, compresses, and heats ambient solar wind material. Behind it, a rarefaction region forms as an expansion wave propagates both back into the trailing portion of the ejecta as well as into the slower solar wind behind. Flow deflections and magnetic field rotations are consistent with many observed events. By providing a picture of the evolution of the CME all the way from the solar surface to 1 AU we can infer the global properties of in situ observations with more confidence. The simulation demonstrates, for example, that the initial flux rope and cavity are, for all practical purposes, the same. This simulation also bears a striking resemblance to a set of magnetic clouds that have been labeled as "double flux-ropes". Although a more detailed analysis is required, the inference from this is that many, if not all of these events can be explained by a single flux rope structure.

Some of these simulations are discussed in more detail in appendix 1.

Acceleration of CMEs

Near the Sun, Coronal Mass Ejections (CMEs) exhibit a wide range in propagation speeds, ranging from ~50 km/s to > 2000 km/s. Moreover half of the CMEs observed within 5 solar radii by the coronagraph onboard the Solar Maximum Mission over a 7 year period, had speeds less than 300 km/s; a result independent of heliographic latitude. By comparison, the average speed of the low latitude solar wind at 1 AU is ~440 km/s. Thus even within the slow solar wind, it is likely that a significant fraction of CMEs are traveling at speeds, at least initially, lower than the ambient solar wind. We have previously investigated the acceleration of slow CMEs embedded within a fast solar wind, indicative of the high-latitude solar wind flow using 1-D gas-dynamic simulations and comparing with Ulysses observations of high latitude CMEs. We found that pressure gradients induced by the initial speed differences between the slow CMEs and the faster ambient solar wind flow generated large accelerations of the CMEs, eventually bringing

them up to the speed of the ambient solar wind flow over scales of 1 to 10 AU.

In the present study, we investigated the acceleration of even slower CMEs embedded within a slow flow indicative of the low-latitude, slow solar wind. We generated an ambient solar wind flow of approximately 440 km/s, and launched a velocity pulse into the inner boundary (at 30 solar radii) consisting of a drop in speed of 250 km/s over an interval of 15 - 20 hours. We considered both square and bell-shaped pulses (which alter the evolution of the disturbances quantitatively. However, they were used primarily as a check that the qualitative results are not dependent on the shape of the pulse). Our results demonstrated that the CMEs are accelerated up to ambient solar winds considerably faster than their high-latitude counterparts. In fact, for the range of inputs considered, the CMEs reach ambient solar wind speeds within a fraction of an AU. The rapid formation and propagation of a compression region at the trailing edge of the CME produces this acceleration. These results, together with others are summarized in a paper accepted for publication in the *Journal of Geophysical Research*, and included in appendix 3.

Relationship between electron density and temperature within CMEs

Osherovich and colleagues have argued that the relationship between electron number density and temperature within magnetic clouds (and CMEs in general) suggests that the adiabatic index is less than one. Others, such as J. T. Gosling, have argued that such a conclusion is not reasonable, since it requires that the temperature within CMEs increases with increasing distance from the Sun. At the heart of the debate, is the question of whether one can infer an adiabatic index from a single slice through a CME. For, under such circumstances, one is not monitoring the variation in a parcel of plasma, but snapshots of different plasma.

We investigated the relationship between temperature and density using a series of 1-D fluid models, where we simulated CME-like pulses and tracked their evolution through the solar wind. The simulation region ranged between our inner boundary, at 30 solar radii, and our outer boundary, at 5 AU. We specified inflow boundary conditions at the inner edge and allowed the system to relax into an equilibrium solution. Into this solution we propagated a pulse mimicking a CME. We varied the duration, speed, density, and/or temperature variations of the pulse. It is important to realize that the equations strictly assume a polytropic relationship between density and temperature. Thus if we set the adiabatic index, gamma = 1.5 in the simulation, then this value holds for all elements of plasma at all times and at every point within the simulation. We launched many test pulses into this ambient solution and found that plots of Log(density) versus Log(temperature) at particular distances can, although not always, display slopes different from 0.5 (the slope of the points gives (gamma-1), thus gamma = 1.5 would produce a slope of 0.5) within the pulse. Thus our interpretation is that the slope is often not indicative of the value of the adiabatic index but reflects the plasma's tendency to achieve pressure balance. The details of these simulations are covered in more detail in a paper and reply to a comment accepted for publication in the *Journal of Geophysical Research*, and included in appendices 4 and 5, respectively.

Analysis of "density holes"

We analyzed a series of low-density intervals in the ACE and WIND plasma data. At least one of these events (May, 1999) has been associated with significant geomagnetic activity at Earth and was the topic of several sessions at the Fall AGU meeting in San Francisco, as well as several popular media reports (also known as "the day the solar wind disappeared"). Although the cause of these events remains unclear, we believe they may represent some type of transient activity akin to coronal mass ejections. Using a 3-D MHD model, we modeled the structure of the solar corona during the intervals containing these density holes. Although the model is not yet capable of initiating the types of perturbations that we believe are responsible for these density holes, it can in principle provide a picture of the underlying equilibrium structure of the corona during these times. We mapped the density holes from their interplanetary location back to the solar corona and found that all events were associated with low density regions in the corona. Moreover, a current sheet crossing could be identified immediately preceding a low density region as was observed in some of the events. Thus we believe that the models provide a reasonable approximation to the equilibrium structure of the solar wind. We suggest that this configuration must be present in order for a low density transient to be initiated. This could explain why we also see low density regions in the model that do not apparently map out to low density events in the solar wind: In addition to this equilibrium configuration, a transient process is also required to initiate the event, in much the same way as a CME is launched. The results of this work were presented at the Fall American Geophysical Union meeting in San Francisco, December, 1999 by Dr. Barbara Thompson in a talk entitled "The Structure of the Sun During Low-Density Solar Wind Periods". We plan to write up this research during the next several months and submit to the *Journal of Geophysical Research.*

Are there two classes of CMEs?

A controversy recently re-surfaced at the SHINE (Solar, Heliospheric, and Interplanetary Environment) 2000 meeting as to whether there are two intrinsic classes of CMEs. The question was stimulated by recent papers by N. Sheeley that argued that, based on the speed of CMEs observed by the LASCO instrument onboard SOHO there exists two classes of CMEs: A fast, impulsive class with little or no acceleration, and a gradual class, showing acceleration throughout the field of view of the instrument. Several important counter-examples have been shown over the years that did not seem to fit either class. The topic, however, was sufficiently stimulating that it was decided to make it one of our "challenges" and will be the focus of a special session at the upcoming spring AGU, as well as a discussion topic at SHINE 2001. As part of this investigation, we assembled tables of these CMEs and began a preliminary analysis for candidate counterparts in *in situ* data sets. Our focus centers on whether we can distinguish two classes of events based on their *in situ* characteristics. However, this will not be an easy task as most Interplanetary CMEs can be binned into two classes based on any one of a

number of features that are not necessarily intrinsic. For example, flux-rope versus non-flux rope; helium enhancement versus no anomalous helium; fast versus slow; over-expanding versus not; etc. In addition, we have developed a website to encourage collaborations on this topic (http://haven.saic.com/twoclass).

Multi-spacecraft observations of CMEs

It has been reported recently that the ICMEs observed by Ulysses at high heliographic latitudes had a compositional makeup significantly different from the CMEs observed by Ulysses at low latitudes. An intriguing inference that can be drawn from this result is that these high latitude CMEs are associated with a different source than low-latitude CMEs. However, without simultaneous measurements at low latitudes of the same events, it has not been possible to confirm this. With the launch of ACE, however, we now have two heliospheric spacecraft with sophisticated instruments measuring composition and elemental abundance (SWICS). To investigate the combined compositional, plasma, and magnetic field properties of CMEs in more detail, we have initiated a collaboration with D. Lario (Applied Physics Laboratory) and T. Zurbuchen (University of Michigan). Our first goal is to study the detailed properties of a CME observed by both ACE and Ulysses in February/March 1999. This event is particularly appealing because, while ACE was located at 1 AU in the ecliptic plane, Ulysses was located at ~5 AU and at 22 deg. south heliolatitude. Thus the two spacecraft were separated significantly both in latitude and heliocentric distance. Our initial analysis has revealed that many of the features of the event are either the same, or comparable at the two spacecraft. Several significant differences, however, were found. For example, the Fe/O ratio at Ulysses remained unchanged, whereas at ACE, the first half of the event was associated with a significant increase, while the second half was associated with a decrease (differences in the C6/C5 ratio at the two spacecraft were also found, however, we are reviewing the ACE data to confirm that these differences are not an artifact of the data reduction process). Also, while both observations showed rotations in the magnetic field, consistent with a magnetic cloud, the axis of rotation was significantly different. We are pursuing force-free flux rope models of these observations with R. Lepping.

2. Scientific Collaborations

In addition to the studies described above, we have also initiated the following fruitful collaborations, related to the structure and evolution of CMEs in the solar wind.

Deceleration of CMEs

N. Gopalswamy (Catholic University) has developed a propagation model for CMEs from the Sun to Earth, by correlating the expansion properties of halo CMEs observed by SOHO with the speeds of counterpart CMEs observed by near-Earth spacecraft. We have

completed several simple fluid simulations to explore the deceleration profiles of CMEs in the solar wind. One such simulation is summarized at the following URL:

http://haven.saic.com/~uk2/research/gopal/summary_sim14.jpg

and the speed and acceleration profiles for the ejecta are shown at:

http://haven.saic.com/~uk2/research/gopal/v_avge_sim14.jpg

These simulations may allow Dr. Gopalswarmy to more accurately predict the deceleration profiles of CMEs observed by LASCO and differentiate between two possible deceleration curves.

Over-Expansion of CMEs both very near to and far from the Sun

We have simulated the evolution of the so-called "over-expanding" CMEs out to large heliocentric distances and provided a table of plasma profiles that can be used to identify possible candidates in Helios data (T. Horbury) near the Sun and Pioneer data (P Gazis) far from the Sun. Until now, this class of CME has been observed exclusively in the Ulysses high-speed data set. These results were published in a table of plasma profiles on the web (http://haven.saic.com/~uk2/research/oe-cmes). As yet, no candidate events have been found in either the Helios or Pioneer datasets.

Relationship between counterstreaming suprathermal electrons and cross helicity

Counterstreaming electrons in *in situ* data sets often indicate that the local field lines are connected back to the Sun at both ends. Thus they provide a direct measure of the topology of the magnetic field. Cross helicity, is a measure of the "Aflvenicity" of the plasma, i.e., the degree to which the fluctuations may be ascribed to Alfven waves. A value of +1 indicates the presence of outwardly propagating waves, a value of –1 indicates the presence of inwardly propagating waves, while 0 may either indicate the absence of waves altogether, or a combination of inwardly and outwardly propagating waves that yield a net helicity of zero. In collaboration with E. Marsch we are currently comparing intervals of counterstreaming electrons with cross-helicity. The presence of closed field lines would lead to a situation where outwardly propagating waves along either end of the field line produce a net helicity of zero. Moreover, if this correlation exists, cross-helicity may be a new unique indicator of closed field lines, and hence CMEs. It may also be possible to use counterstreaming and cross helicity signatures together to avoid false alarms of CME events caused by field line connection to shocks.

Interpretation of Planar Magnetic Structures in the Solar Wind

We initiated a collaboration with Geraint Jones at Imperial College to identify the cause

and origin of Planar magnetic structures in the Ulysses data set. Our working interpretation is that they represent the "legs" of CMEs.

Anomolous composition measurements within CMEs

During early February, 1998 a CME passed by the ACE spacecraft. One of the instruments, SWEPAM, recorded very large helium to proton abundance ratios, with proportionate increases in other heavy ions. This event is discussed in more detail in appendix 6.

In May, 1998, a CME was observed by the SWEPAM instrument onboard ACE with with an unusually large enhancement of He+, strongly suggesting the presence of prominence material. In fact, both a disappearing filament and prominence were observed at the Sun and could be associated with this event. This event is discussed in more detail in appendix 7.

Connecting SOHO coronal observations with Ulysses observations of CMEs

During October, 1996 to January 1997, Ulysses was located above the west limb of the Sun at approximately 4.6 AU. Thus there existed the possibility to observe CMEs observed by the LASCO instrument onboard SOHO and subsequently measured in situ by Ulysses. We analyzed three such events in detail, and were able to identify intervals of plasma that were accelerated or decelerated between the LASCO and Ulysses observations. This study is described in more detail in appendix 8.

3. Scientific Presentations and Papers

During the course of this investigation, the results have been presented at nine scientific meetings:

(1) An oral presentation on the analysis of the CMEs observed by Ulysses was presented at the Spring meeting of the American Geophysical Union on May 29, 1998, in Boston, MA: "The properties and radial trends of coronal mass ejecta and their associated shocks observed by Ulysses" by Pete Riley, J. T. Gosling, D. J. McComas, and R. J. Forsyth.

(2) Results from the modeling aspect of this investigation were presented during an invited review talk at the Solar Wind 9 conference on October 5, 1998 in Nantucket, MA): "CME dynamics in a structured solar wind" by Pete Riley.

(3) A poster presentation on the hybrid simulations conducted as part of this investigation was presented at the Fall meeting of the American Geophysical Union on December 6, 1998, in San Francisco, CA: "Global Hybrid Simulations of the Structure and Evolution of Coronal Mass Ejections in the Solar Wind" by Pete Riley, N. Omidi, and J. T. Gosling.

(4) An oral summary of the work outlined here was made at the Ulysses Science Working Team meeting in San Diego in October, 1999 .

(5) An oral presentation on the simulations performed to investigate the origin of density holes in the solar wind was presented by Dr. B. Thompson at the Fall AGU meeting, San Francisco, in December, 1999.

(6) An oral presentation on Ulysses and WIND plasma observations, including the identification of CMEs, was presented at the Whole Sun Month III workshop at the Goddard Spaceflight Center, Maryland, in January, 2000.

(7) Several informal presentations related to this investigation were made at the Elmau workshop on coronal mass ejections in Elmau, Germany (27 March - 1 April 2000).

(8) Results of this investigation were presented at the Ulysses Science Working Team at the Applied Physics Laboratory, Maryland from May 25 to May 26, 2000.

(9) Several informal presentations related to this investigation were made at the SHINE 2000 workshop in Lake Tahoe, Nevada.

Eight papers were completed, submitted, or accepted based on the work performed in this investigation:

(1) CME dynamics in a structured solar wind, Pete Riley, in *Solar Wind 9,* edited by S. R. Habbal, R. Esser, J. V. Hollweg, and P. A. Isenberg, published by The American Institute of Physics, pp131-136, 1999.

(2) Properties and radial trends of coronal mass ejecta and their associated shocks observed by Ulysses in the ecliptic plane, Pete Riley, J. T. Gosling, D. J. McComas, and R. J. Forsyth, *Journal of Geophysical Research*, 105, 12,617, 2000.

(3) Fluid aspects of solar wind disturbances driven by coronal mass ejections, J. T. Gosling and Pete Riley, Submitted to the *Journal of Geophysical Research*, 2000.

(4) Investigation of the polytropic relationship between density and temperature within interplanetary coronal mass ejections using numerical simulations, Pete Riley, J. T. Gosling, and V. J. Pizzo, in press, *Journal of Geophysical Research*, January, 2001.

(5) Reply to "Comment on the paper "On the determination of electron polytrope indices within coronal mass ejections in the solar wind"", J. T. Gosling, Pete Riley, and R. Skoug, accepted for publication in the *Journal of Geophysical Research*, July, 2000.

(6) An unusual coronal mass ejection: First solar wind electron, proton, alpha monitor (SWEPAM) results from the Advanced Composition Explorer, by D. J. McComas, S. J.

Bame, P. L. Barker, D. M. Delapp, W. C. Feldman, J. T. Gosling, E. Santiago, R. M. Skoug, R. L. Tokar, P. Riley, J. L. Phillips, and J. W. Griffee, *Geophysical Research Letters, 25,* 4289, 1998.

(7) A prolonged He+ enhancement within a coronal mass ejection in the solar wind, by R. M. Skoug, S. J. Bame, W. C. Feldman, J. T. Gosling, D. J. McComas, J. T. Steinberg, R. L. Tokar, P. Riley, L. F. Burlaga, N. F. Ness, and C. W. Smith, *Geophysical Research Letters, 26,* 161, 1999.

(8) Combined Ulysses solar wind and SOHO coronal observations of several west limb coronal mass ejections, by H. O. Funsten, J. T. Gosling, P. Riley, O. C. St. Cyr, R. J. Forsyth, R. A. Howard, and R. Schwenn, *Journal of Geophysical Research*, 104, 6679, 1999.

These papers are included in the appendices.

4. APPENDICES

Appendix 1

CME dynamics in a structured solar wind

Pete Riley

Solar Wind 9, edited by S. R. Habbal, R. Esser, J. V. Hollweg, and P. A. Isenberg, published by The American Institute of Physics, pp131-136, 1999.

CME Dynamics in a Structured Solar Wind

Pete Riley

Science Applications International Corporation, San Diego, CA 92121.

Abstract. Models of coronal mass ejection (CME) propagation and evolution in the solar wind, which range from simple one-dimensional fluid to three-dimensional MHD algorithms, continue to provide important insight into the dynamics of CMEs and are a valuable tool in the interpretation of interplanetary in situ observations. In this paper we summarize and discuss the current state of knowledge with respect to these models. In particular, we highlight the structure of the ambient solar wind into which the CME propagates which plays a significant and complex role in the evolution of CME-driven disturbances.

INTRODUCTION

In this paper we will illustrate, with the aid of numerical simulations, how coronal mass ejections (CMEs) and their associated disturbances evolve as they move away from the Sun through the interplanetary medium. In particular, we will focus on more recent topics, such as the so–called "over–expanding" CMEs, and highlight the significant and often complex role that is played by the ambient solar wind on the evolution of CMEs and their associated disturbances.

The study of CMEs is important for a number of reasons. First, CMEs appear to play a fundamental role in the way the corona responds to changes in the solar magnetic field associated with the 11 year solar activity cycle (1). The CMEs effectively provide a mechanism for the Sun to shed magnetic flux, which is thought to be essential to the cyclic renewal of the solar dynamo. Second, CMEs contribute a small, but significant amount to the overall solar wind flow at low latitudes; perhaps as much as 15% of the average mass flux in the low–latitude solar wind during solar maximum (16). Third, fast CMEs have been identified as the leading cause of non–recurrent geomagnetic storms and they can also enhance the geoeffectiveness of recurrent storms (6).

We will begin by discussing spherically symmetric, or one–dimensional (1–D), fluid simulations of CMEs in an unstructured solar wind. These types of simulations span almost 30 years (9), yet their results continue to be relevant and provide an effective way to introduce the basic dynamical processes associated with CME evolution. We will mention two important classes: fast CMEs and so-called "over-expanding" CMEs. Next we will discuss axisymmetric, or 2-D, simulations and finally 3-D simulations. As you can see, this is quite an ambitious task, and the examples we have chosen from the literature are illustrative, but certainly not comprehensive.

We will only discuss CME evolution outside of the outermost solar critical point. This avoids, or perhaps more honestly evades, interesting but considerably more complex problems associated with the initiation and launch of CMEs. Most of the simulations we will discuss model CME evolution between an inner boundary at $\sim 20-30$ solar radii ($R_\odot$) and an outer boundary between 1 and 100 astronomical units (AU).

ONE–DIMENSIONAL MODELS

The basic technique of 1–D fluid simulations is as follows. First, a radial grid is defined. Inflow boundary conditions are prescribed at the inner boundary and outflow boundary conditions are prescribed at the outer boundary. Next, the grid is filled with some initial plasma values, and the algorithm is allowed to run in time until a dynamic equilibrium is achieved. To simulate the launch of a CME, or more simply a shock, the inner boundary conditions are perturbed; speed, density, temperature, or any combination thereof may be varied over some interval of time. An important class of CMEs at low heliographic latitudes are fast CMEs, which drive a fast Forward (F) shock and sweep up and compress both magnetic field and plasma ahead of them (9). As Ulysses moved into the southern high-speed polar solar wind, a new class of CMEs was discovered (7). Unlike the fast CMEs near the ecliptic plane that drive a shock disturbance by virtue of the relative difference in speed between the CME and the ambient solar wind, these high-latitude disturbances are driven by a relative difference in pressure. An interesting question concerning these so–called "over-expanding" CMEs relates to their ulti-

CP471, *Solar Wind Nine*, edited by S. R. Habbal, R. Esser, J. V. Hollweg, and P. A. Isenberg

"Page missing from available version"

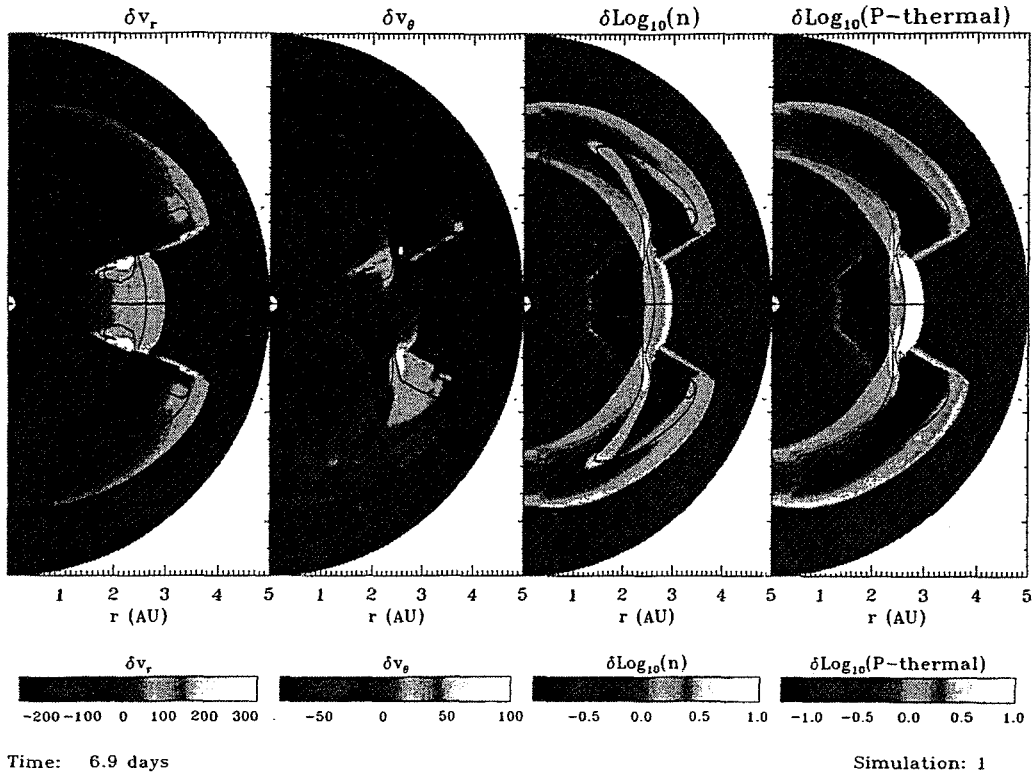

FIGURE 1. Grey–scale difference contours (i.e., the ambient solar wind values have been subtracted) of radial velocity, meridional velocity (positive southward), density, and pressure $\sim$ 7 days after the launch of a coronal mass ejection. The CME is introduced into the ambient solar wind as a bell–shaped pressure pulse (in the form of a density enhancement) over an interval of 10 hours, with a speed and temperature equal to that of the high–latitude solar wind. The CME initially extends $\pm 45°$. The sold line marks the boundary of the CME

(iv) The region of high pressure at low latitudes that forms because the CME is overtaking and compressing the solar wind ahead is not confined to low latitudes. Instead, it expands poleward by at least 10° into the fast solar wind.

(v) At low latitudes, two pairs of waves are generated (8). The first F/R pair is associated with the CME overtaking and compressing the solar wind ahead, and forming a region of high pressure bounded by F/R waves. The second pair is associated with the expansion of the pulse. It turns out that since the CME is propagating away from the slow ambient solar wind faster than the R wave associated with the expansion of the CME can propagate away from it, this wave does not develop substantially. Also, the F wave from the expansion of the CME interacts with the R wave from the compression region such that both are weakened in the process. Thus all that remains is a relatively strong F shock. At high latitudes, on the other hand, because the CME is propagating at the same speed as the ambient solar wind, only a F/R shock pair is generated from the expansion of the CME and the whole high-latitude disturbance looks relatively symmetric.

A simulation qualitatively similar to this was compared with simultaneous observations of a CME by IMP 8 and Ulysses in February-March, 1994 while Ulysses was located at 3.53 AU and 54° south heliographic latitude (14). The comparison indicated that the simulations could reproduce the essential features of the observations.

The pulse discussed in the previous example was launched simultaneously into the high and low speed solar wind. And, while it might well represent a reasonable initial condition at our inner boundary, it is quite likely that, closer to the Sun, the CME was originally contained exclusively within the slow solar wind, and penetrated into the higher-speed wind as it propagated away from the Sun. To investigate this possibility, we launched a pulse into the same ambient solar wind, but restricted the initial latitudinal extent of the pulse to 15°. Figure 2 again presents plasma parameters at 7 days after the launch of the CME. Many of the features are qualitatively similar to the previous example, but some have changed substantially. We note the following:

"Page missing from available version"

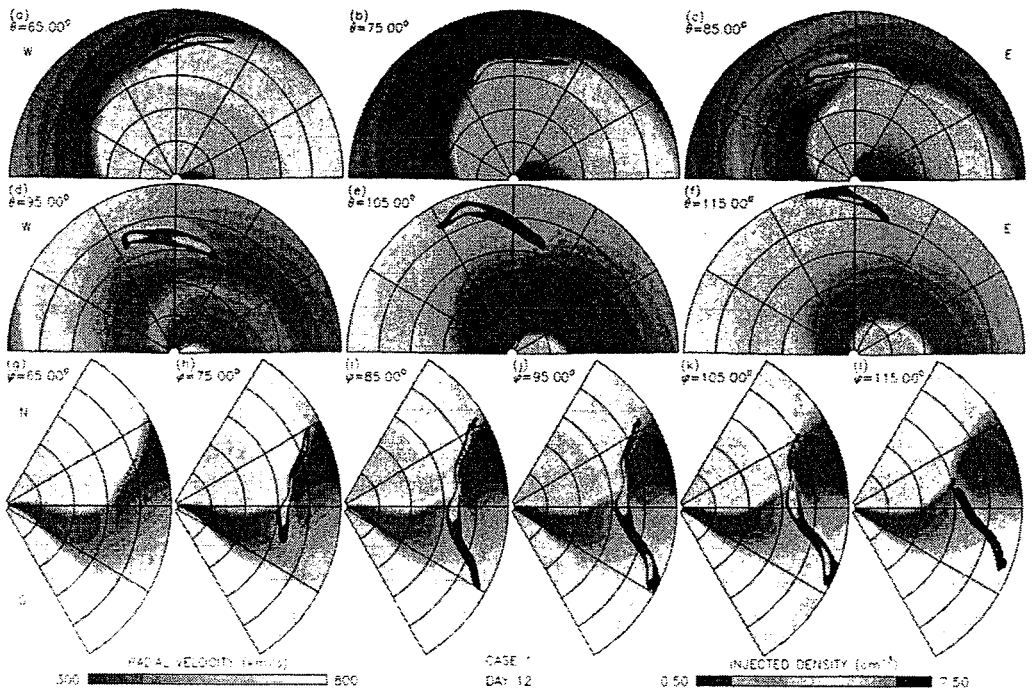

FIGURE 3. Grey–scale contours of radial velocity and density in: (a–f) azimuthal planes at different co–latitudes; and (g–i) meridional planes at different longitudes 12 days following the launch of a CME pulse. The CME is delineated by the darkest contour. Within the CME, the shading represents density. Outside the CME, the shading represents radial velocity. Row 1 (a–c) shows cuts in azimuthal planes above the heliographic equator and row 2 (d–f) shows cuts below the heliographic equator. The density has been renormalized to 1 AU by dividing by $R(AU)^2$. From (11).

Reprinted from Odstrcil, D. and Pizzo, V., *Journal of Geophysics Research.*, ©1998a by the American Geophysical Union.

Figure 3 presents a snapshot at 12 days following the launch of a CME. In this case, the CME consisted of a pulse with a speed equal to the high–latitude solar wind and a pressure eight times higher than the low–latitude wind. The pulse was launched from the center of the slow flow band. The top two rows show grey–scale contours in different azimuthal planes for various co-latitudes. The first 3 panels (top row) display azimuthal planes above the heliographic equator, and the second three (middle row) display azimuthal planes below the heliographic equator. The last row shows meridional cuts at different longitudes. The light grey shading on the plots shows radial velocity. The darkly–bounded regions demark the ejecta and the shading within these regions represents the density of the ejecta.

Consider the bottom row first. Note how much more asymmetric and variable the profiles of the ejecta appear when compared with the 2–D simulations. At low latitudes, for example, the CME is much thicker. Here, there is predominantly fast wind ahead of the ejecta, and slow wind behind it. Since the ejecta was travelling initially significantly faster than the slow wind, these conditions allow the ejecta to expand both at its leading edge and trailing edge. In contrast, at mid–latitudes, the solar wind ahead of the CME is slow wind, while the flow behind it is fast. These naturally act to compress the CME and further squeeze the ejecta to higher latitudes. This effect is most pronounced at the boundary where the slow wind, ejecta, and fast wind all meet.

There are also notable variations in the ejecta profile in the different azimuthal planes. Comparing panels a to f, there is, for example, a trend for the orientation of the CME to move from being aligned with the prevailing spiral pattern at northen latitudes, to being almost perpendicular to it in the southern hemisphere. This effect can be understood in terms of the ambient wind in which the ejecta is immersed. At southern latitudes, for example, the western (left) edge is immersed in faster solar wind, whereas the eastern portion of the ejecta is immersed in slower wind. Thus a refraction process takes place such that the western portion of the CME is convected outward more quickly than the eastern portion. Further details on these simulations can be found in (11, 12).

SUMMARY AND DISCUSSION

In this paper, we have discussed a number of models aimed at investigating the large scale dynamical evolution of CME–driven distubances in the solar wind. We

Appendix 2

Properties and radial trends of coronal mass ejecta and their associated shocks observed by Ulysses in the ecliptic plane

Pete Riley, J. T. Gosling, D. J. McComas, and R. J. Forsyth

Journal of Geophysical Research, 105, 12,617, 2000

JOURNAL OF GEOPHYSICAL RESEARCH, VOL. 105, NO. A6, PAGES 12,617–12,626, JUNE 1, 2000

Properties and radial trends of coronal mass ejecta and their associated shocks observed by Ulysses in the ecliptic plane

Pete Riley

Science Applications International Corporation, San Diego, California

J. T. Gosling and D. J. McComas

Los Alamos National Laboratory, Los Alamos, New Mexico

R. J. Forsyth

Blackett Laboratory, Imperial College, London

Abstract. In this paper, magnetic and plasma measurements are used to analyze 17 interplanetary coronal mass ejections (CMEs) identified by Ulysses during its in-ecliptic passage to Jupiter. We focus on the expansion characteristics of these CMEs (as inferred from the time rate of change of the velocity profiles through the CMEs) and the properties of 14 forward shocks unambiguously associated with these CMEs. We highlight radial trends from 1 to 5.4 AU. Our results indicate that the CMEs are generally expanding at all heliocentric distances. With regard to the shocks preceding these ejecta, we note the following: (1) There is a clear tendency for the shock speed (in the upstream frame of reference) to decrease with increasing heliocentric distance as the CMEs transfer momentum to the ambient solar wind and slow down; (2) 86% of the shock fronts are oriented in the ecliptic plane such that their normals point westward (i.e., in the direction of planetary motion about the Sun); (3) 86% of the shocks are propagating toward the heliographic equator; and (4) no clear trend was found in the strength of the shocks versus heliocentric distance. These results are interpreted using simple dynamical arguments and are supported by fluid and MHD simulations.

1. Introduction

The Ulysses spacecraft was launched in October 1990 and during the next 16 months traveled outward to Jupiter where it received a gravitational assist necessary to propel it into a polar orbit about the Sun. During this near-ecliptic phase of the mission, at least 25 coronal mass ejections (CMEs) were encountered [*Phillips* 1997].

In this paper, we analyze the expansion characteristics of these ejecta and the properties of the shocks associated with them and attempt to identify radial trends. Specifically, we focus on the speed profiles within the ejecta which allow us to determine the expansion properties of the ejecta, and we compute the orientation, speed, and strength of the 14 fast-mode forward shocks that could be unambiguously associated with these ejecta.

Paper number 1999JA000169.
0148-0227/00/1999JA000169$09.00

Several previous studies have analyzed specific CME-driven events during the in-ecliptic phase of the Ulysses mission [e.g., *Phillips et al.*, 1992; *Lanzerotti et al.*, 1992]. Other studies have summarized the properties of shocks observed during this period but did not distinguish between corotating and CME-associated shocks [e.g., *Burton et al.*, 1992; *Balogh et al.*, 1995]. Several studies have summarized the general properties of these transient events. *Phillips* [1997] provided a list of the CMEs, including start times, and possible associations with transient shocks. *González-Esparza et al.* [1998] analyzed several dynamic properties of these CMEs and, in particular, found an apparent lack of correlation between the radial widths of the ejecta and heliocentric distance. The authors interpreted this result as an indication that the ejecta had established a pressure equilibrium with the surrounding ambient solar wind and were no longer expanding. In contrast, *González-Esparza and Bravo* [1998] compared Ulysses observations with near-Earth IMP observations to infer that the radial width of the ejecta was larger at Ulysses than at IMP, demonstrating that the ejecta were expanding as they propagated away from the Sun.

In an earlier study, *Gosling et al.* [1987] examined the flow properties at the leading edge of 19 fast CMEs using data from ISEE 3. They found that 17 events displayed eastward flow deflections across the leading edge of the ejecta. Thus the normal vectors to the ejecta fronts were tilted toward the west (i.e., in the direction of planetary motion). In contrast, no pattern was found in the meridional flow deflections. Gosling et al. proposed that the observed eastward flow deflections were a consequence of solar rotation and the Parker spiral pattern that resulted from it. As the ejecta propagate approximately radially outward from the Sun, westward pressure gradients acted to 'refract' the ejecta fronts so that they became more aligned with the prevailing Parker spiral.

The data analyzed in this study derive from the Solar Wind Over the Poles of the Sun (SWOOPS) ion sensor [*Bame et al.*, 1992] and the magnetometer instrument [*Balogh et al.*, 1992] on board the Ulysses spacecraft. The plasma moments produced from the SWOOPS instrument have a typical resolution of 4–8 min, while the magnetic field components have a typical resolution of 1–2 s.

This paper is structured as follows. In section 2 we discuss the expansion characteristics of the ejecta. In section 3 we describe the analysis techniques that were performed on the transient forward shocks and discuss the results of this analysis. Finally, in section 4 we discuss the results of this study and compare with numerical models of CME evolution.

2. Plasma Characteristics of the Ejecta

The coronal mass ejections encountered by Ulysses during its outward passage to Jupiter were identified primarily by the presence of counterstreaming suprathermal electrons (CSEs) [*Phillips* 1997]. In addition, Phillips required that at least one other characteristic commonly associated with ejecta (e.g., anomalously low proton temperature [e.g., *Gosling et al.*, 1973] or high helium abundance [e.g., *Hirshberg et al.*, 1972]) also be present. These combined criteria led to the identification of 25 CMEs. However, among these events there was considerable variability. Many, for example, did not display helium abundance enhancements or rotations in the magnetic field, which are commonly associated with flux ropes. In some cases the boundaries of the ejecta were difficult to ascertain.

To mimimize variability due to different trajectories through the CME-driven disturbances, we restrict our analysis to only those events for which at least two other plasma and/or magnetic field signatures were present in addition to the signature of CSEs. By so doing, our initial list of 25 events was reduced to 17. Table 1 summarizes all 25 CMEs that were observed by Ulysses during its transit to Jupiter. The two left columns provide the inferred start dates and times and the two middle columns provide the inferred stop dates and times. The two right columns indicate whether a fast forward shock was obviously associated with the ejecta and whether the CME was included in the current study.

Table 1. Coronal Mass Ejections Observed by Ulysses During Its In-Ecliptic Outward Transit to Jupiter

Start Date	Start Time, UT	Stop Date	Stop Time, UT	Shock	Used in Current Study
11/29/90	0253	11/29/90	0615	no	yes
12/01/90	0425	12/01/90	1230	no	yes
12/11/90	0225	12/13/90	1800	yes	no
12/26/90	1530	12/28/90	1140	yes	no
01/11/91	0325	01/11/91	1100	no	no
01/16/91	1629	01/19/91	0040	yes	yes
02/27/91	0444	02/27/91	1700	yes	yes
03/05/91	0100	03/07/91	2345	yes	yes
03/15/91	2245	03/18/91	1300	yes	yes
03/21/91	1230	03/21/91	2045	yes	yes
03/24/91	0631	03/26/91	1140	yes	no
03/27/91	0915	03/29/91	1200	yes	yes
03/29/91	1200	04/02/91	1845	no	no
04/08/91	1610	04/11/91	1505	yes	no
05/29/91	1515	05/31/91	1430	yes	yes
06/04/91	0135	06/05/91	0800	yes	yes
08/09/91	1700	08/11/91	0600-1800	no	no
09/10/91	0530	09/13/91	0800	yes	yes
09/18/91	1100	09/19/91	1100	yes	yes
10/27/91	1200	10/28/91	0205	yes	yes
11/10/91	1220	11/13/91	1235	yes	no
11/17/91	1500	11/20/91	1400	no	yes
12/27/91	0300	12/27/91	2030	yes	yes
01/12/92	1115	01/13/92	1530	yes	yes
01/21/92	1550	01/22/92	0950	no	yes

Figure 1 shows the speed profiles for the 17 CMEs. In each case, speed is plotted as a function of time in days, as indicated by the legend in the upper left. The first two CMEs occurred in 1990, the last two occurred in 1992, and the remaining events occurred in 1991. In each panel the data begin at the leading edge of the ejecta (left) and end at the trailing edge (right). Superimposed on each plot is a least squares fit to the data. A negative slope indicates that the leading edge of the CME is traveling faster than the trailing edge. Furthermore, if the change between the two boundaries is relatively monotonic, then the CME is expanding; 71% (12 of 17) of the events displayed negative gradients, indicating that the majority of the ejecta were expanding. Presumably, the positive gradients in the remaining events are the result of compression and acceleration of the ejecta by faster solar wind behind the CME.

Using the least squares fits calculated above, we can define an "expansion rate" for each CME as $-dv/dt$. We emphasize, however, that since we measure the CME parameters at a single point in space, this rate is in reality a convolution of both temporal and radial effects. Furthermore, $-dv/dt$ is likely to be sensitive to a number of intrinsic properties of the CMEs, as well as to properties of the ambient solar wind into which the CMEs are propagating. Simulation results [e.g., *Gosling et al.*, 1995b; *Riley et al.*, 1997; *Riley and Gosling*, 1998] illustrate that the relative speed between the ejecta and the ambient solar wind can have a substantial impact on the rate of expansion of CMEs. Thus, in an effort to minimize scatter and amplify any underlying trends, we further restrict our analysis to those ejecta that were propagating sufficiently fast to drive a forward shock. Figure 2a shows $-dv/dt$ for the 14 events that were unambiguously associated with shocks (see Table 1). Eleven of the 14 events lie above zero, indicating expansion. The least squares fit to the points suggests that the rate at which CMEs expand tends to decrease with increasing heliocentric distance. However, this fit may be biased by several events observed at $\sim$ 2.3 AU (corresponding to the time period March–April, 1991, during which time there was major solar activity [*Phillips et al.*, 1992]). Thus at best, these results should be viewed tentatively.

It is straightforward to show that for fast plasma outrunning slower plasma ballistically (i.e., such that each parcel of plasma maintains constant speed), a gradient evolves between them such that $dv/dt \propto 1/R$, where R is the heliocentric distance of the ejecta. In reality, however, dv/dt will decrease faster than $1/R$ as a rarefaction (or expansion wave) propagates into the surrounding plasma. On the other hand, if the expansion of the ejecta is impeded by the surrounding plasma, dv/dt would decrease less rapidly than $1/R$. Thus in Figure 2b we display $-Rdv/dt$ as a function of heliocentric distance. The large scatter and lack of any obvious trend do not allow us to infer an expansion rate appreciably different from $1/R$.

3. Shock Analysis

We now turn our attention to an analysis of the transient forward shocks associated with these ejecta. In particular, there are several methods for calculating the orientation of shock fronts [*Abraham-Shrauner and Yun*, 1976]. The two approaches most often used are magnetic coplanarity and velocity colinearity. Velocity colinearity is only an approximate result, which is most valid when the shock is nearly perpendicular and the magnetosonic Mach number is high [*Abraham-Shrauner and Yun*, 1976]. The errors associated with this method have been discussed in detail by *Riley et al.* [1996]. Magnetic coplanarity is, on the other hand, at least theoretically an exact method. However, while this is true for nearly perpendicular shocks, the technique can become inaccurate as the angle between the upstream and downstream magnetic field vectors, $\mathbf{B}_1$ and $\mathbf{B}_2$, becomes small. This is especially true when large fluctuations exist, as are often observed in solar wind magnetic field measurements. In this study we use magnetic coplanarity to determine the orientation of the shock normal, $\mathbf{n}$:

$$\mathbf{n} = \pm \frac{(\mathbf{B}_1 \times \mathbf{B}_2) \times (\mathbf{B}_1 - \mathbf{B}_2)}{|(\mathbf{B}_1 \times \mathbf{B}_2) \times (\mathbf{B}_1 - \mathbf{B}_2)|}. \quad (1)$$

Typically, in the analysis of interplanetary shocks, windows upstream and downstream of the shock are chosen, and the plasma and magnetic field parameters are first averaged before calculating the properties of the shocks. However, because of potential contamination by waves, the approach we adopt is to match all the points in the upstream region with all the points in the downstream region and calculate $\mathbf{n}$ for each. Thus for p points upstream and downstream we actually calculate p^2 unit normals. Since $\mathbf{n}$ is a unit vector, it can be expressed as a function of two coordinates (θ, ϕ). Here θ is defined as the latitudinal angle and is positive northward, and ϕ is defined as the azimuthal angle and is positive in the direction of planetary motion about the Sun. Thus the radial direction is represented by (0,0). Since the distributions of calculated unit normals tend to be fairly circular in (θ, ϕ) space for any given shock, we assume that $\mathbf{n} = (< \theta >, < \phi >)$. Each shock calculation is checked by visually inspecting the cluster of normals in the (θ, ϕ) plane. This technique has been used previously to calculate the orientation of interplanetary corotating shocks [*Riley et al.*, 1996; *Gosling et al.*, 1997] as well as the orientation of the polar coronal hole boundary [*McComas et al.* 1998] using velocity colinearity.

Once the orientation of the shock front has been determined, we use mass conservation to determine the speed of the shock in the spacecraft frame of reference:

$$v_{\text{shock}} = \frac{1}{p} \sum_{i=1}^{p} \frac{\Delta [N_i \mathbf{v}_i] \cdot \mathbf{n}}{\Delta [N_i]}, \quad (2)$$

where N_i is the proton number density and $\mathbf{v}_i$ is the proton velocity in the spacecraft frame of reference. Here

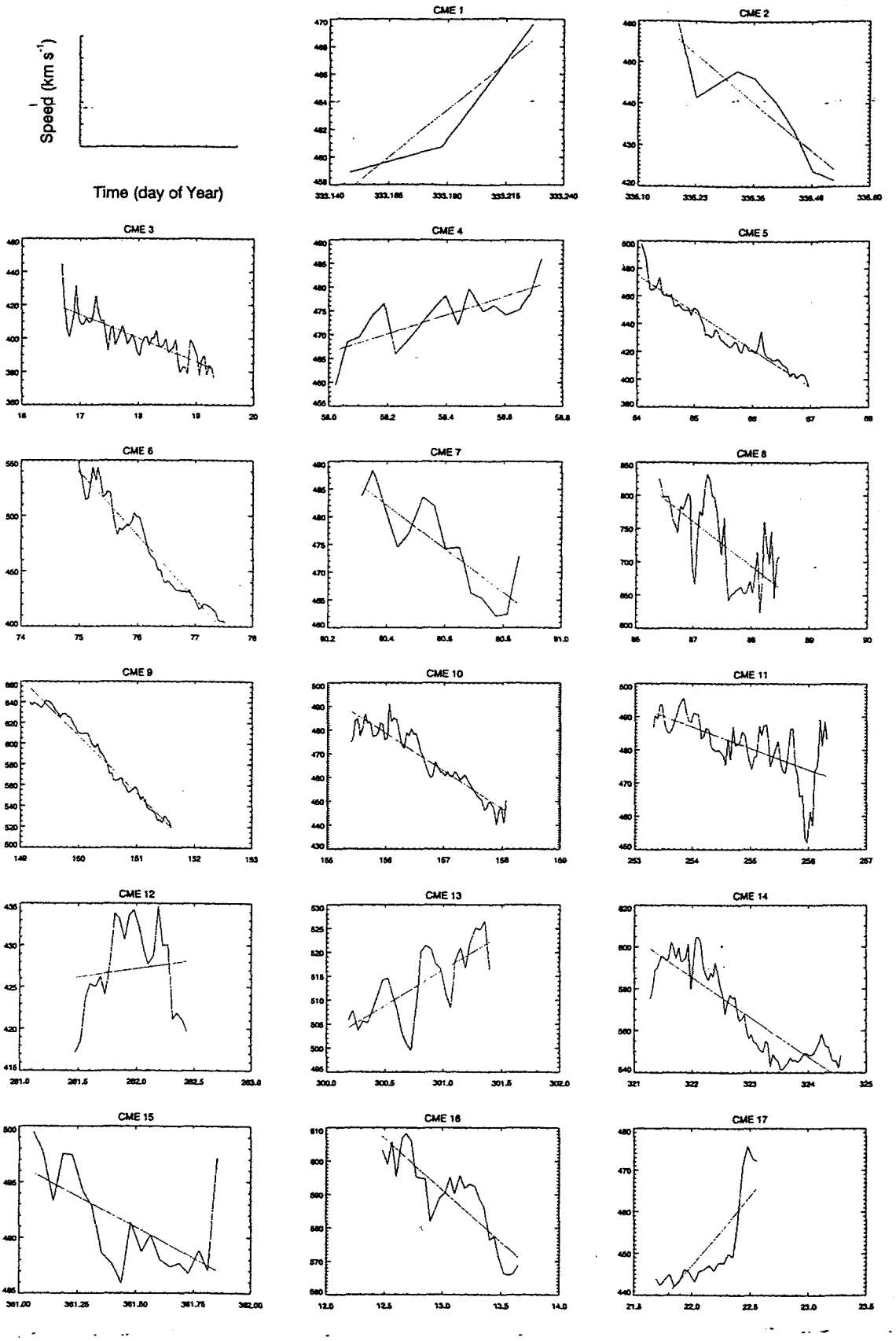

Figure 1. Speed profiles for 17 coronal mass ejections (CMEs). The top left diagram identifies the axes for each subsequent plot. CMEs 1 and 2 are from 1990, CMEs 16 and 17 are from 1992, and the remaining CMEs are from 1991. The straight dashed line in each panel is a least squares fit to the data. A negative slope indicates that the leading edge of the CME is traveling faster than the trailing edge, indicating that the CME is expanding.

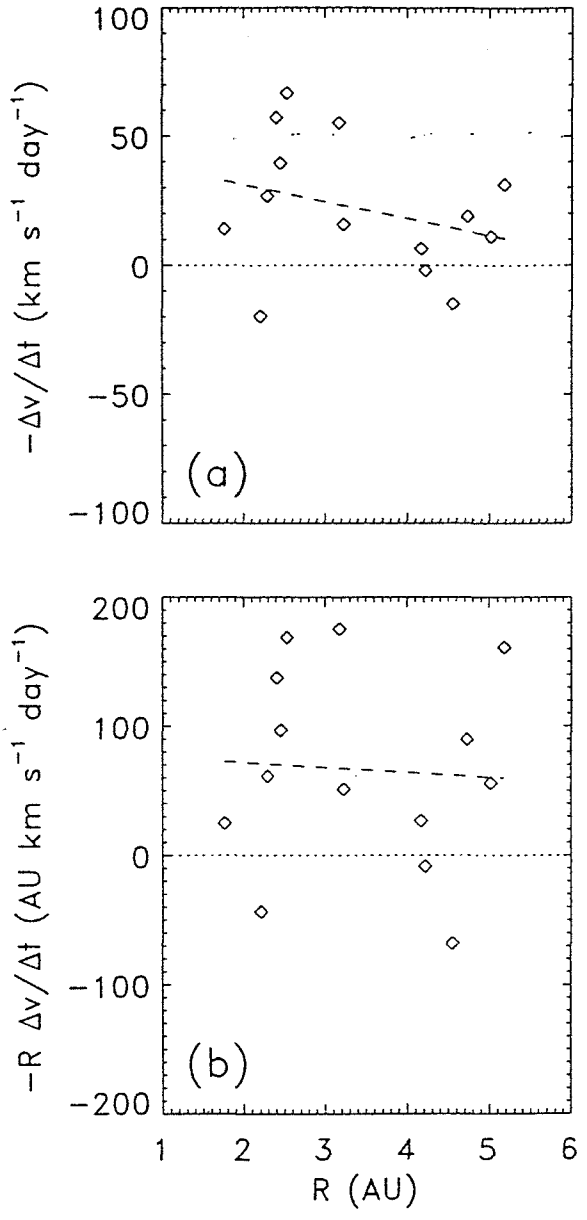

Figure 2. (a) The expansion rate, defined as the negative of the slopes calculated from Figure 1, plotted against heliocentric distance for the 14 CMEs that drove shocks. The dashed line is a least squares fit to the data. (b) Expansion rate multiplied by the heliocentric distance of the ejecta.

$\Delta[\,]$ denotes the difference between the downstream and upstream quantities and the summation over i runs over p measurements. It is usually more meaningful to discuss the speed of the shock relative to the upstream solar wind ($v^*_{\rm shock}$) which is obtained by subtracting $v_1 \cdot \mathbf{n}$ from the right-hand side of (2).

Following *Gosling et al.* [1995a], we define the shock strength χ_{ss} to be the ratio of the downstream to upstream density minus 1:

$$\chi_{ss} = \frac{N_2}{N_1} - 1. \qquad (3)$$

This definition of χ_{ss} is such that for an infinitely weak shock, $\chi_{ss} \to 0$. From simple theoretical considerations we would predict a maximum value, $\chi_{ss} \sim 3$, when the ratio of specific heats γ is equal to $\frac{5}{3}$.

The difference between the resolution of the magnetic field measurements (1-2 s) and the plasma measurements (4-8 min) makes the choice of upstream and downstream windows difficult. On one hand, the windows should be sufficiently narrow and close to the shock front so as to reduce potential contamination by waves and/or discontinuities. On the other hand, the windows must be sufficiently wide and/or far away from the shock front so as to include at least one meaningful plasma data point. Our approach was to analyze each event by hand, choosing the windows so as to (1) minimize the scatter in plots of n in (θ, ϕ) space and (2) include at least one representative plasma data point within each window. As a check, we also applied velocity colinearity to larger windows to determine the shock normal, shock speed, and shock strength. Although we found quantitative differences between the two approaches, the conclusions reached in the study were insensitive to the particular technique. A detailed comparison of these as well as other techniques will be presented elsewhere.

The 14 shocks used in this study are listed in Table 2. All were (fast-mode) forward shocks that preceded CMEs by anywhere from 4 hours to 2.5 days. All events fit the paradigm of a fast ejecta plowing through a slower ambient solar wind and driving a shock wave ahead.

Figure 3 presents shock speed, in the upstream solar wind reference frame, as a function of heliocentric distance. The numerical values are summarized in Table 2. Although there is significant scatter, the trend is for shock speed to decrease with increasing distance from the Sun. The dashed line represents a least squares fit to the points.

Figure 4a presents the shock strengths, as defined by (3). There appears to be no obvious trend with increasing distance from the Sun. Shock strength is, however, one of the least accurately determined shock parameters and is likely to be more sensitive to the initial properties of the individual ejecta (i.e., mass and speed). For comparison, Figures 4b and 4c display the ratio of downstream to upstream magnetic field strength and the magnetosonic Mach number as calcuated by *Balogh et al.* [1995]. These parameters provide an independent verification of a lack of trend in shock strength with heliocentric distance. It is also noteworthy, and reassuring, that there is a relatively good correlation between point-to-point variations in the parameters, in spite of the fact that the windows were chosen independently.

In Figure 5 we have computed the sound speed c_s, Alfvén speed v_A, and magnetosonic speed v_s immediately upstream of each shock. Of interest here is the modest (17 km s^{-1}) decrease in the magnetosonic wave speed, which is driven primarily by a decrease in the Alfvén speed.

Figure 6 displays the orientations of the shock normals. The top panel presents shock tilts in the merid-

Table 2. Shock Parameters

Year	Day of Year	Time, UT	θ	ϕ	v_{shock}	v^*_{shock}	χ	R, AU
1990	343	19:17	16.70	-5.13	496.99	137.67	0.81	1.347
1990	358	16:00	8.90	7.61	426.70	64.86	1.45	1.501
1991	014	07:55	-6.29	21.78	464.32	99.32	0.78	1.728
1991	062	23:49	32.67	16.97	500.88	134.02	0.37	2.266
1991	078	22:25	60.15	17.93	340.47	131.41	0.71	2.438
1991	082	15:40	25.42	-9.24	567.17	165.49	2.21	2.479
1991	097	04:46	9.88	19.78	543.16	135.51	3.21	2.633
1991	154	17:06	12.61	-4.45	508.56	84.35	2.77	3.219
1991	251	08:27	-23.41	4.24	477.70	89.51	1.24	4.117
1991	261	07:10	28.52	18.90	398.64	64.35	0.58	4.204
1991	299	22:03	-9.26	8.76	545.36	106.47	2.29	4.535
1991	313	08:21	28.66	2.31	413.30	63.12	2.13	4.646
1991	360	19:45	15.99	40.96	388.39	42.57	2.85	5.033
1992	012	04:00	-35.67	1.11	535.33	52.84	0.48	5.162

ional plane. Twelve of the 14 events have a positive tilt. Thus 86% of the shock normals are tilted northward in the meridional plane. Since Ulysses' trajectory was displaced southward of the heliographic equator during this period, we infer that the shock normals were also tilted preferentially toward the heliographic equator. The bottom panel shows shock orientations in the azimuthal plane. From this we deduce that 86% are also tilted toward the west (although the two events that are tilted toward the east are not the same two events that are tilted toward the south).

4. Summary and Discussion

In this study we have analyzed the expansion properties of 17 coronal mass ejections observed by Ulysses during its outward bound trip to Jupiter and computed the basic shock parameters of 14 transient forward shocks that were associated with these ejecta.

Our results indicate that CMEs are generally expanding as they propagate away from the Sun and that the rate of expansion tends to decrease with increasing distance from the Sun. This is not a surprising result; coronagraph observations indicate that CMEs near the

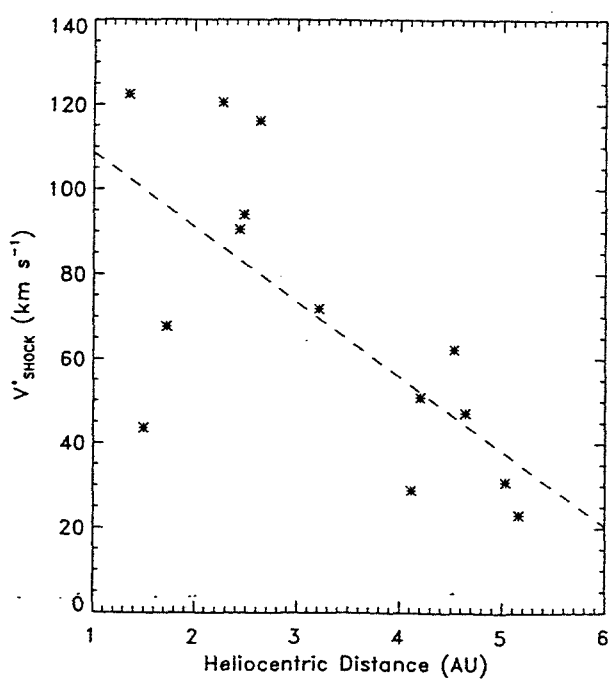

Figure 3. Shock speed relative to the upstream solar wind reference frame (v^*_{shock}) versus heliocentric distance for 14 fast-mode shocks.

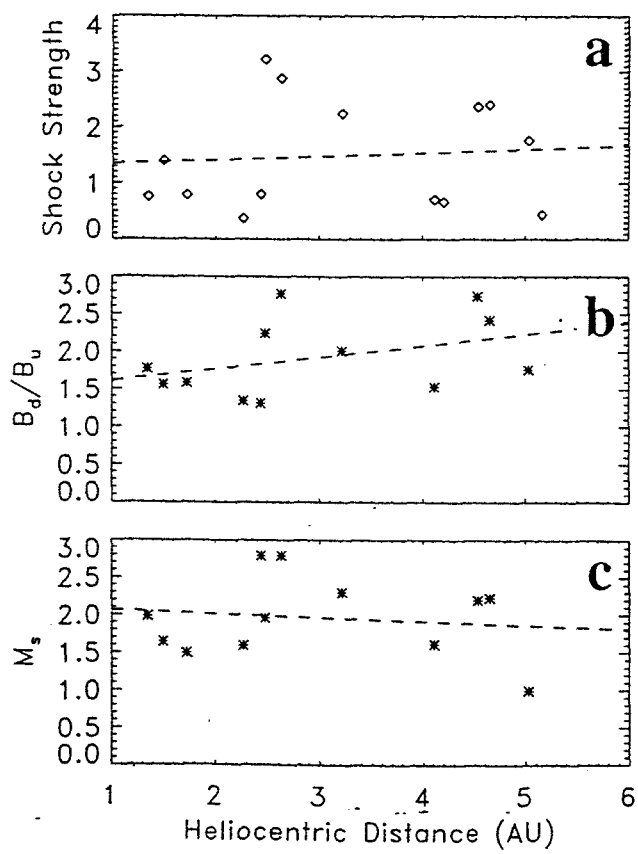

Figure 4. (a) Shock strength (as inferred from the ratio of downstream density to upstream density minus 1) versus distance from the Sun. (b) Ratio of downstream to upstream magnetic field strength. (c) Magnetosonic Mach number.

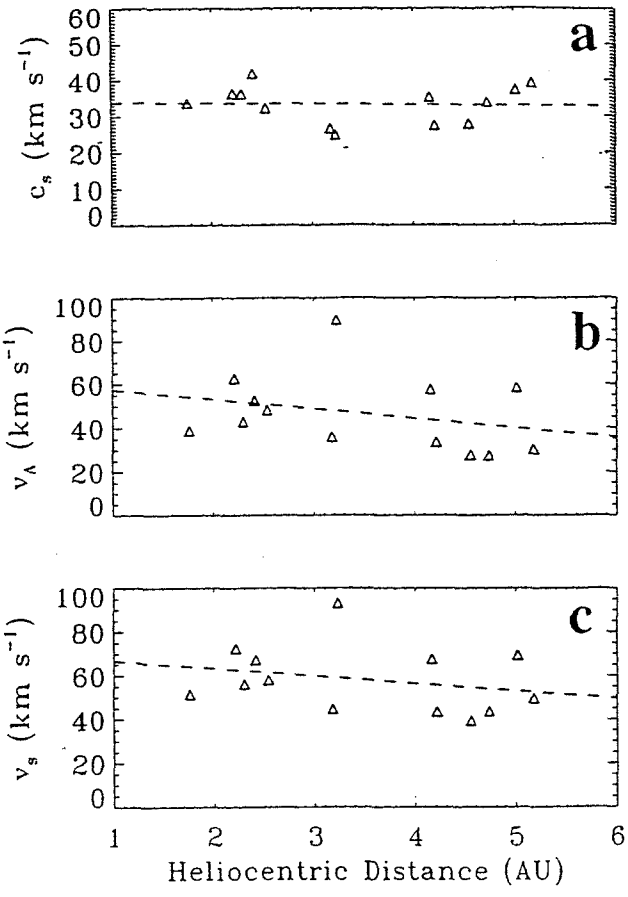

Figure 5. (a) Sound speed. (b) Alfvén speed. (c) Magnetosonic speed immediately upstream of the shocks.

Sun are expanding. They are inferred to have pressures considerably higher than the ambient solar wind into which they are propagating. Thus initially, the high pressure within the ejecta drives a strong expansion, but as the CME propagates farther from the Sun and evolves toward pressure balance with the ambient solar wind, the rate of expansion decreases. CME expansion in the solar wind may also be the result of other effects [e.g., *Gosling and Riley*, 1996]. For example, CMEs traveling faster than the trailing ambient solar wind and/or slower than the leading wind expand as they are accelerated into the rarefaction caused by the difference in speed between the CME and the ambient solar wind. Also, expansion may simply be the result of the leading edge of the CME being ejected faster than the trailing edge. Unfortunately, the scatter in the calculated expansion rates precludes us from inferring an expansion rate significantly different from $1/R$, which would be expected based on the evolution of ballistic trajectories.

Our results may be compared with a study by *González-Esparza et al.* [1998], who examined the variation in the radial width of these ejecta (computed by integrating the solar wind bulk speed between the leading and trailing edges of the ejecta) as a function of heliocentric distance and concluded that there was no evidence for expansion between 1 and 5 AU. Their method, however, was sensitive to a number of factors, including the initial intrinsic properties of the CMEs and the trajectory taken by the spacecraft through the event. On the other hand, our approach provides a more direct measure of expansion since clearly a CME is expanding if its leading edge is moving faster than its trailing edge. Our results support the study by *González-Esparza and Bravo* [1998] who found that ejecta observed by both Ulysses and IMP displayed larger radial widths at larger heliocentric distances.

As a fast CME plows through the solar wind traveling at speeds (in the rest frame of the upstream solar wind plasma) in excess of the fast magnetosonic wave, it drives a shock ahead of it, providing the necessary mechanism to communicate the presence of the outward moving CME to the solar wind ahead. Momentum coupling, however, between the ejecta and the slower leading and trailing solar wind acts to slow the ejecta down. In turn, the speed of the shock relative to the upstream solar wind diminishes. Our results suggest that, on average, the rate of change in velocity with distance is $\sim$15 km s^{-1} AU^{-1}. However, for any particular event, the rate of deceleration is likely to be sensitive to the initial properties of the ejecta as well as to the ambient wind into which it is propagating.

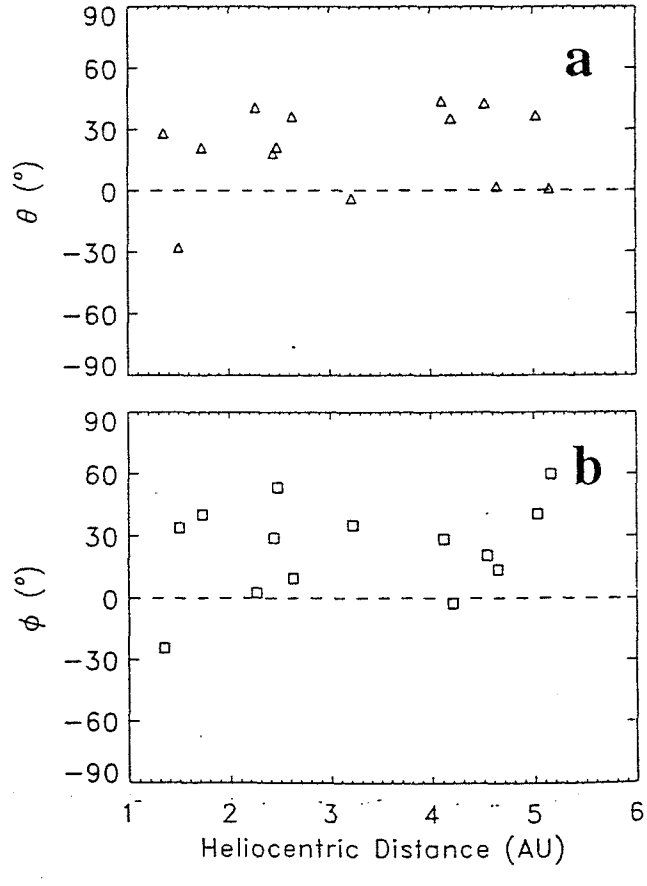

Figure 6. (a) Meridional tilt of shock normals (θ). (b) Azimuthal tilt of shock normals (ϕ) versus heliocentric distance.

Our results suggest that there is no underlying trend in the strength of shocks (as defined by the ratio of downstream density to upstream density) preceding a fast CME as a function of heliocentric distance. This is supported by a comparison of the variation of B_d/B_u and the magnetosonic Mach number with heliocentric distance as calculated by *Balogh et al.* [1995]. We suggest that the competing effects of (1) the shock slowing down and (2) the characteristic wave speed of the upstream solar wind decreasing conspire to produce this result. Both of these effects are evident in the data, although the decrease in the magnetosonic wave speed upstream of the shocks is relatively modest.

To explore whether one might expect to observe a systematic variation in shock strength with distance from the Sun, we have utilized one-dimensional (1-D) fluid simulations of fast transient disturbances. In simulating CIR evolution, 2- and 3-D effects have been shown to be important in the evolution of shocks bounding interaction regions [*Pizzo,* 1981]. However, fast CMEs propagate radially away from the Sun, suggesting that multidimensional effects may not be as significant. This is supported by 2-D [*Riley et al.,* 1997] and 3-D [*Odstrčil and Pizzo,* 1999a, b] simulations that show that while the large-scale morphology of ejecta and their associated disturbances are affected by the dimensionality of the simulation, the essential features of the disturbance along some radial trajectory are captured by 1-D results [e.g., *Gosling et al.,* 1995b]. The algorithm employed is based on an Eulerian finite difference scheme with inflow boundary conditions specified at the inner boundary (30 R_{Sun}) and outflow boundary conditions specified at the outer boundary (6 AU) [e.g., *Riley and Gosling,* 1998; *Riley et al.,* 1997]. The simulation region is filled with typical solar wind values, and the system is allowed to evolve into an equilibrium. A bell-shaped pulse is then launched at the inner boundary in the form of a speed perturbation while holding the density and temperature constant.

In Figure 7 we compare two profiles of a pulse mimicking a fast CME-driven disturbance at 83 hours (1.75 AU) and 250 hours (5 AU) following its launch. Over an interval of 10 hours the speed was raised smoothly by 300 km s^{-1} and then lowered smoothly while holding the remaining plasma parameters constant. Figure 7a shows speed, Figure 7b shows number density, and Figure 7c shows the thermal pressure of the fluid as functions of heliocentric distance. The point to note from Figure 7 is that the strength of the shock at the leading edge of the disturbance (which, by virtue of the logarithmic scaling, is directly proportional to the change in density) does not change appreciably between ~1.75 and ~5 AU. In contrast, the speed of the shock decreased substantially over that distance range. Numerical experiments such as this one were repeated for a variety of speed profiles. For several cases the simulation region was extended to 50 AU to investigate whether trends might only become apparent over sufficiently large distances. In some cases the shock strength increased slightly, while in other cases it decreased. However, these variations were never more than 10-15%. Thus, although shocks slow down as the CME-driven disturbances propagate away from the Sun, the characteristic wave speed of the medium into which they are propagating also decreases, and the net effect is that the strength of the shock does not change appreciably over large distances. These results are in qualitative agreement with 1-D simulations of corotating interaction regions (CIRs) by *Hundhausen* [1973], who found that the strength of shocks either remained constant or increased between 1 and 6 AU.

Linearized fluid models [*Burton et al.,* 1992], two-dimensional MHD simulations [*Odstrčil et al.,* 1996], and three-dimensional hydrodynamic simulations [*Odstrčil and Pizzo,* 1999a, b] suggest that the large-scale meridional structure of the ejecta and shock fronts near the eclipic is concave outward. Thus the normal vectors to the fronts are tilted toward the heliographic equator in both hemispheres. Ulysses was located in the Southern Hemisphere ($\lesssim$ 6°S heliographic latitude) during this interval, and hence the northward (i.e., e-

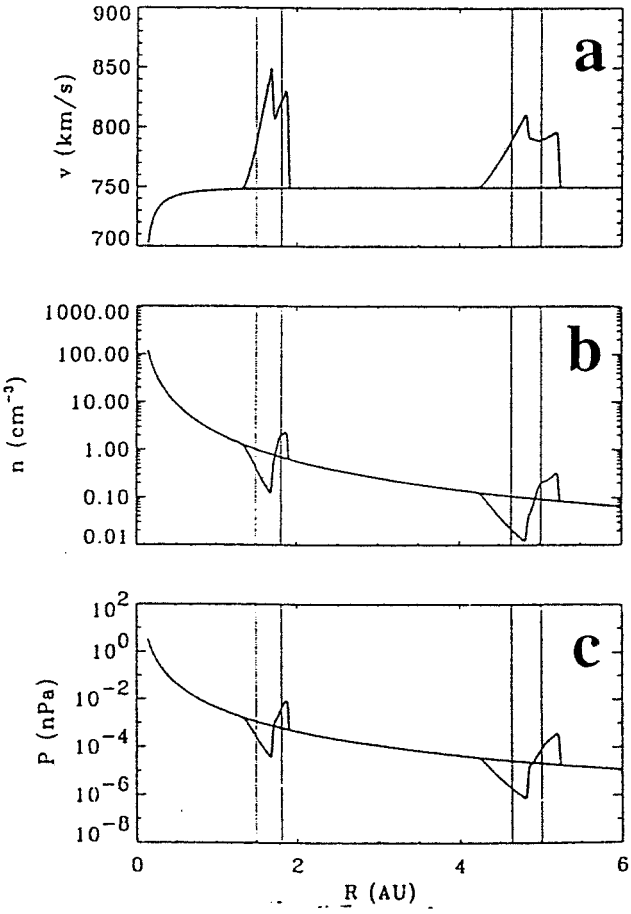

Figure 7. (a) Solar wind speed, (b) number density, and (c) pressure profiles at two times (83 and 350 hours) following the launch of a pulse introduced at the inner boundary. The vertical lines mark the boundary of the pulse.

quatorward) tilts of the shock normals are consistent with this picture. Slower, denser flow equatorward of the observation acts to retard the disturbance more and thus effectively refracts the shock normal toward the equatorial plane. Thus these orientations imply that at least part of the ejecta was embedded within the streamer belt. Another possibility is that the majority of the ejecta were centered south of the spacecraft. However, this would imply a meridional asymmetry in the launch characteristics of CMEs at the Sun for a period of ~16 months.

The inferred azimuthal orientation of the shock fronts is consistent with an earlier study by *Gosling et al.* [1987] of flow deflections at the leading edges of fast ejecta. Taken together, these two studies suggest that these tilts may be a large-scale phenomenon. Gosling et al. proposed that the azimuthal ejecta tilts may be the result of one (or a combination) of two effects, both related to the Parker spiral pattern. First, as the fast CME sweeps up the ambient solar wind magnetic field ahead, the draping of the field lines takes place asymmetrically, with more draping occurring on the westward side. The net result is an east-west magnetic pressure gradient that causes the ejecta to rotate toward the west. Second, inhomogeneities organized about the Parker spiral could cause the observed azimuthal tilts. In particular, as the fast CME approaches and overtakes the slower, denser material of a slow stream, it will encounter the slow stream at its westward edge first and thus be retarded more there. Three-dimensional hydrodynamic simulations of CME evolution in a simple two-stream tilted dipole model [*Odstrčil and Pizzo,* 1999a, b] support the idea that significant azimuthal tilts can be generated by the prevailing Parker corotating flow pattern. However, this model only predicts the observed westward asymmetry for certain launch characteristics. In particular, the CME must be launched at the eastward edge of the slow-flow stream. Under such conditions, as it moves away from the Sun, it interacts with the slow-flow wind as described above. In contrast, if the CME is launched from the center of the slow flow wind, the ejecta can display an eastward tilt. When an ejection is launched to the west of the slow wind, there is no slow ambient flow ahead for it to interact with; no shock forms, and the ejection does not display a significant tilt.

Since inhomogeneities occur in the solar wind on all measurable scales, it is not clear that the observed tilts are global effects; if the ejecta respond only to small-scale inhomogeneities, the fronts may be tilted locally westward but globally remain relatively untilted. Since individual spacecraft sample only one cut through the shock surface, accurate shock timing by several spacecraft would be required to differentiate between "global" and "local" shock tilts.

In this paper we have shown that the CMEs observed by Ulysses during its in-ecliptic passage to Jupiter were generally expanding and that the rate of expansion decreases with increasing heliocentric distance. Analysis of the shocks preceding these ejecta suggests that while the speed of the shocks (in the upstream frame of reference) decreases with increasing distance from the Sun, there is no discernible trend in shock strength. We suggest that the combination of decreasing shock speed and decreasing wave speed (in the upstream wind) moving away from the Sun is responsible for this result. We found that 12 out of 14 (86%) shock normals are tilted toward the equator in the meridional plane and that 12 out of 14 (86%) shock normals are tilted toward the west in the azimuthal plane. The observed meridional tilts are consistent with simulations, suggesting that slow, dense flow equatorward of the observations is responsible for "refracting" the front normals toward the equator. Although several possible explanations for the azimuthal tilts were discussed, their cause, ultimately, remains unknown.

Acknowledgments. We thank D. Odstrčil, V. J. Pizzo, J. Americo González-Esparza, and Zoran Mikic for useful discussions. We are grateful to the referees for their comments and in particular to one of them for pointing out the relationship between dv/dt and R for ballistic expansion. This work was performed under the auspices of the U.S. Department of Energy, with support from NASA. P.R. gratefully acknowledges the support of the U.S. Department of Energy (subcontract G35240018-97), the National Aeronautics and Space Administration (grants NASW-98007 and NASW-98030), and the National Science Foundation (Space Weather Program grant ATM9613834).

Janet G. Luhmann thanks Marcia Neugebauer and another referee for their assistance in evaluating this paper.

References

Abraham-Shrauner, B., and S. H. Yun, Interplanetary shocks seen by Ames plasma probe on Pioneer 6 and 7, *J. Geophys. Res., 81,* 2097, 1976.

Balogh, A., T. J. Beek, R. J. Forsyth, P. C. Hedgecock, R. J. Marquedant, E. J. Smith, D. J. Southwood, and B. T. Tsurutani, The magnetic field investigation on the Ulysses mission: Instrumentation and preliminary scientific results, *Astron. Astrophys. Suppl. Ser., 92,* 221, 1992.

Balogh, A., J. A. González-Esparza, R. J. Forsyth, M. E. Burton, B. E. Goldstein, E. J. Smith, and S. J. Bame, Interplanetary shock waves: Ulysses observations in and out of the ecliptic plane, in *The High Latitude Heliosphere, Proceedings of the 28th ESLAB Symposium,* edited by R. G. Marsden, pp. 171-180, Kluwer Acad., Norwell, Mass., 1995.

Bame, S. J., D. J. McComas, B. L. Barraclough, J. L. Phillips, K. J. Sofaly, J. C. Chavez, B. E. Goldstein, and R. K. Sakurai, The Ulysses solar wind plasma experiment, *Astron. Astrophys. Suppl. Ser., 92,* 237, 1992.

Burton, M. E., E. J. Smith, B. E. Goldstein, A. Balogh, R. J. Forsyth, and S. J. Bame, Ulysses: Interplanetary shocks between 1 and 4 AU, *Geophys. Res. Lett., 19,* 1287, 1992.

González-Esparza, J. A., and S. Bravo, Two spacecraft observations of transient shocks and ejecta in the interplanetary medium, *J. Geophys. Res., 103,* 29,643, 1998.

González-Esparza, J. A., M. Neugebauer, E. J. Smith, and J. L. Phillips, Radial evolution of ejecta characteristics and transient shocks: Ulysses in-ecliptic observations, *J. Geophys. Res., 103,* 4767, 1998.

Gosling, J. T., and P. Riley, The acceleration of slow coronal mass ejections in the high-speed solar wind, *Geophys. Res. Lett., 23,* 2867, 1996.

Gosling, J. T., V. J. Pizzo, and S. J. Bame, Anomalously low proton temperatures in the solar wind following interplanetary shock waves: Evidence for magnetic bottles?, *J. Geophys. Res., 78,* 2001, 1973.

Gosling, J. T., M. F. Thomsen, S. J. Bame, and R. D. Zwickl, The eastward deflection of fast coronal mass ejecta in interplanetary space, *J. Geophys. Res., 92,* 12,399, 1987.

Gosling, J. T., S. J. Bame, D. J. McComas, J. L. Phillips, V. J. Pizzo, B.E. Goldstein, and M. Neugebauer, Solar wind corotating stream interaction regions out of the ecliptic plane: Ulysses, *Space Sci. Rev., 72,* 99, 1995a.

Gosling, J. T., D. J. McComas, J. L. Phillips, V. J. Pizzo, B.E. Goldstein, R. J. Forsyth, and R. P. Lepping, A CME-driven solar wind disturbance observed at both low and high heliographic latitudes, *Geophys. Res. Lett., 22,* 1753, 1995b.

Gosling, J. T., S. J. Bame, W. C. Feldman, D. J. McComas, P. Riley, B. E. Goldstein, and M. Neugebauer, The northern edge of the band of solar wind variability: Ulysses at ~4.5 AU, *Geophys. Res. Lett., 24,* 309, 1997.

Hirshberg, J., S. J. Bame, and D. E. Robbins, Solar flares and solar wind helium enrichments: July 1965-July 1967, *Sol. Phys., 23,* 467, 1972.

Hundhausen, A. J., Evolution of large-scale solar wind structures beyond 1 AU, *J. Geophys. Res., 78,* 2035, 1973.

Lanzerotti, L. J., C. G. Maclennan, R. E. Gold, S. E. Hawkins III, S. J. Tappin, and R. J. Forsyth, Solar particle composition: Measurements in the March 1991 event at 2.5 AU, *Geophys. Res. Lett., 19,* 1251, 1992.

McComas, D. J., P. Riley, J. T. Gosling, A. Balogh, and R. J. Forsyth, Ulysses' rapid crossing of the polar coronal hole boundary, *J. Geophys. Res., 103,* 1955, 1998.

Odstrčil, D., M. Dryer, and Z. Smith, Propagation of an interplanetary shock along the heliospheric plasma sheet, *J. Geophys. Res., 101,* 19,973, 1996.

Odstrčil, D., and V. J. Pizzo, Three-dimensional propagation of coronal mass ejections in a structured solar wind flow, 1, CME launched within the streamer belt, *J. Geophys. Res., 104,* 483, 1999a.

Odstrčil, D., and V. J. Pizzo, Three-dimensional propagation of coronal mass ejections in a structured solar wind flow, 2, CME launched adjacent to the streamer belt, *J. Geophys. Res., 104,* 493, 1999b.

Phillips, J. L., Coronal mass ejections encountered by the Ulysses spacecraft during the in-ecliptic mission phase, *Rep. 97-1086,* Los Alamos Natl. Lab., Los Alamos, N. M., 1997.

Phillips, J. L., S. J. Bame, J. T. Gosling, D. J. McComas, B. E. Goldstein, E. J. Smith, A. Balogh, and R. J. Forsyth, Ulysses plasma observations of coronal mass ejections near 2.5 AU, *Geophys. Res. Lett., 19,* 1239, 1992.

Pizzo, V. J., An evaluation of corotating solar wind stream models, in *Solar Wind Four, Rep. MPAE-W-100-81-31,*, pp. 153–158, Max-Planck-Inst. Fur Aeron., Katlenburg-Lindau, Germany, 1981.
edited by H. Rosenbauer, published by Max-Planck-Institut fur Aeronomie, Katlenburg-Lindau, and Max-Planck-Institut fur extraterrestrische Physik, Garching, Germany, p. 153, 1981.

Riley, P. and J. T. Gosling, Do coronal mass ejections implode in the solar wind?, *Geophys. Res. Lett., 25,* 1529, 1998.

Riley, P., J. T. Gosling, L. A. Weiss, and V. J. Pizzo, The tilts of corotating interaction regions at midheliographic latitudes, *J. Geophys. Res., 101,* 24,349, 1996.

Riley, P., J. T. Gosling, and V. J. Pizzo, A two-dimensional simulation of the radial and latitudinal evolution of a solar wind disturbance driven by a fast, high-pressure coronal mass ejection, *J. Geophys. Res., 102,* 14,677, 1997.

R. J. Forsyth, Space and Atmospheric Physics, Blackett Laboratory, Imperial College, London SW7 2BZ, England, United Kingdom. (r.forsyth@ic.ac.uk)

J. T. Gosling and D. J. McComas, Los Alamos National Laboratory, Los Alamos, NM 87545. (jgosling@lanl.gov; dmccomas@lanl.gov)

P. Riley, Science Applications International Corporation, San Diego, CA 92121. (uk2@haven.saic.com)

(Received May 13, 1999; revised January 31, 2000; accepted January 31, 2000.)

Appendix 3

Fluid aspects of solar wind disturbances driven by coronal mass ejections

J. T. Gosling and Pete Riley

Submitted to the *Journal of Geophysical Research*, 2000.

LA-UR- 99-5887

Approved for public release; distribution is unlimited.

Title: FLUID ASPECTS OF SOLAR WIND DISTURBANCES DRIVEN BY CORONAL MASS EJECTIONS

Author(s): John T. Gosling, NIS-1
Pete Riley, SAIC, San Diego, California

Submitted to: Journal of Geophysical Research

Los Alamos
NATIONAL LABORATORY

km s^{-1} in some of the faster events [e.g., *Gosling et al.*, 1976; *Hundhausen et al.*, 1994; *Sheeley et al.*, 1999]. Many CMEs have outward speeds and internal plasma and magnetic field pressures that are quite different from that of the ambient wind into which they are injected. Such CMEs produce transient disturbances in the solar wind that should propagate to the far reaches of the heliosphere.

Transient disturbances in the solar wind initiated by coronal eruptions have been modeled for many years, beginning with the self-similar analytical models of *Parker* [1961; 1963] and *Simon and Axford* [1966]. The first numerical computer code (one-dimensional, gas dynamic) to study disturbance propagation in the solar wind was developed in the late 1960s [*Hundhausen and Gentry*, 1969], and a variety of other codes ranging from simple one-dimensional gas dynamic codes through three-dimensional gas dynamic and magnetohydrodynamic codes have been developed in subsequent years. For the most part, these codes have been applied to the problem of disturbances driven by fast CMEs propagating into a structureless solar wind. *Pizzo* [1985] provided an excellent summary of the level of understanding achieved from such simulation studies through about 1984, and other reviews have subsequently become available [e.g., *Dryer*, 1994; *Pizzo*, 1997; *Riley*, 1999]. More recently, some attention has been focused on disturbances generated by slow CMEs [e.g., *Gosling and Riley*, 1996], on disturbances driven by CMEs having high internal pressures [e.g., *Gosling et al.*, 1994a; 1994b; 1998; *Riley and Gosling*, 1998], and disturbance propagation effects associated with a structured ambient solar wind [e.g., *Odstrcil et al.*, 1996; 1999a; 1999b; *Riley et al.*, 1997].

Our purpose here is to provide a brief tutorial on fluid aspects of solar wind disturbances derived from numerical gas dynamic simulations. For the most part we illustrate disturbance evolution by propagating idealized perturbations, mimicking different types of CMEs, into a structureless solar wind using a simple one-dimensional, adiabatic (except at shocks), gas dynamic code. The simulations begin outside the critical point where the solar wind becomes supersonic and thus do not address questions of how the CMEs themselves are initiated. Limited to one dimension (the radial direction), the simulation code predicts too strong an interaction between newly ejected solar material and the ambient wind because it neglects azimuthal and meridional motions of the plasma that help relieve pressure stresses. Moreover, the code ignores magnetic forces and thus also underestimates the speed with which pressure disturbances propagate in the wind. Despite these

"Page missing from available version"

plasma is compressed and accelerated as it encounters the forward shock and the faster wind is compressed and decelerated as it encounters the reverse shock. The vertical lines in Figure 1 bracket the last 30 hours of slow wind introduced at the inner boundary. This plasma parcel is compressed into an ever smaller volume as the forward shock passes through it. When the fast and slow plasmas have equal densities at the inner boundary, as in this example, momentum conservation dictates that a step function increase in speed produces nearly equal and opposite speed changes in the slow and fast wind. (The changes would be precisely equal and opposite were it not for the overall R^{-2} fall off in density, where R is heliocentric distance.) Essentially the same result is obtained if the speed increase at the inner boundary is more gradual than a step function, but the interaction develops more slowly and the shocks form farther from the Sun.

Figure 2 shows two superimposed snapshots illustrating the radial evolution of a disturbance initiated at the inner boundary in the opposite manner from that in Figure 1. In this case the steady state expansion produced an asymptotic flow speed at large distances of about 750 km s^{-1}. The disturbance was initiated by changing the speed at the inner boundary from 700 to 400 km s^{-1} in a step function decrease while holding the density and pressure constant there. A region of low pressure quickly forms at the interface between the two flows as the faster plasma runs away from the slower. This region of low pressure is commonly called a rarefaction (our preference) or an expansion wave. The slower plasma behind the interface is accelerated as it encounters the enhanced outward pressure gradient associated with the rarefaction, while the faster plasma ahead of the interface is decelerated by the reverse pressure gradient associated with the leading portion of the rarefaction. It is of interest that the rarefaction in Figure 2 expands much more quickly than does the compression in Figure 1 because it is superimposed upon diverging flows. With increasing heliocentric distance, the overall speed profile flattens as the rarefaction spreads into the surrounding plasma. Vertical lines in the figure bracket the first 30 hours of slow plasma introduced at the inner boundary. This parcel of plasma broadens as it moves out from the Sun and eventually all of the plasma within the parcel is accelerated to a higher speed as it encounters the low-pressure rarefaction. The greatest acceleration is experienced by the plasma at the leading edge of the parcel; however, the change in speed of the leading edge of the parcel remains less than half the original difference in speed between the fast and slow flows because of momentum conservation in a plasma whose overall density varies as R^{-2}. The spherical nature of the overall

"Page missing from available version"

sharing its momentum with both the leading and the trailing ambient wind via the compression and rarefaction waves, the CME slows considerably as it propagates out into the heliosphere. The simulation thus explains why CMEs with speeds considerably higher than that of the normal wind are only occasionally observed far from the Sun. Only those CMEs with exceptionally large inertia will not be slowed substantially as they interact with a slower ambient solar wind. Finally, although the simulated CME was not expanding at the inner boundary and has a radial width near 1.7 AU that is comparable to its width (0.22 AU) at the inner boundary, it does expand once the reverse wave has passed through its back edge. When the perturbation at the inner boundary is of shorter duration than in the present example, the reverse wave passes more quickly through the CME and expansion begins sooner. The simple simulation shown in Figure 3 is qualitatively consistent with near-ecliptic observations of many CME-driven solar wind disturbances, although reverse shocks are only rarely detected in these disturbances except possibly along their central axes [e.g., *Gosling et al.*, 1988] where the interaction is most nearly one-dimensional in nature.

Disturbances Produced by Slow CMEs

It is instructive to consider the inverse problem of a slow CME injected into a much faster surrounding solar wind such as might happen at high latitudes. Figure 4 shows two superimposed snapshots of calculated radial speed and pressure profiles of a solar wind disturbance produced in our one-dimensional simulation by introducing a very slow pulse into a faster ambient wind. Starting with the same steady state solution as in Figure 3, the disturbance is initiated at the inner boundary by dropping the flow speed from 350 to 200 km s^{-1} and then raising it back up to 350 km s^{-1} in a square wave pulse 15-hours long. Because of the speed gradient at the leading edge of the CME, a rarefaction quickly forms there that rapidly spreads forward into the ambient wind and back through the CME. Simultaneously a compression region, which is bounded by a forward-reverse shock pair, forms on the trailing edge of the CME as the faster trailing wind overtakes the CME. After 41 hours the forward shock and the trailing edge of the rarefaction have passed through one another in opposite directions such that the forward shock lies within the heart of the CME while the rarefaction extends nearly to its back edge. After 111 hours the rarefaction extends well behind the CME but still leads the reverse shock, while the

"Page missing from available version"

temperature of the plasma within a CME typically decrease with increasing heliocentric distance more rapidly than does that of the normal solar wind. Thus, at 1 AU CMEs in the solar wind often are characterized by anomalously low kinetic temperatures [e.g., *Gosling et al.*, 1973; 1987; *Montgomery et al.*, 1974; *Richardson and Cane*, 1995], and, at distances beyond about 3 AU, by unusually low plasma densities as well [*Gosling et al.*, 1998].

Several processes can contribute to the expansion of a CME. A CME can expand simply because it is injected into the solar wind with a substantial front-to-rear speed gradient. Another possibility is that expansion is a CME's response to a rarefaction wave produced by relative motion between the CME and the surrounding solar wind, as discussed above. Finally, a CME may expand because it has a higher internal pressure than that of the surrounding solar wind. The higher pressure can be a result of a higher density, a higher temperature, a stronger magnetic field, or some combination thereof. We have used the term "overexpansion" to describe CME events where a higher internal pressure contributes substantially to the expansion. The relative importance of these various expansion processes differs from event to event, depending on the physical character of the CME and on initial conditions within the surrounding solar wind.

Figure 5 show snapshots of solar wind speed and pressure as a function of heliocentric distance obtained in a simulation of an overexpanding CME. In this case the initial steady state boundary conditions produced a highly supersonic flow with a speed of 750 km s^{-1} at 6.0 AU and a density of 2.5 cm^{-3} at 1 AU, matching average high-latitude flow conditions observed by Ulysses on the declining phase of the last solar cycle [e.g., *Phillips et al.*, 1995]. The disturbance was initiated at the inner boundary by increasing the density (and hence also the pressure) by a factor of four in a bell-shaped pulse 10-hours long while simultaneously holding the temperature and speed constant. This mimics the injection of a dense CME into the heliosphere whose internal pressure is higher than that of the surrounding wind and whose speed is the same. The temporal duration of the initial pulse corresponds to a radial width of 0.17 AU at the inner boundary.

Because of its initial high internal pressure, the CME expands as it travels out from the Sun so that at 3.2 AU it has a radial width of 0.40 AU. The overall disturbance width at this distance is 0.67 AU since the expansion drives a forward compression wave into the ambient wind ahead and a reverse compression wave into the trailing wind. These pressure waves steepen into relatively weak shocks by the time they reach 3.2 AU. The expansion also produces a declining front-to-

"Page missing from available version"

was initiated by increasing the flow speed by a factor of two in a bell-shaped pulse, also 10-hours long, while holding the density and pressure constant. This disturbance evolves much the same as the one shown in Figure 3, although differences arise because of the shorter and more gradual nature of the initial perturbation at the inner boundary when compared to the example in Figure 3.

Finally, the disturbance shown at the right in Figure 6 was initiated by combining these perturbations in a single pulse. That is, the disturbance was initiated at the inner boundary by simultaneously increasing both the speed (by a factor of two) and the density (by a factor of four) in a bell-shaped pulse 10-hours long while holding the temperature constant. This input mimics the injection of a moderately fast, high pressure CME into a slower ambient solar wind. We note that the resulting disturbance near 1 AU includes only a single forward-reverse shock pair. Primarily because of the greater initial momentum of the CME in this simulation, the forward shock near 1 AU is considerably stronger than in the example shown in the middle of the figure, and the CME slows less rapidly as it travels out from the Sun. After 59.1 hours the CME is also broader than the disturbances in the other panels because both the trailing rarefaction and the initial over pressure contribute to the expansion. The reverse shock in this simulation is associated with expansion of the compression region on the leading edge of the CME. It is weakened and retarded considerably as it encounters the forward wave associated with CME overexpansion. The weaker forward expansion wave is nearly obliterated by that interaction. On the other hand, the reverse compression wave associated with overexpansion of the CME never really develops fully in this case because the CME runs away from the trailing plasma faster than the reverse wave can effectively expand back into it. Overall, the disturbance bears a greater resemblance to the example driven by a pure speed pulse (middle panel) than that driven by a pure pressure pulse (left panel). This simulation thus illustrates the dominant role that relative speed plays in the evolution of most CME-driven solar wind disturbances.

Figure 7 provides a somewhat similar comparison for the case of slow CMEs injected into a much faster ambient solar wind flow (asymptotic speed of 750 km s^{-1} in this case). The disturbance in the left panel was initiated by dropping the speed from 700 to 400 km s^{-1} at the inner boundary and then raising it back up to 700 km s^{-1} in a bell-shaped pulse 30-hours long. In this case the outer edges of the simulated CME have the same high speed as the ambient wind, while the central portion of the CME has a much lower speed. Because of the more gradual nature

"Page missing from available version"

Disturbance Propagation Effects Associated With Latitudinal Structure in the Ambient Solar Wind

The examples shown in Figures 1-7 illustrate most of the basic fluid effects underlying CME-driven disturbance evolution in the solar wind. They also illustrate the sensitivity of that evolution to initial conditions and provide considerable guidance for interpreting observations. Real solar wind disturbances are, of course, often more complex than those illustrated by these simple simulations. Because of spatial structure within the ambient solar wind and within the CMEs themselves, as well as the possibility of transverse flows, we can not hope to replicate all the details of these disturbances with one-dimensional simulations. Additional effects arise when one considers spatial inhomogenieties and allows for transverse flow in the simulations. Figure 8 provides an example of some of these effects [*Riley et al.*, 1997]. The figure shows the result of a two-dimensional fluid simulation of a CME propagating into a solar wind characterized by dense, slow radial flow from the equator to a latitude of 20° and by tenuous, fast radial flow above 20°. At large heliocentric distances the steady state flow prior to initiation of the disturbance was ~450 km s^{-1} at low latitudes and ~750 km s^{-1} at high latitudes. This approximates the average latitudinal structure observed by Ulysses during its first polar orbit about the Sun on the declining phase of solar cycle 22 [e.g., *Phillips et al.*, 1995]. It represents the limiting case of a three-dimensional model in which the ambient flow close to the Sun is structured into a band of low-speed wind above the magnetic equator and a considerably higher-speed wind at higher magnetic latitudes. In this case the tilt of the solar magnetic dipole relative to the rotation axis of the Sun is exactly zero so that there is no stream structure at low or high heliographic latitudes and thus corotating interaction regions (CIRs) do not form.

The disturbance shown in Figure 8 was initiated at 0.14 AU by introducing a fast, hot and dense bell-shaped pulse of 10-hour duration into the simulation. The pulse extended from the equator to 45° latitude, extending well across the boundary between the low and high-latitude flows. The speed of the plasma in the pulse at all latitudes was identical to that in the ambient wind at high latitudes and the maximum gas pressure within the pulse was 6 times greater than that which prevailed at both low and high latitudes in the ambient wind. The simulation thus mimics injection into the solar wind of a CME that initially has a speed equal to that of the ambient wind at high

"Page missing from available version"

velocities (50 km s^{-1}) within the disturbance.

The disturbance profiles produced in this two-dimensional simulation at high and low latitudes are similar to disturbance profiles observed in the ecliptic plane at 1 AU by IMP 8 and at S54° and 3.5 AU by Ulysses during a CME-driven disturbance in February 1994 [*Gosling et al.*, 1995]. Although the two-dimensional simulation introduces additional complexities and provides a global perspective not possible in the one-dimensional simulations, the basic nature of the disturbances at high and low latitudes is correctly inferred from the simpler one-dimensional simulations.

Disturbance Propagation in a More Realistic Three-Dimensional Geometry

The geometry of the ambient solar wind flow close to the Sun is probably never as simple as assumed in Figure 8. Stream structure and CIRs always are present to some degree in the solar wind at low heliographic latitudes. A more realistic, but still highly idealized, geometry is that which has been used to simulate three-dimensional aspects of CIRs [*Pizzo*, 1991; 1994; *Pizzo and Gosling*, 1994]. In those simulations it is assumed that a uniform band of slow, dense wind encircles the Sun at low heliographic latitudes, while uniform regions of fast, tenuous wind emanate from higher latitudes. Fast and slow flow regimes are separated by a relatively sharp transition and the slow flow band, centered on the solar magnetic equator, is tilted relative to the heliographic equator. Typical tilts range from about 10° to 30°, reflecting observed tilts of the solar magnetic dipole relative to the rotation axis of the Sun. Gas dynamic and MHD simulations using this type of geometry provide a credible approximation to the gross latitudinal structure of the solar wind observed by Ulysses on the declining phase of the most recent solar activity cycle [e.g., *Phillips et al.*, 1995], and successfully reproduce the observed three-dimensional structure of CIRs over a wide range of latitudes out to distances of at least 5 AU [*Pizzo and Gosling*, 1994].

In the three-dimensional simulation used to produce Figure 9 [*Odstrcil and Pizzo*, 1999a], the slow flow band was 30° wide and was centered on the magnetic equator which, in turn, was tilted 20° relative to the heliographic equator. Initial conditions at the inner boundary at 0.14 AU were chosen to be 600 (300) km s^{-1}, 125 (500) cm^{-3} and 2 (0.5) x 10^6 K in the fast (slow) wind. These produced an ambient background state with speed 718 (359) km s^{-1}, density 2.08 (8.45) cm^{-3}, and temperature 1.30 (0.33) x 10^5 K in the fast (slow) wind at 1 AU, which are close to

"Page missing from available version"

can be discerned in Figures 9 and 10 as regions where the density contours are most closely spaced. Shock strengths are greatest, and the entire structure narrowest, where the forward and reverse shocks, driven by the relative motion and expansion of the CME, merge with the CIR shocks into a single shock pair north of the equator. At those latitudes the CME becomes entrained within the CIR. At southern latitudes a relatively weak forward shock - the result of both relative motion between the CME and the ambient wind and the expansion of the CME - stands well off in front of the CME. At the highest southern latitudes of the CME the front does not appear to be a shock. A relatively weak reverse shock, the result of overexpansion of the CME, trails most of the southern portion of the CME.

This three-dimensional simulation, although highly idealized, graphically demonstrates the complexities that arise in a CME-driven disturbance propagating into a spatially structured solar wind (see also *Odstrcil and Pizzo* [1999b]). The CME becomes distorted in all dimensions and the shock strengths and stand-off distances (relative to the CME) are strong functions of position. Even when the CME itself is spatially uniform close to the Sun, the disturbance the CME produces in the solar wind is a strong function of latitude and longitude as well as heliocentric distance.

Concluding Comments

Our goal in this paper has been to provide a simple physical description of fluid aspects of the evolution of CME-driven disturbances in the solar wind. This evolution becomes ever more complex as one proceeds from idealized speed perturbations introduced into a structureless solar wind using a simple one-dimensional fluid code to compound pressure and speed perturbations introduced into a solar wind that is highly structured in all three dimensions using a three-dimensional fluid code. Although the two and three-dimensional simulations provide unique global perspectives of disturbance evolution and include effects that simply can not be explored with the one-dimensional simulations, most of the basic physical processes and effects in both types of simulations are most simply understood in the context of the one-dimensional simulations.

We note that even the three-dimensional simulations are highly idealized approximations to what nature actually provides. The ambient solar wind nearly always contains detailed structure beyond

"Page missing from available version"

evolution in the solar wind. Nevertheless, (1) the magnetic field increases the characteristic speed with which small amplitude pressure signals propagate in the wind, and (2) the magnetic pressure typically is comparable to, and can be greater than, the thermal pressure of the plasma, depending on the plasma beta (the ratio of plasma to magnetic field pressure). This indicates, for example, that solar wind disturbances spread more rapidly than is suggested by the fluid simulations, and overexpanding CMEs may actually be a result more of an enhanced magnetic pressure than an enhanced thermal pressure. We would not expect that either of these effects would seriously modify the conclusions drawn from the fluid simulations, although they would affect detailed comparisons of simulation results with observations.

In closing, we wish to emphasize that, even though the magnetic field usually plays a secondary role in disturbance evolution, it is a vital part of any CME-driven disturbance. Field line topology provides important clues for understanding CME origins in processes close to the Sun, and the strength and orientation of the field are crucial elements of a disturbance's interaction with the Earth's magnetosphere. Both the strength and orientation of the field are strongly affected by the evolution of CME-driven disturbances. The ambient field must drape about a fast CME as the CME pushes its way outward into the heliosphere, and the both the ambient field and that within the CME are enhanced as the plasma is compressed. Thus, a model that includes both fluid and magnetic field effects ultimately is needed for predicting space weather effects of these disturbances.

Acknowledgment. This paper is based on a tutorial presented at the SHINE workshop held in Boulder, Colorado in June, 1999. JTG thanks N. Crooker for travel support to the workshop. We thank D. Odstrcil and V. Pizzo for providing Figures 9 and 10 and J. Steinberg for comments on the manuscript. Work at Los Alamos was performed under the auspices of the U. S. Department of Energy with support from the National Aeronautics and Space Administration. Work at SAIC was performed with support from the National Aeronautics and Space Administration (Grant NASW-98007, SR&T program, and SEC-TP) and the National Science Foundation (Space Weather Program).

"Page missing from available version"

associated with transient disturbances in the solar wind at 1 AU, *J. Geophys. Res., 93*, 8741, 1988.

Gosling, J. T., S. J. Bame, D. J. McComas, J. L. Phillips, E. E. Scime, V. J. Pizzo, B. E. Goldstein, and A. Balogh, A forward-reverse shock pair in the solar wind driven by over expansion of a coronal mass ejection: Ulysses observations, *Geophys. Res. Lett., 21*, 237, 1994a.

Gosling, J. T., D. J. McComas, J. L. Phillips, L. A. Weiss, V. J. Pizzo, B. E. Goldstein, and R. J. Forsyth, A new class of forward-reverse shock pairs in the solar wind, *Geophys. Res. Lett., 21*, 2271, 1994b.

Gosling, J. T., D. J. McComas, J. L. Phillips, V. J. Pizzo, B. E. Goldstein, R. J. Forsyth, and R. P. Lepping, A CME-driven solar wind disturbance observed at both low and high heliographic latitudes, *Geophys. Res. Lett., 22*, 1753, 1995.

Gosling, J. T., P. Riley, D. J. McComas, and V. J. Pizzo, Overexpanding coronal mass ejections at high heliographic latitudes: Observations and simulations, *J. Geophys. Res., 103*, 1941, 1998.

Hundhausen, A. J., Some macroscopic properties of shock waves in the heliosphere, in *Collisionless Shocks in the Heliosphere: A Tutorial Review, Geophys. Monogr. Ser.*, vol. 34, edited by R. G. Stone and B. T. Tsurutani, pp 37-58, 1985.

Hundhausen, A. J., Coronal mass ejections, in *Cosmic Winds and the Heliosphere*, edited by J. R. Jokipii, C. P. Sonett, and M. S. Giampapa, University of Arizona Press, Tucson pp 259-296, 1997.

Hundhausen, A. J., and R. A. Gentry, Numerical simulation of flare-generated disturbances in the solar wind, *J. Geophys. Res., 74*, 2908, 1969.

"Page missing from available version"

Pizzo, V. J., The evolution of corotating stream fronts near the ecliptic plane in the inner solar system, 2. Three-dimensional tilted-dipole fronts, *J. Geophys. Res., 96*, 5405, 1991.

Pizzo, V. J., Global, quasi-steady dynamics of the distant solar wind, 1, Origins of north-south flows in the outer heliosphere, *J. Geophys. Res., 99*, 4173, 1994.

Pizzo, V. J., Global modeling of CME propagation in the solar wind, in *Coronal Mass Ejections, Geophys. Monogr. Ser.*, vol. 99, edited by N. Crooker, J. A. Joselyn, and J. Feynman, pp 261-267, 1997.

Pizzo, V. J., and J. T. Gosling, 3-D simulation of high-latitude interaction regions: Comparison with Ulysses results, *Geophys. Res. Lett., 21*, 2063, 1994.

Phillips, J. L., S. J. Bame, W. C. Feldman, B. E. Goldstein, J. T. Gosling, C. M. Hammond, D. J. McComas, M. Neugebauer, E. E. Scime, and S. T. Suess, Ulysses solar wind plasma observations at high southerly latitudes, *Science, 268*, 1030, 1995.

Richardson, I. G., and H. V. Cane, Regions of abnormally low proton temperature in the solar wind (1965-1991) and their association with ejecta, *J. Geophys. Res., 100*, 23,397, 1995.

Riley, P., CME dynamics in a structured solar wind, in *Solar Wind Nine*, edited by S. R. Habbal, R. Esser, J. V. Hollweg, and P. A. Isenberg, AIP Conf. Proc., 471, Woodbury, NY, pp 131-136, 1999.

Riley, P., and J. T. Gosling, Do coronal mass ejections implode?, *Geophys. Res. Lett., 25*, 1529, 1998.

Riley, P., J. T. Gosling, and V. J. Pizzo, A two-dimensional simulation of the radial and latitudinal evolution of a solar wind disturbance driven by a fast, high-pressure coronal mass

"Page missing from available version"

Figure Captions

Figure 1. Simulated solar wind speed and pressure versus heliocentric distance 83 and 250 hours after introducing a 300 km s^{-1} step function increase in speed at 0.14 AU. Vertical lines bound the last 30 hours of slow wind introduced into the simulation prior to the speed increase. Adapted from *Gosling and Riley* [1996].

Figure 2. Simulated solar wind speed and pressure versus heliocentric distance 83 and 250 hours after introducing a 300 km s^{-1} step function decrease in speed at 0.14 AU. Vertical lines bound the first 30 hours of slow wind introduced at the inner boundary. Adapted from *Gosling and Riley* [1996].

Figure 3. Simulated solar wind speed and pressure versus heliocentric distance for a solar wind disturbance initiated by a 15-hour long, 250 km s^{-1}, square wave increase in speed at 0.14 AU. The snapshots shown were obtained 27, 69 and 125 hours after onset of the perturbation. Vertical lines bound the material introduced at higher speed at the inner boundary, and thus mark the CME in the simulation. Adapted from *Gosling* [1999].

Figure 4. Simulated solar wind speed and pressure versus heliocentric distance for a solar wind disturbance initiated by a 15-hour long, 150 km s^{-1}, square wave decrease in speed at 0.14 AU. The snapshots shown were obtained 41 and 111 hours after onset of the perturbation. Vertical lines bound the material introduced at lower speed at the inner boundary, and thus mark the CME in the simulation. Adapted from *Gosling* [1999].

Figure 5. Simulated solar wind speed and pressure versus heliocentric distance for a solar wind disturbance initiated by a 10-hour long, factor of four, bell-shaped increase in density at 0.14 AU. The snapshots shown were obtained 55 and 194 hours after onset of the perturbation. Vertical lines bound the material within the density pulse, and thus identify the CME in the simulation. Adapted from *Gosling et al.* [1998].

"Page missing from available version"

equator. Plasma within the pulse, which lasted for 14 hours, had the same speed as the high-latitude wind and an internal pressure eight times greater than that within the ambient wind at both high and low latitudes. Right: Longitudinal slices of the disturbance at four different polar angles 12 days after its launch from 0.14 AU. The slices extend from 2.5 to 5 AU and cover azimuths from 50° to 130°. The initial disturbance was centered at an azimuth of 90°. The radial velocity is indicated by the gray scale and the density is indicated by contours. The injected material density, representing the CME, is normalized to 1 AU values and is color-coded. Adapted from *Odstrcil and Pizzo* [1999a].

Figure 10. Similar to Figure 9 except that this shows a meridional cut at the central longitude of the disturbance obtained 10 days after the initial perturbation at 0.14 AU. The cut extends from 1 to 5 AU and covers polar angles from 30° to 150°. Adapted from *Odstrcil and Pizzo* [1999b].

"Page missing from available version"

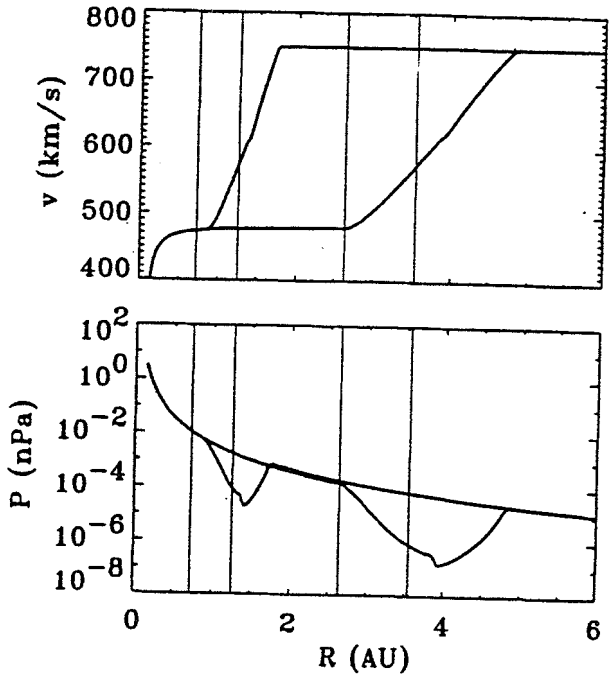

Figure 2

"Page missing from available version"

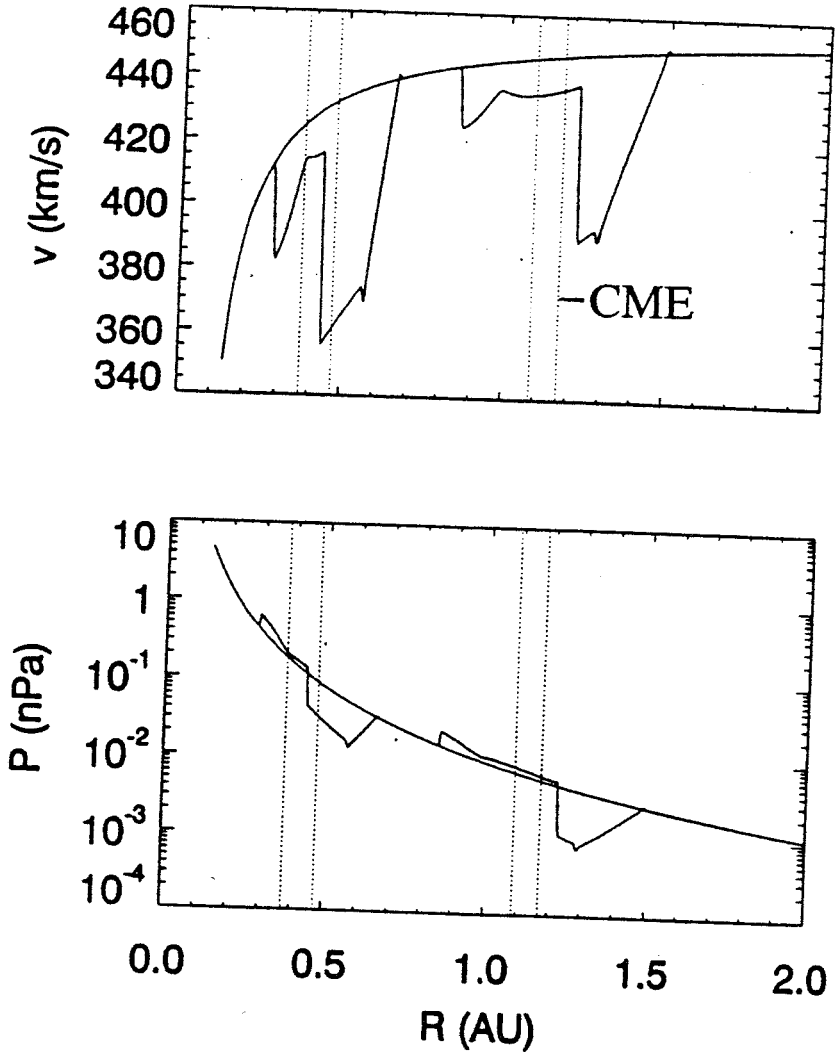
460
440
420
400
380
360
340
v (km/s)
CME
10
1
10^-1
10^-2
10^-3
10^-4
P (nPa)
0.0
0.5
1.0
1.5
2.0
R (AU)

Figure 4

"Page missing from available version"

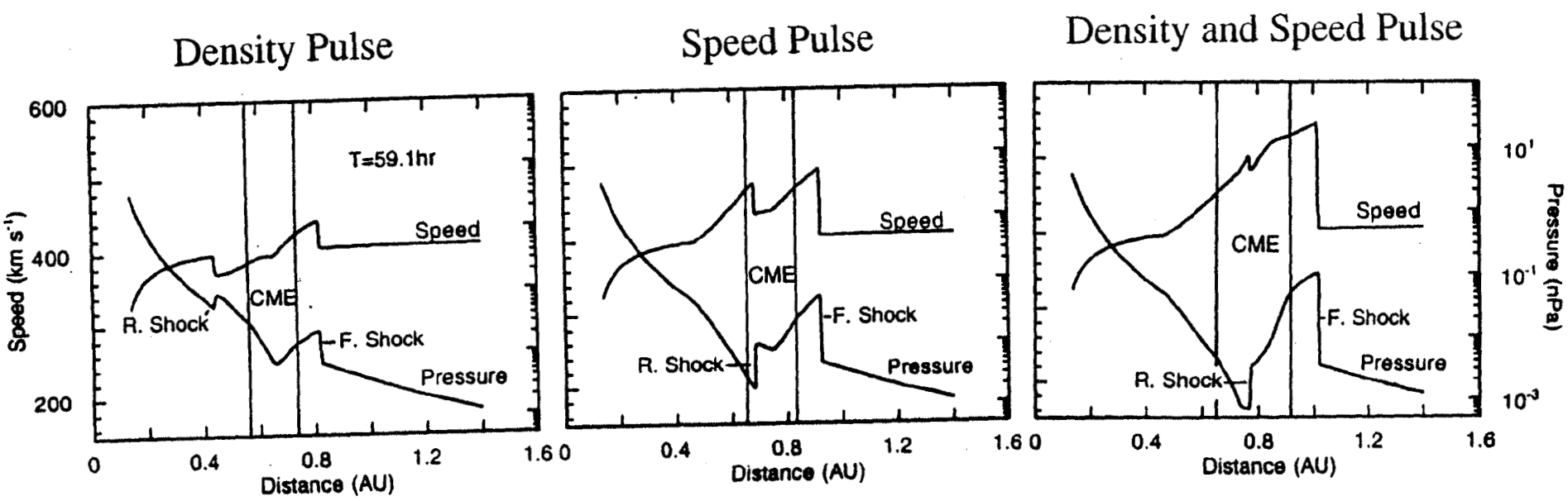
Density Pulse
Speed Pulse
Density and Speed Pulse
600
400
200
Speed (km s⁻¹)
T=59.1hr
Speed
CME
R. Shock
F. Shock
Pressure
0
0.4
0.8
1.2
1.6
Distance (AU)
10¹
10⁻¹
10⁻³
Pressure (nPa)

Figure 6

"Page missing from available version"

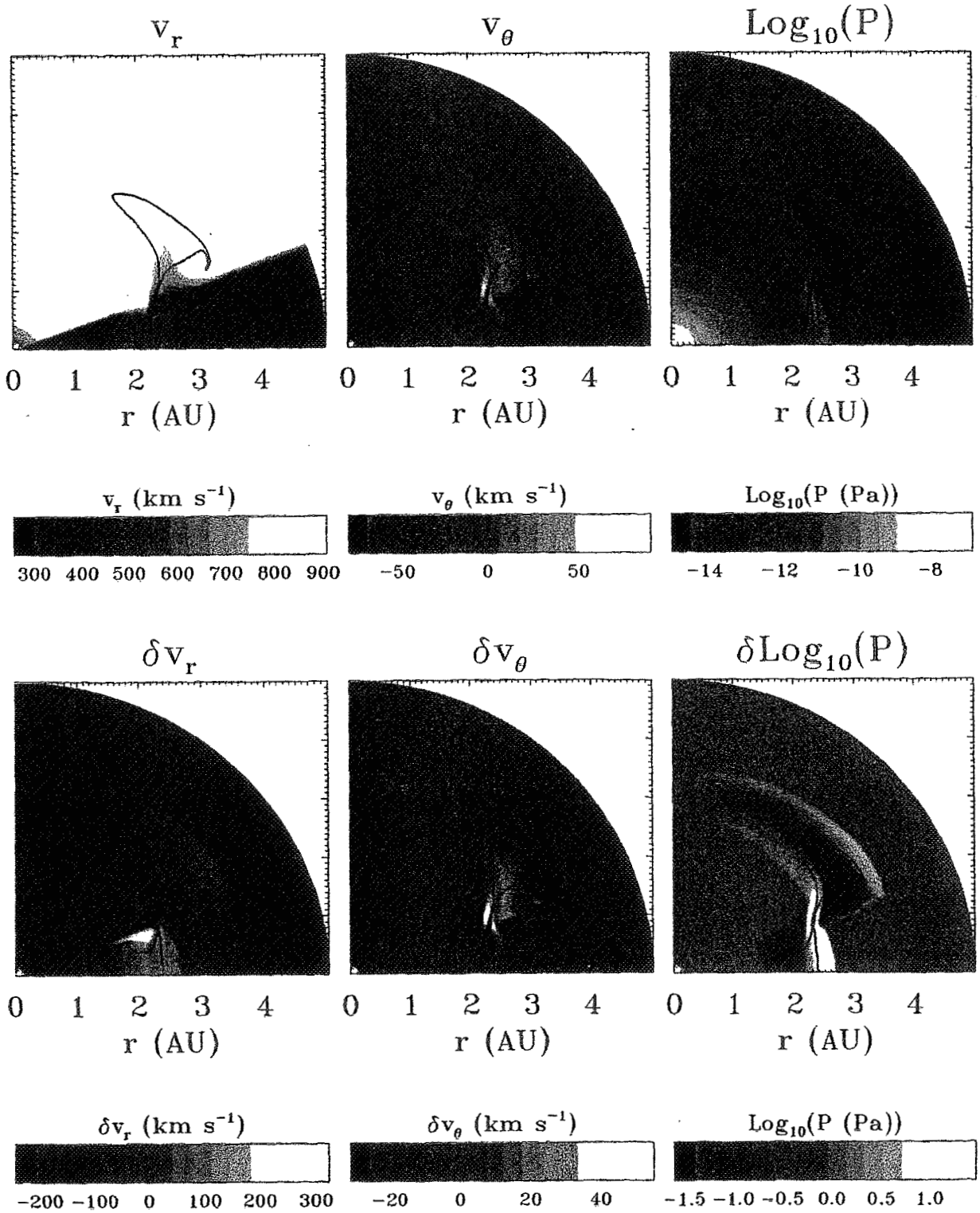
v_r
v_θ
$Log_{10}(P)$
0 1 2 3 4
r (AU)
v_r (km s^{-1})
300 400 500 600 700 800 900
v_θ (km s^{-1})
−50 0 50
Log_{10}(P (Pa))
−14 −12 −10 −8
δv_r
δv_θ
$\delta Log_{10}(P)$
δv_r (km s^{-1})
−200 −100 0 100 200 300
δv_θ (km s^{-1})
−20 0 20 40
Log_{10}(P (Pa))
−1.5 −1.0 −0.5 0.0 0.5 1.0

Figure 8

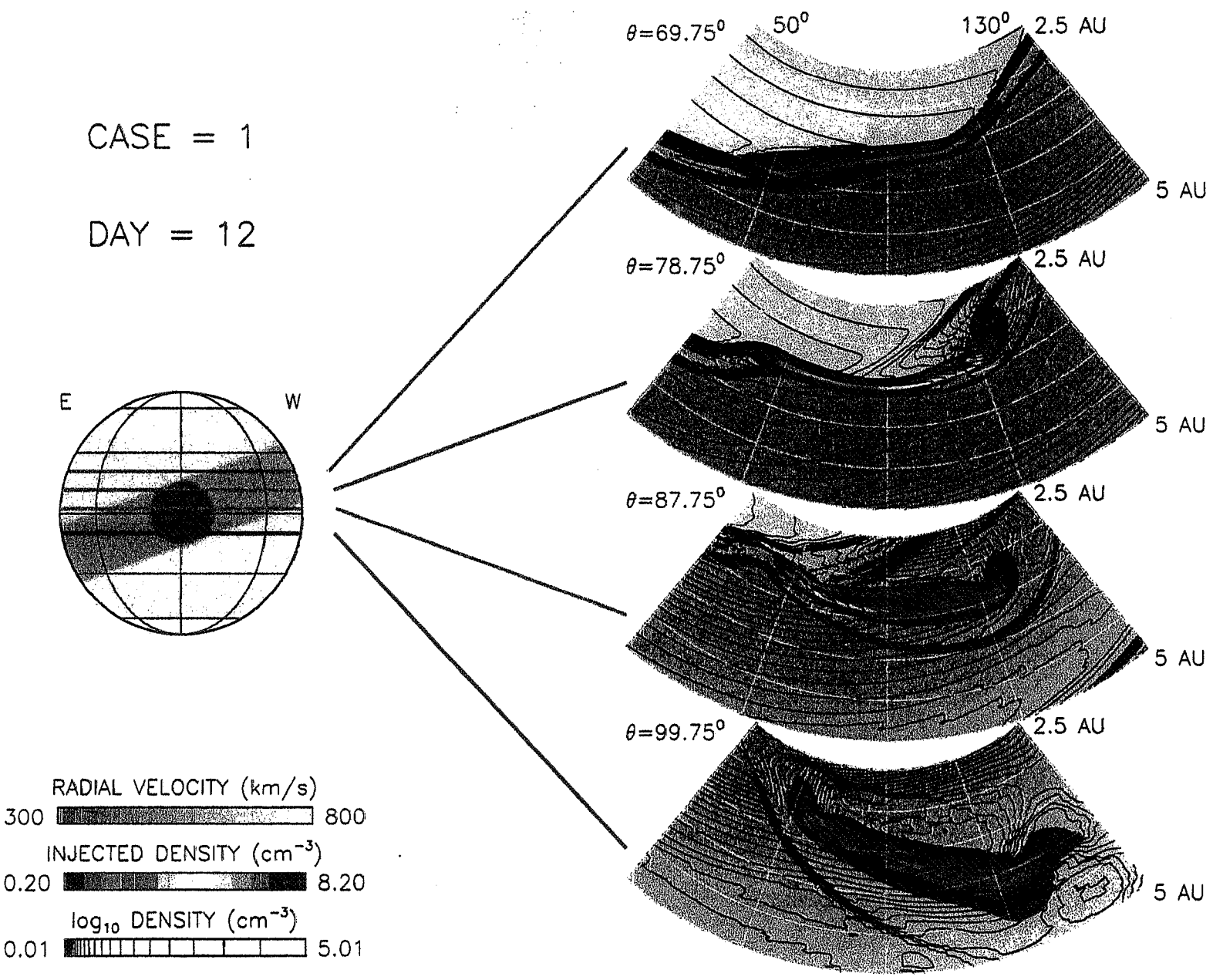
CASE = 1
DAY = 12
E
W
θ=69.75°
50°
130°
2.5 AU
5 AU
θ=78.75°
2.5 AU
5 AU
θ=87.75°
2.5 AU
5 AU
θ=99.75°
2.5 AU
5 AU
RADIAL VELOCITY (km/s)
300
800
INJECTED DENSITY (cm⁻³)
0.20
8.20
log10 DENSITY (cm⁻³)
0.01
5.01

Figure 9

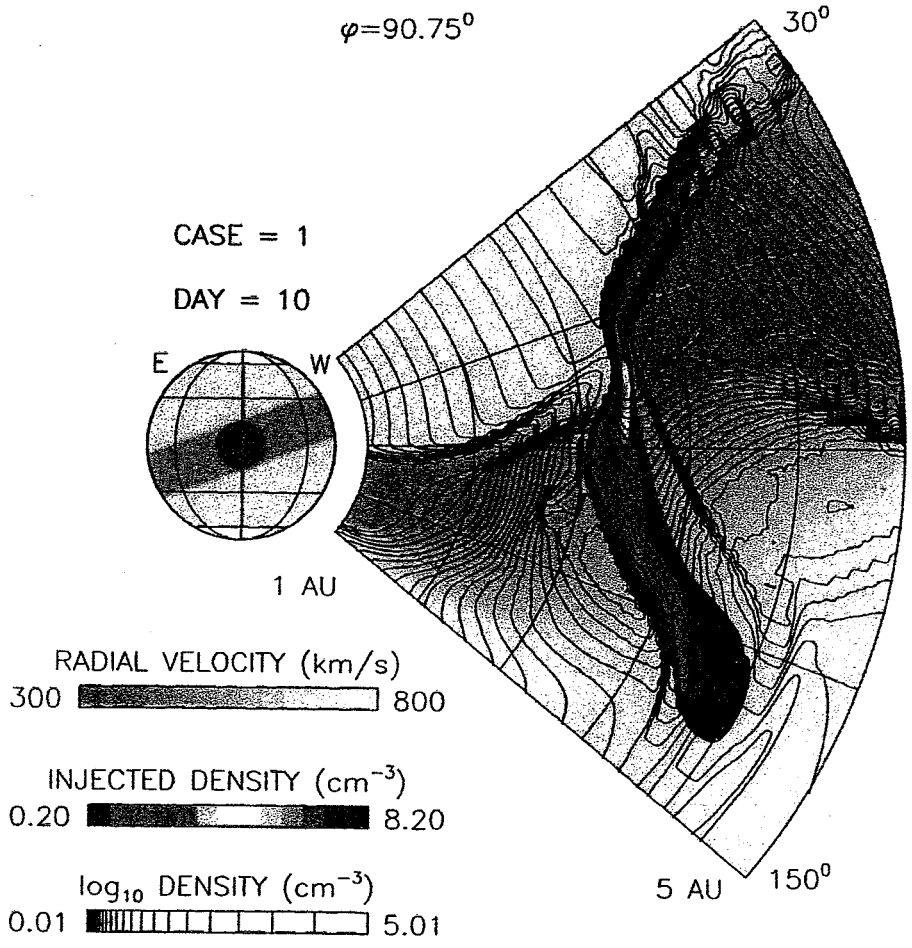
φ=90.75°
30°
CASE = 1
DAY = 10
E
W
1 AU
5 AU
150°
RADIAL VELOCITY (km/s)
300
800
INJECTED DENSITY (cm⁻³)
0.20
8.20
log₁₀ DENSITY (cm⁻³)
0.01
5.01

Figure 10

Appendix 4

Investigation of the polytropic relationship between density and temperature within interplanetary coronal mass ejections using numerical simulations

Pete Riley, J. T. Gosling, and V. J. Pizzo

in press, *Journal of Geophysical Research*, January, 2001.

Investigation of the polytropic relationship between density and temperature within interplanetary coronal mass ejections using numerical simulations

Pete Riley

Science Applications International Corporation, San Diego, California

J. T. Gosling

Los Alamos National Laboratory, Los Alamos, New Mexico

V. J. Pizzo

Space Environment Center, NOAA, Boulder, Colorado

Abstract.

Single-point spacecraft measurements within coronal mass ejections (CMEs) often exhibit a negative correlation between electron density and temperature. At least two opposing interpretations have been suggested for this relationship. If, on one hand, these single spacecraft observations provide direct measures of the polytropic properties of the plasma, then they imply that the polytropic index for the electrons γ_e is often < 1. Moreover, since the electrons carry the bulk of the pressure (via their significantly higher temperature), this further implies that the dynamics of CME evolution are dominated by an effective polytropic index $\gamma_{eff} < 1$. On the other hand, $\gamma < 1$ implies that as the ejecta propagate away from the Sun and expand, they also heat up; a result clearly at odds with in situ observations. In contrast to these CME intervals, many studies have shown that the quiescent solar wind exhibits a positive correlation between electron density and temperature, suggesting that $\gamma_e > 1$. In this study we simulate the evolution of a variety of CME-like disturbances in the solar wind using a one-dimensional, single-fluid model, to address the interpretation of the relationship between electron density and temperature within CMEs at fixed locations in space. Although we strictly impose a polytropic relationship (with γ = constant) throughout our simulations, we demonstrate that a variety of correlations can exist between density and temperature at fixed points. Furthermore, we demonstrate that the presence of only local uncorrelated random fluctuations in density and temperature can produce a negative correlation. Consequently, we conclude that these single-point observations of negative correlations between electron density and temperature cannot be used to infer the value of γ_e. Instead, we suggest that entropy variations, together with the plasma's tendency to achieve pressure balance with its surroundings, are responsible for the observed profiles.

1. Introduction

A number of studies have demonstrated that a negative correlation often exists between electron density n_e and temperature T_e within magnetic clouds [e.g., *Osherovich et al.,* 1993a, b] and, more generally, coronal mass ejections (CMEs) in the solar wind [e.g., *Hammond et al.,* 1996]. In particular, *Osherovich et al.*

[1993a] found that, on average, the slope of a logarithmic plot of T_e versus n_e equaled $\sim 1/2$ within magnetic clouds. These results may be contrasted with studies of the quiescent solar wind at different heliocentric distances for which a positive correlation is found [e.g., *Sittler and Scudder,* 1980; *Pilipp et al.,* 1990; *Phillips et al.,* 1993, 1995].

The relationship between temperature and density in a plasma has important ramifications for hydrodynamic and MHD models of space plasmas and particularly models of CME evolution in the solar wind, since most models do not explicitly include energy conservation in their description of the fluid [e.g., *Riley,* 1999]. Instead, the (magneto-) fluid equations are closed by assuming a polytropic relationship between pressure and density. In this case the energy transport equation reduces to

$$\frac{\partial}{\partial t}\left(\frac{P}{n^\gamma}\right) + v \cdot \nabla\left(\frac{P}{n^\gamma}\right) = 0, \qquad (1)$$

where P is the thermal pressure, n is the number density, γ is the polytropic index, and v is the bulk velocity of the plasma. Combining this with the equation for an ideal gas, $P = nK_BT$, leads to

$$\frac{D}{Dt}\left(\frac{T}{n^{\gamma-1}}\right) = 0, \qquad (2)$$

where K_B is the Boltzmann constant, T is the temperature of the plasma, and we have replaced the temporal (Eulerian) and spatial derivatives with the total (Lagrangian) derivative (D/Dt). Thus along any streamline,

$$log(T) = (\gamma - 1)log(n) + log(S), \qquad (3)$$

where the constant S is the thermodynamic entropy of the plasma. If (3) holds, then the slope of a logarithmic plot of T versus n should yield a straight line with a slope equal to $(\gamma - 1)$ and an intercept related to the entropy of the plasma.

Osherovich and colleagues [e.g., *Osherovich et al.,* 1993a, b, 1995; *Fainberg et al.,* 1996; *Osherovich et al.,* 1998, 1999] have argued that (3) holds for single-point spacecraft measurements within magnetic clouds in the solar wind. Although strictly the relationship holds only along a given streamline, they contend that because of the assumed axisymmetry implicit in their model, together with the assumption of infinite conductivity, the entropy term must be constant throughout the magnetic cloud. Furthermore, they reason that the entropy term cannot vary significantly during the passage of the magnetic cloud, for otherwise there would

not be a unique linear relationship between $\log(T)$ and $\log(n)$ as is commonly observed.

Osherovich et al. [1993a] derived an analytic theory for the evolution of self-similar, axisymmetric, radially-expanding, magnetic flux ropes and applied the model to magnetic clouds in the solar wind. Their solution, however, required $\gamma < 1$ to produce the observed expansions of clouds. On the other hand, *Vandas et al.* [1996] modeled the evolution of force-free objects within an ambient solar wind flow using three-dimensional MHD simulations and showed that good agreement could be found between the simulation results and Osherovich et al.'s analytic theory without the requirement that $\gamma < 1$ in the simulations.

Osherovich and Burlaga [1997] analyzed several magnetic clouds, as well as the sheath region that surrounded them and the ambient solar wind. They found that the application of (3) to each region yielded electron polytropic indices of 0.4-0.5 (for the magnetic cloud), 0.7-0.8 (for the sheath region), and 1.2 (for the ambient solar wind). From this, *Osherovich and Burlaga* [1997, p. 157] concluded that "single-fluid MHD models can approximate any one of these states, but not all three."

Other studies, however, have disputed the polytropic interpretation of the $n_e - T_e$ relationship within magnetic clouds and, more generally CMEs. *Hammond et al.* [1996] studied the relationship between core electron temperature and density and found a similar negative correlation for five CMEs that were observed by the Ulysses spacecraft during its in-ecliptic journey from Earth to Jupiter. They also found that a negative correlation existed during CME (but not cloud-like) intervals, when axisymmetry was probably not a good assumption. They suggested that the core $n_e - T_e$ profile was not the result of a polytropic relationship, but that it derives from differences in the collision histories of the electrons, that is, denser plasma cools more quickly than less dense plasma [*Phillips and Gosling,* 1990].

Gosling [1999] has also argued against the inference that the polytropic index is < 1 within CMEs. He reasoned that if $\gamma_e < 1$, then the temperature within CMEs must increase as they propagate away from the Sun, a result that is clearly at odds with both solar observations and in situ CME observations at different heliocentric distances. He suggested that the observed relationship occurs primarily because of the plasma's tendency to reach local pressure balance.

Skoug et al. [2000] studied a single CME observed by both ACE and Ulysses at widely different heliocentric distances. They showed that while the slope derived

from each spacecraft individually was indeed negative, the least squares fit for the combined ACE-Ulysses data set was positive ($\gamma_e = 1.4$).

In contrast to the properties of the electron population within magnetic clouds, proton density and temperature often display a positive correlation. *Osherovich et al.* [1993a], for example, found that $\gamma_p = 1.1-1.3$ in the analysis of several magnetic clouds. However, Osherovich et al. have argued that since T_e/T_p is typically 6 to 7 within magnetic clouds (reaching ~ 10 near the magnetic cloud axis), the pressure gradient term in the momentum equation is dominated by the electron contribution. Thus the evolution of the magnetic cloud is governed principally by the properties of the electrons, with the protons playing a relatively minor role.

Using the relationship between density and temperature, derived from measurements at different heliocentric distances, to determine the polytropic relationship of electrons and protons in the quiescent solar wind appears to be on firmer ground. *Gosling* [1999] reviewed many of these studies. Here we remark only that most studies found values in the range $\gamma_p = 1.4 - 1.6$ and $\gamma_e = 1.1 - 1.6$. Suffice to say that $\gamma > 1$ for both electrons and protons in the normal solar wind. *Newbury et al.* [1997] also found a positive correlation between proton density and temperature in the vicinity of stream interfaces but cautioned that care must be taken to isolate solar wind originating from different coronal source regions. In particular, they presented an event for which a negative correlation was found between density and temperature when data both preceding and following a stream interface were plotted collectively. On the other hand, when the data were separated into two sets (an interval preceding the interface and an interval following it), each displayed a positive correlation. *Skoug et al.* [2000] also identified intervals within the ACE and Ulysses data sets that were not associated with CMEs yet also displayed a negative correlation. Indeed, negative correlations of electron density and temperature are common everywhere in the solar wind [e.g., *Phillips and Gosling,* 1990].

In this study we use numerical simulations to investigate the relationship between fluid density and temperature for a variety of perturbations, some of which have been shown previously to mimic the propagation and evolution of CMEs through the solar wind. This is a particularly appropriate avenue of investigation in view of the argument made that single-fluid simulations relying on a single $\gamma > 1$ are not applicable for modeling CME evolution in the solar wind [*Osherovich and*

Burlaga, 1997]. We reduce the modeling to its simplest terms; we consider a single-fluid, spherically symmetric system and neglect magnetic fields. We demonstrate that, in spite of these simplifications, we can generate a variety of relationships between density and temperature, depending on the launch profiles of the plasma. Since our fluid algorithm strictly enforces γ = constant throughout the simulation domain, we conclude that any departure in the slope from $(\gamma - 1)$ does not indicate a change in the polytropic index of the gas. We also demonstrate that, in addition to the large-scale perturbations mimicking CMEs, random fluctuations in density and temperature can also produce negative n-T correlations. Thus we conclude that single-point measurements of density and temperature during limited intervals are often not good indicators of γ.

2. Simulation Technique

To mimic the evolution of transient disturbances and, in particular, CME-driven disturbances in the solar wind, we employ an Eulerian finite difference code [*Stone and Norman,* 1992]. The energy transport equation is reduced to (1), and the polytropic index γ is set to a constant value. For the simulations presented here, $\gamma = 3/2$ (although selected runs were also made with $\gamma = 5/3$ with no substantial differences). The code has been previously applied to modeling CME disturbances in one and two dimensions [e.g., *Gosling and Riley,* 1996; *Riley et al.,* 1997; *Gosling et al.,* 1998; *Riley and Gosling,* 1998]. Since our goal is to investigate the relationship between n and T at fixed locations in space for a variety of perturbations and not to reproduce the details of CME evolution in the solar wind, we make a number of simplifying assumptions. First, we neglect the magnetic field. Thus our simulations are strictly only valid for high-β perturbations [*Riley et al.,* 1997; *Riley and Gosling,* 1998]. Second, we restrict our analysis to a spherically symmetric (one-dimensional) geometry. As such, the interactions between adjacent parcels of plasma are probably too strong, since velocity shear transverse to the radial direction is not permitted. A practical benefit of these assumptions is that the simulations are computationally fast. Thus we can explore the evolution of many types of perturbations. In total, > 200 launch profiles were simulated and analyzed for this study. In the interests of brevity, only a handful of representative cases are discussed.

For all the simulations an ambient solar wind is first established and then a perturbation is introduced at the inner boundary. To produce an ambient solar wind, we specify the speed, density, and temperature at the in-

ner boundary of the simulation (30 R_{Sun}). We enforce inflow boundary conditions at the inner boundary and outflow boundary conditions at the outer boundary (6 AU). The simulation region is filled with approximately correct values and allowed to reach an equilibrium state. Values of $n = 128$ cm^{-3}, $v = 702$ km s^{-1}, and $T = 10^6$ K at the inner boundary yielded the equilibrium flow profiles summarized in Figure 1 and match well with Ulysses observations at high heliographic latitudes. In the present study the particular values of the ambient wind used are largely immaterial; we could have chosen values more indicative of the slow solar wind. This would only have had the effect of increasing the time taken to complete a particular simulation without affecting our conclusions.

Figure 1

Introducing a time-dependent perturbation can, in principle, mimic the launch of a CME through the inner boundary of the simulation. We considered variations in the following parameters: (1) the shape of the pulse (square- and bell-shaped); (2) the duration of the pulse (10, 30, and 50 hours); (3) the height of the pulse ($\times 4$, $\times 10$, and $\times 30$ above or below ambient values); and (4) which parameters were perturbed (density, temperature, and/or speed). In addition, for some cases, the speed was linearly increased or decreased during the perturbation interval. Some of these profiles have been previously shown to compare favorably with observed CME-driven disturbances in the solar wind [e.g., *Gosling and Riley,* 1996; *Riley et al.,* 1997; *Gosling et al.,* 1998], while others have no obvious counterpart in solar wind data sets that we have studied. Nevertheless, they allow us to explore how a broad range of perturbations evolve as they propagate through the solar wind and, in particular, how density and temperature are related at fixed locations in space. Finally, in addition to these large-scale perturbations, we also modeled smaller-scale random fluctuations in density and temperature.

3. Results

We have chosen seven examples from the set of simulations to support the main conclusion of this study, namely, that in spite of the fact that γ = constant in the model, a variety of relationships between density and temperature can be observed at fixed heliocentric distances. The first five examples consist of large-scale perturbations, while the last two examples consist of smaller-scale random fluctuations in density and temperature. They are summarized in Figure 2.

Figure 2

The perturbation for our first case study is summarized in Figure 2a. It consisted of a bell-shaped increase

in speed of 300 km s^{-1} above the ambient speed in concert with a $\times 4$ enhancement in both density and temperature. Thus the gas pressure peaked at $\times 16$ above background values. The perturbation lasted for 50 hours. These variations approximate the launch of a fast, dense, hot CME propagating through a slower, more tenuous, and cooler ambient solar wind. Figure 3 shows the resulting solar wind disturbances at 102 and 208 hours following its launch. The two pairs of vertical lines in each panel mark the boundary of the pulse. The development and evolution of this type of disturbance is well known and discussed elsewhere [e.g., *Hundhausen and Gentry,* 1969; *Riley et al.,* 1997]. Our interest here lies in the variation of temperature and density at fixed points in space, since this is how single-spacecraft measurements are made. In Figure 4 we plot temperature against density logarithmically at 3 AU. The cross marks the ambient solar wind, which, at a particular heliocentric distance has a single value. The small dots identify disturbed solar wind, while the larger dots identify the ejecta. (The boundaries of the ejecta were tracked using test particles in the simulations.) The dots are equally spaced in time, thus larger separations suggest larger temporal (logarithmic) gradients in density and/or temperature. Inspection of Figure 3 reveals the temporal sense of the curve in Figure 4: Moving from right to left in Figure 3, we note that the corresponding variations in Figure 4 are from ambient solar wind (the cross) to the sheath region of the disturbance (small dots, from the lower left to top center and then to the upper right) to ejecta (large dots, from upper right to lower left) and finally back to ambient solar wind flow. The solid straight line is a least squares fit to the ejecta portion and has a numerical value of 0.450. If this slope were indicative of the polytropic index of the gas, we would infer a value of $\gamma = 1.45$. This is similar, but not identical, to the imposed model value of 1.5.

The perturbation used for our second example is summarized in Figure 2b. Both the speed and temperature were held constant, while the density (and hence pressure) was increased smoothly by a factor of 4 and then returned to its equilibrium value over a period of 30 hours. This type of pulse was used to successfully model a new class of CMEs observed at high heliographic latitudes by the Ulysses spacecraft [*Gosling et al.,* 1994]. Figure 5 summarizes the plasma density and temperature variations at 1 and 3 AU. The disturbance consists of an ejecta bounded by forward and reverse shocks. The ejecta and sheath regions are now much more symmetric with respect to the temporal midpoint of the ejecta (where the temperature is a minimum). Note

F3

F4

F5

that the slope within the ejecta changes from predominantly negative at 1 AU to predominantly positive at 3 AU. The least squares fit to the results of Figure 5a lead to a slope of - 0.402, whereas the fit to Figure 5b leads to a slope of 2.033. The sheath region in both panels (dots) maintains a slope of ~ 0.5.

For our third example we consider a perturbation in speed only. The initial profile of the pulse is shown in Figure 2c. The speed was decreased by 300 km s^{-1} over an interval of 30 hours and then returned to its initial value while maintaining constant density and temperature. Since density and temperature do not change, thermodynamic entropy also remains constant. *Gosling and Riley* [1996] discussed this type of pulse in relation to the acceleration of CMEs in the high-speed solar wind. In Figure 6 we again compare density and temperature at 1 and 3 AU from the Sun. A least squares fit to the points within the ejecta gives $+0.589$ and -0.385, respectively. Note, once again, that the compressed region at both locations gives a slope of ~ 0.5. Moreover, the straight-line portion of the sheath region (extending from the ambient solar wind point (cross) to the lower left corner of each panel) occurs in the region trailing the CME and corresponds to a rarefaction [see also *Gosling and Riley,* 1996, Figure 3]. Figures 6a and 6b also suggest that the value of the slope may be a function of heliocentric distance. In fact, inspection of plots at other heliocentric distances (not shown) confirms that the ejecta profile evolves from a predominantly positive slope near the Sun to a predominantly negative slope at larger heliocentric distances.

F6

The perturbation for our fourth example is shown in Figure 2d. This profile consisted of a smooth decrease in density (by a factor of 4) with a corresponding increase in temperature (so as to maintain constant pressure), over a period of 10 hours, while maintaining constant speed. We are not aware of any specific event for which this perturbation is intended to mimic. Nevertheless, it would correspond to the expulsion of a hot, tenuous transient that was initially in thermal pressure balance. Figure 7 displays the relationship between temperature and density at 3 AU. The least squares fit to the ejecta portion of the data gives a slope of -1.003. Again, the slope of the sheath region equals 1/2.

F7

As our fifth example we consider a perturbation in density and temperature, such that the entropy of gas remains constant (Figure 2e). From (3) we have that the thermodynamic entropy, $S = T/n^{(\gamma-1)}$, which for $\gamma = 3/2$ becomes $S = T/n^{1/2}$. Thus a pulse consisting of a peak density enhancement of $\times 4$ must be accompanied by a corresponding peak temperature increase of

$\times 2$ to maintain constant entropy. The peak pressure is then $\times 8$ above ambient values. The resulting relationship between density and temperature at 3 AU is shown in Figure 8. The least squares fit to the ejecta gives a slope of 0.490. Note that although this perturbation is qualitatively similar to our second example (compare Figures 2b and 2e), the resulting temperature-density relationship is significantly different (compare Figures 5 and 8).

The perturbations for our final two examples are shown in Figures 2f and 2g. Both consisted of random fluctuations in density and temperature. In the latter case, however, these fluctuations were embedded within an ambient solar wind consisting of the same type of fluctuations. Figure 9 displays $\log(T)$ versus $\log(n)$ at 0.13 AU and 3 AU for the perturbations shown in Figure 2f. At 0.13 AU the "ejecta" (or, in this case, the interval initially containing all the fluctuations) consists of a random distribution of points. However, by 3 AU, these points all fall close to a least squares fit line with slope -0.908. On the other hand, the perturbations that have propagated outside the initial boundaries of the ejecta tend to lie along a line with a positive gradient. In Figure 10, $\log(T)$ is plotted against $\log(n)$ at 0.13 and 3 AU for the fluctuations summarized in Figure 2g. In this case the ejecta interval is no different from the ambient wind and is distinguishable, only because we track the "boundaries" at $t = 0$ hours and $t = 10$ hours. The point we wish to draw attention to is that while the points were initially randomly distributed in $\log(T)$-$\log(n)$ space, by 3 AU the presence of circular patterns indicates that a degree of coherence has developed as neighboring parcels of plasma strive to reach pressure equilibrium with one another.

F8

F9

F10

4. Summary and Discussion

In this report we have shown that one-dimensional, hydrodynamic simulations mimicking the evolution of CME-like disturbances in the solar wind are capable of producing a variety of temperature-density relationships. In fact, even random fluctuations in density and temperature are capable of reproducing the negative correlations often observed within CMEs. Since we strictly impose a polytropic relationship with $\gamma =$ constant throughout our simulation domain, we conclude that a negative correlation between density and temperature cannot be used to infer the value of γ at a fixed location in space.

Our examples suggest that the negative correlations are driven by variations in the thermodynamic entropy of the plasma. Our fifth example (Figures 2e and 8)

shows that when the entropy of the perturbed gas remains the same as that of the ambient solar wind, the temperature-density relationship may be a fair indicator of the polytropic index of the gas. In apparent contradiction our third example (Figures 2c and 6) also appears to maintain constant entropy (since it contains no variations in density or temperature) and yet does not yield a slope of 0.5. The concept of entropy we have been using, however, is strictly only applicable to individual parcels of plasma as they propagate away from the Sun and evolve. A more realistic definition of entropy at a particular location in space, such as the inner boundary of our simulations, must also take into account the speed of the plasma. Thus we suggest that entropy flux ($S \times v$) must be conserved for temperature-density relationships to be able to provide a meaningful value of the polytropic index. It is also worth remarking that as a shock propagates through a medium, it increases the entropy of the gas. Thus, in addition to the results discussed in this paper, the concept of deriving a polytropic index from temperature-density profiles clearly cannot be applied to plasma that has been processed by the passage of a shock, such as in the sheath regions of magnetic clouds/CMEs.

Our simulations support the idea suggested by *Gosling* [1999] that the negative correlation is the result of structure within the CMEs and pressure balance. However, other effects may play a role. It is possible, for example, that kinetic effects of the electrons drive the observed negative correlation, such as proposed by *Hammond et al.* [1996], which are not included in the fluid simulations.

In closing, we reiterate that our simulations demonstrate that a negative correlation between density and temperature can exist for a variety of launch profiles, in spite of the fact that we strictly impose $\gamma =$ constant in our model. We suggest that the observed relationships are driven by entropy variations and the plasma's desire to establish pressure balance with its surroundings. In contrast to the conclusions reached by *Osherovich and Burlaga* [1997], we have shown that single-fluid models can reproduce the types of observed temperature-density variations in CMEs, sheath regions, and ambient solar wind, without resorting to nonphysical arguments requiring $\gamma < 1$.

Acknowledgments. P.R. gratefully acknowledges the support of the National Aeronautics and Space Administration (grant NASW-98007 and Space Physics Theory Program contract NAS5-96081). Work by J.T.G. was performed under the auspices of the U.S. Department of Energy with support from NASA and the Ulysses project. Work by V.J.P. was performed at NOAA Space Environment Cen-

ter and supported by NASA grants.

Janet G. Luhmann thanks Robert Forsyth, Martin A. Lee, and another referee for their assistance in evaluating this paper.

References

Fainberg, J., V. A. Osherovich, R. G. Stone, and R. J. MacDowall, Ulysses observations of electron and proton components in a magnetic cloud and related wave activity, in *Solar Wind Eight, Am. Inst. Phys. Conf. Proc. 382,* edited by D. Winterhalter et al., p. 554, College Park, Md., 1996.

Gosling, J. T., On the determination of electron polytrope indices within coronal mass ejections in the solar wind, *J. Geophys. Res., 104,* 19,851, 1999.

Gosling, J. T., and P. Riley, The acceleration of slow coronal mass ejections in the high-speed solar wind, *Geophys. Res. Lett., 23,* 2867, 1996.

Gosling, J. T., D. J. McComas, J. L. Phillips, L. A. Weiss, V. J. Pizzo, B. E. Goldstein, and R. J. Forsyth, A new class of forward-reverse shock pairs in the solar wind, *Geophys. Res. Lett., 21,* 2271, 1994.

Gosling, J. T., P. Riley, D. J. McComas, and V. J. Pizzo, Overexpanding coronal mass ejections at high heliographic latitudes: Observations and simulations, *J. Geophys. Res., 103,* 1941, 1998.

Hammond, C. M., J. L. Phillips, G. K. Crawford, and A. Balogh, The relationship between electron density and temperature inside coronal mass ejections, in *Solar Wind Eight, Am. Inst. Phys. Conf. Proc. 382,* edited by D. Winterhalter et al., p. 558, College Park, Md., 1996.

Hundhausen, A. J., and R. A. Gentry, Numerical simulations of flare-generated disturbances in the solar wind, *J. Geophys. Res., 74,* 2908, 1969.

Newbury, J. A., C. T. Russell, and G. M. Lindsay, Solar wind polytropic index in the vicinity of stream interactions, *Geophys. Res. Lett., 24,* 1431, 1997.

Osherovich, V. A., and L. F. Burlaga, Magnetic clouds, in *Coronal Mass Ejections: Causes and Consequences, Geophys. Monogr. Ser.,* vol. 99, edited by N. Crooker, J. A. Joselyn, and J. Feynman, p. 157, A64, Washington, D.C., 1997.

Osherovich, V. A., C. J. Farrugia, L. F., Burlaga, R. L. Lepping, J. Fainberg, and R. G. Stone, Polytropic relationship in interplanetary magnetic clouds, *J. Geophys. Res., 98,* 15,331, 1993a.

Osherovich, V. A., C. J. Farrugia, and L. F. Burlaga, Dynamics of aging magnetic clouds, *Adv. Space Res., 13*(6), 57, 1993b.

Osherovich, V. A., C. J. Farrugia, and L. F. Burlaga, Nonlinear evolution of magnetic flux ropes, 2, Finite beta plasma, *J. Geophys. Res., 100,* 12,307, 1995.

Osherovich, V. A., C. J. Farrugia, R. G. Stone, R. Fitzenreiter, and A. F. Vinas, Measurement of polytropic index in the January 10-11, 1997 magnetic cloud observed by WIND, *Geophys. Res. Lett., 25,* 3003, 1998.

Osherovich, V. A., C. J. Farrugia, and R. G. Stone, Multitube model for interplanetary magnetic clouds, *Geophys. Res. Lett., 26,* 401, 1999.

Phillips, J. L., and J. T. Gosling, Radial evolution of solar wind thermal electron distributions due to expansion and

collisions, *J. Geophys. Res., 95,* 4217, 1990.
Phillips, J. L., S. J. Bame, J. T. Gosling, D. J. McComas, B. E. Goldstein, and A. Balogh, Solar wind thermal electrons from 1.15 to 5.34 AU: Ulysses observations, *Adv. Space Res., 13*(6), 47, 1993.
Phillips, J. L., W. C. Feldman, J. T. Gosling, and E. E. Scime, Solar wind plasma electron parameters based on aligned observations by ICE and Ulysses, *Adv. Space Res., 16*(9), 95, 1995.
Pilipp, W. G., H. Miggenrieder, K.-H. Muhlhauser, H. Rosenbauer, and R. Schwenn, Large-scale variations of thermal electron parameters in the solar wind between 0.3 and 1 AU, *J. Geophys. Res., 95,* 6305, 1990.
Riley, P., CME dynamics in a structured solar wind, in *Solar Wind 9,* edited by S. R. Habbal, et al., p. 131, Am. Inst. of Phys., College Park, Md., 1999.
Riley, P., and J. T. Gosling, Do coronal mass ejections implode in the solar wind?, *Geophys. Res. Lett., 25,* 1529, 1998.
Riley, P., J. T. Gosling, and V. J. Pizzo, A two-dimensional simulation of the radial and latitudinal evolution of a solar wind disturbance driven by a fast, high-pressure coronal mass ejection, *J. Geophys. Res., 102,* 14,677, 1997.
Sittler, E. C., and J. D. Scudder, An empirical polytrope law for solar wind thermal electrons between 0.45 and 4.76 AU: Voyager 2 and Mariner 10, *J. Geophys. Res., 85,* 5131, 1980.
Skoug, R. M., W. C. Feldman, J. T. Gosling, and D. J. McComas, Solar wind electron characteristics inside and outside coronal mass ejections, *J. Geophys. Res., 105,* 23,069, 2000.
Stone, J. M., and M. L. Norman, ZEUS-2D: A radiation magnetohydrodynamics code for astrophysical flows in two dimensions, I, The hydrodynamic algorithms and tests, *Astrophys. J., 80,* 753, 1992.
Vandas, M., S. Fischer, M. Dryer, Z. Smith, and T. Detman, Parametric study of loop-like magnetic cloud propagation, *J. Geophys. Res., 101,* 15,645, 1996.

J. T. Gosling, Los Alamos National Laboratory, Los Alamos, NM 87545. (jgosling@lanl.gov; dmccomas@lanl.gov)

V. J. Pizzo, NOAA/SEC, Code R/E/SE 325 South Broadway, Boulder, CO 80303. (vpizzo@sec.noaa.gov)

P. Riley, Science Applications International Corporation, San Diego, CA 92121. (uk2@haven.saic.com)

(Received July 14, 2000; revised November 28, 2000; accepted November 28, 2000.)

Paper number 2000JA000276.
0148-0227/01/2000JA000276$09.00

Figure 1. Solar wind equilibrium solution. Speed v, number density n, and gas pressure P are plotted against heliocentric distance R.

Figure 1. Solar wind equilibrium solution. Speed v, number density n, and gas pressure P are plotted against heliocentric distance R.

Figure 2. Seven perturbations introduced at the inner boundary of the equilibrium solution summarized in Figure 1. Speed v, number density n, and gas pressure P are plotted against time t. (a) Combined bell-shaped density, temperature, and speed enhancement lasting 50 hours. (b) Bell-shaped density enhancement lasting 30 hours. (c) Box-shaped speed decrease lasting 30 hours. (d) Bell-shaped density decrease and corresponding temperature enhancement (to maintain constant pressure) lasting 10 hours. (e) Bell-shaped density enhancement and corresponding temperature enhancement (to maintain constant entropy) lasting 10 hours. (f) Random fluctuations in density and temperature over an interval of 10 hours. (g) Random fluctuations in density and temperature embedded within an ambient solar wind also consisting of the same fluctuations.

Figure 2. Seven perturbations introduced at the inner boundary of the equilibrium solution summarized in Figure 1. Speed v, number density n, and gas pressure P are plotted against time t. (a) Combined bell-shaped density, temperature, and speed enhancement lasting 50 hours. (b) Bell-shaped density enhancement lasting 30 hours. (c) Box-shaped speed decrease lasting 30 hours. (d) Bell-shaped density decrease and corresponding temperature enhancement (to maintain constant pressure) lasting 10 hours. (e) Bell-shaped density enhancement and corresponding temperature enhancement (to maintain constant entropy) lasting 10 hours. (f) Random fluctuations in density and temperature over an interval of 10 hours. (g) Random fluctuations in density and temperature embedded within an ambient solar wind also consisting of the same fluctuations.

Figure 3. Simulated speed v, number density n, and gas pressure P versus heliocentric distance R at 102 and 208 hours following the launch of the pulse summarized in Figure 2a. The boundary of the pulse (i.e., ejecta) is marked by the two pairs of vertical lines.

Figure 3. Simulated speed v, number density n, and gas pressure P versus heliocentric distance R at 102 and 208 hours following the launch of the pulse summarized in Figure 2a. The boundary of the pulse (i.e., ejecta) is marked by the two pairs of vertical lines.

Figure 4. Logarithmic plot of temperature T versus number density n at 3 AU for the pulse profile summarized in Figure 2a. The ambient solar wind is marked by a single cross. Large (small) dots indicate the ejecta (sheath) region. The straight line is a least squares fit to the ejecta interval.

Figure 4. Logarithmic plot of temperature T versus number density n at 3 AU for the pulse profile summarized in Figure 2a. The ambient solar wind is marked by a single cross. Large (small) dots indicate the ejecta (sheath) region. The straight line is a least squares fit to the ejecta interval.

Figure 5. Same parameters displayed as in Figure 4, but for the pulse profile summarized in Figure 2b, showing results at (a) 1 AU and (b) 3 AU.

Figure 5. Same parameters displayed as in Figure 4, but for the pulse profile summarized in Figure 2b, showing results at (a) 1 AU and (b) 3 AU.

Figure 6. Same parameters displayed as in Figure 4, but for the pulse profile summarized in Figure 2c, showing results at (a) 1 AU and (b) 3 AU.

Figure 6. Same parameters displayed as in Figure 4, but for the pulse profile summarized in Figure 2c, showing results at (a) 1 AU and (b) 3 AU.

Figure 7. Same parameters displayed as in Figure 4, but for the pulse profile summarized in Figure 2d at 3 AU.

Figure 7. Same parameters displayed as in Figure 4, but for the pulse profile summarized in Figure 2d at 3 AU.

Figure 8. Same parameters displayed as in Figure 4, but for the pulse profile summarized in Figure 2e at 3 AU.

Figure 8. Same parameters displayed as in Figure 4, but for the pulse profile summarized in Figure 2e at 3 AU.

Figure 9. Same parameters displayed as in Figure 4, but for the pulse profile summarized in Figure 2f at (a) 0.13 AU and (b) 3 AU.

Figure 9. Same parameters displayed as in Figure 4, but for the pulse profile summarized in Figure 2f at (a) 0.13 AU and (b) 3 AU.

Figure 10. Same parameters displayed as in Figure 4, but for the pulse profile summarized in Figure 2g at (a) 0.13 AU and (b) 3 AU.

Figure 10. Same parameters displayed as in Figure 4, but for the pulse profile summarized in Figure 2g at (a) 0.13 AU and (b) 3 AU.

Supplemental Abstract for *JGR–Space Physics* Manuscripts

2000JA000276

Single-point spacecraft measurements within coronal mass ejections (CMEs) often exhibit a negative correlation between electron density and temperature. At least two opposing interpretations have been suggested for this relationship. If, on one hand, these single spacecraft observations provide direct measures of the polytropic properties of the plasma, then they imply that the polytropic index for the electrons γ_e is often < 1. Moreover, since the electrons carry the bulk of the pressure (via their significantly higher temperature), this further implies that the dynamics of CME evolution are dominated by an effective polytropic index $\gamma_{eff} < 1$. On the other hand, $\gamma < 1$ implies that as the ejecta propagate away from the Sun and expand, they also heat up; a result clearly at odds with in situ observations. In contrast to these CME intervals, many studies have shown that the quiescent solar wind exhibits a positive correlation between electron density and temperature, suggesting that $\gamma_e > 1$. In this study we simulate the evolution of a variety of CME-like disturbances in the solar wind using a one-dimensional, single-fluid model, to address the interpretation of the relationship between electron density and temperature within CMEs at fixed locations in space. Although we strictly impose a polytropic relationship (with γ = constant) throughout our simulations, we demonstrate that a variety of correlations can exist between density and temperature at fixed points. Furthermore, we demonstrate that the presence of only local uncorrelated random fluctuations in density and temperature can produce a negative correlation. Consequently, we conclude that these single-point observations of negative correlations between electron density and temperature cannot be used to infer the value of γ_e. Instead, we suggest that entropy variations, together with the plasma's tendency to achieve pressure balance with its surroundings, are responsible for the observed profiles.

RILEY ET AL.: DENSITY-TEMPERATURE CORRELATION IN CMES

RILEY ET AL.: DENSITY-TEMPERATURE CORRELATION IN CMES

RILEY ET AL.: DENSITY-TEMPERATURE CORRELATION IN CMES

RILEY ET AL.: DENSITY-TEMPERATURE CORRELATION IN CMES

RILEY ET AL.: DENSITY-TEMPERATURE CORRELATION IN CMES

RILEY ET AL.: DENSITY-TEMPERATURE CORRELATION IN CMES

RILEY ET AL.: DENSITY-TEMPERATURE CORRELATION IN CMES

RILEY ET AL.: DENSITY-TEMPERATURE CORRELATION IN CMES

RILEY ET AL.: DENSITY-TEMPERATURE CORRELATION IN CMES

RILEY ET AL.: DENSITY-TEMPERATURE CORRELATION IN CMES

RILEY ET AL.: DENSITY-TEMPERATURE CORRELATION IN CMES

RILEY ET AL.: DENSITY-TEMPERATURE CORRELATION IN CMES

RILEY ET AL.: DENSITY-TEMPERATURE CORRELATION IN CMES

RILEY ET AL.: DENSITY-TEMPERATURE CORRELATION IN CMES

RILEY ET AL.: DENSITY-TEMPERATURE CORRELATION IN CMES

RILEY ET AL.: DENSITY-TEMPERATURE CORRELATION IN CMES

RILEY ET AL.: DENSITY-TEMPERATURE CORRELATION IN CMES

RILEY ET AL.: DENSITY-TEMPERATURE CORRELATION IN CMES

RILEY ET AL.: DENSITY-TEMPERATURE CORRELATION IN CMES

RILEY ET AL.: DENSITY-TEMPERATURE CORRELATION IN CMES

RILEY ET AL.: DENSITY-TEMPERATURE CORRELATION IN CMES

RILEY ET AL.: DENSITY-TEMPERATURE CORRELATION IN CMES

RILEY ET AL.: DENSITY-TEMPERATURE CORRELATION IN CMES

RILEY ET AL.: DENSITY-TEMPERATURE CORRELATION IN CMES

RILEY ET AL.: DENSITY-TEMPERATURE CORRELATION IN CMES

RILEY ET AL.: DENSITY-TEMPERATURE CORRELATION IN CMES

RILEY ET AL.: DENSITY-TEMPERATURE CORRELATION IN CMES

RILEY ET AL.: DENSITY-TEMPERATURE CORRELATION IN CMES

RILEY ET AL.: DENSITY-TEMPERATURE CORRELATION IN CMES

RILEY ET AL.: DENSITY-TEMPERATURE CORRELATION IN CMES

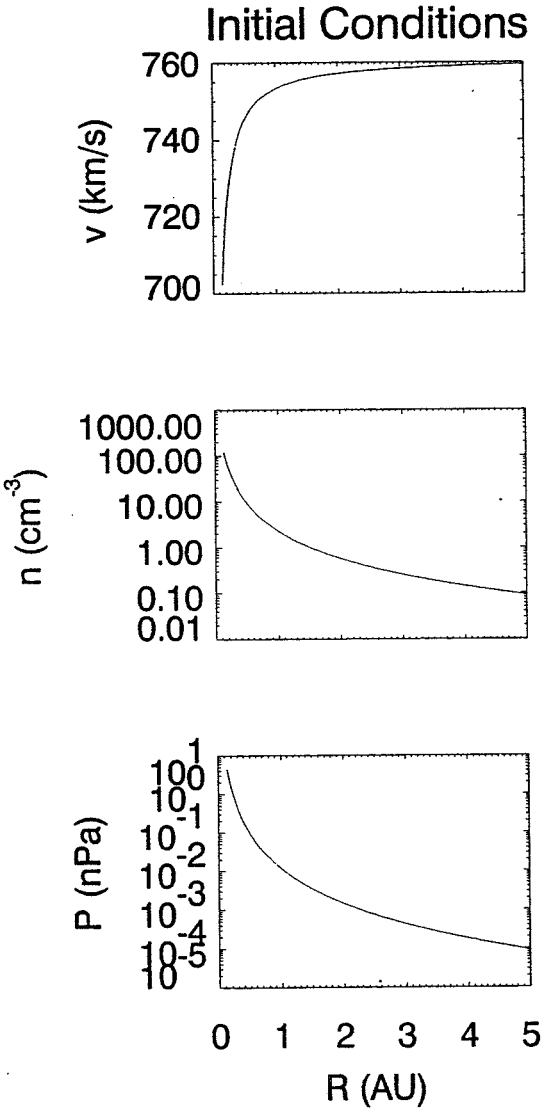
Initial Conditions
v (km/s)
760
740
720
700
n (cm-3)
1000.00
100.00
10.00
1.00
0.10
0.01
P (nPa)
1
10-1
10-2
10-3
10-4
10-5
0 1 2 3 4 5
R (AU)

Figure 1

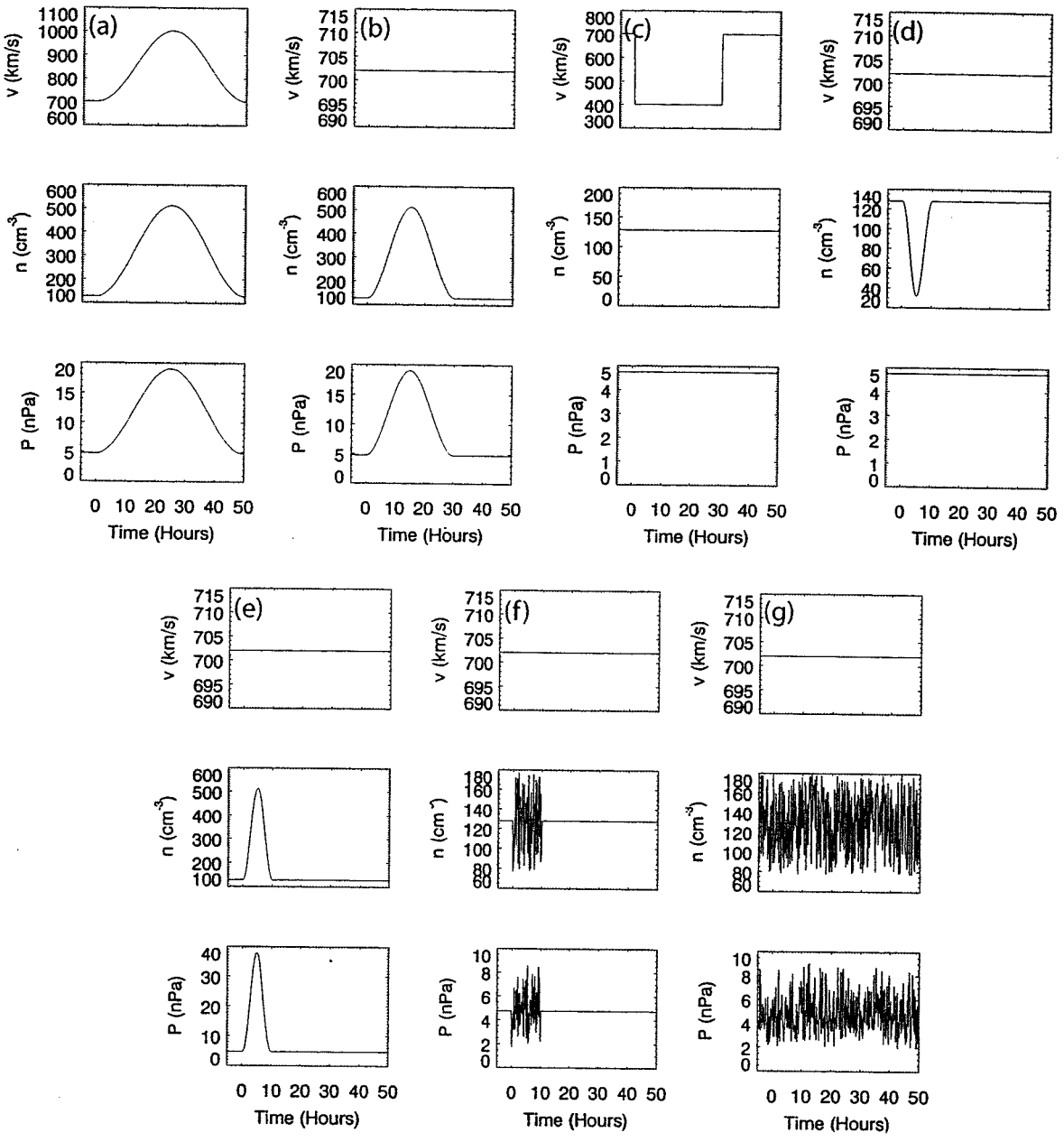

Figure 2

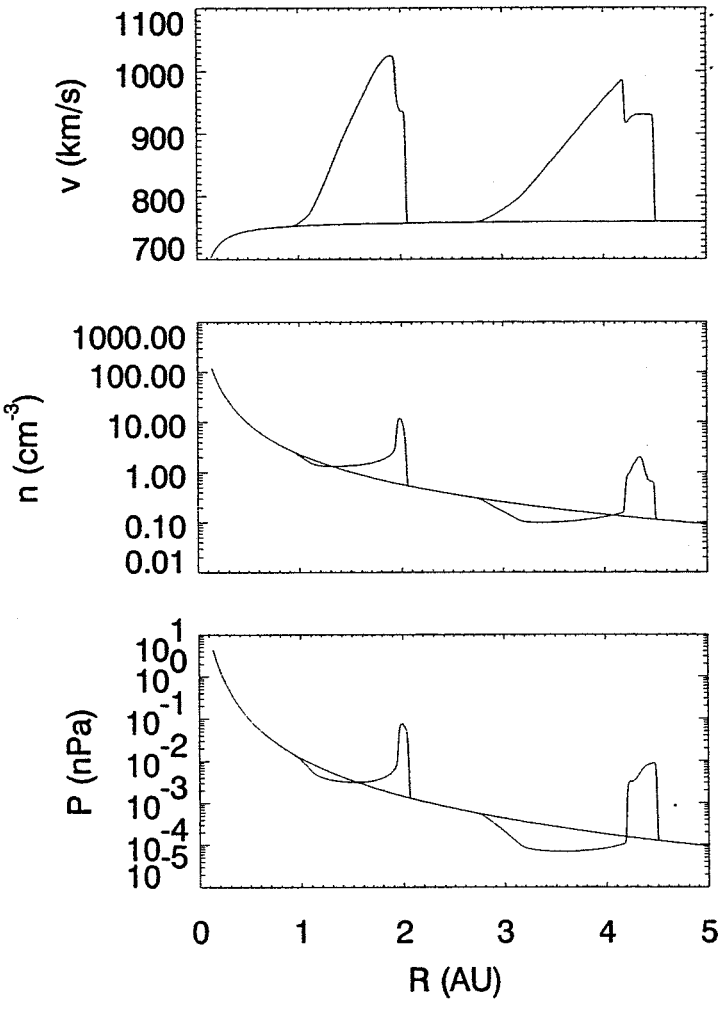
1100
1000
900
800
700
v (km/s)
1000.00
100.00
10.00
1.00
0.10
0.01
n (cm-3)
P (nPa)
0
1
2
3
4
5
R (AU)

Figure 3

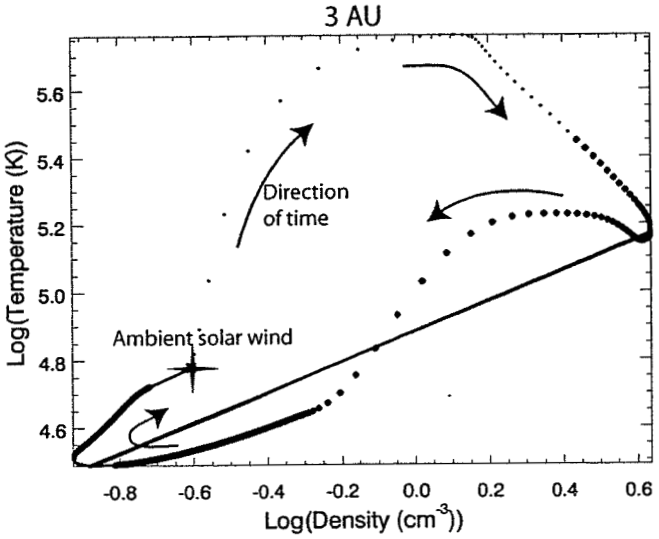
3 AU
Direction
of time
Ambient solar wind
Log(Temperature (K))
5.6
5.4
5.2
5.0
4.8
4.6
-0.8
-0.6
-0.4
-0.2
0.0
0.2
0.4
0.6
Log(Density (cm^{-3}))

Figure 4

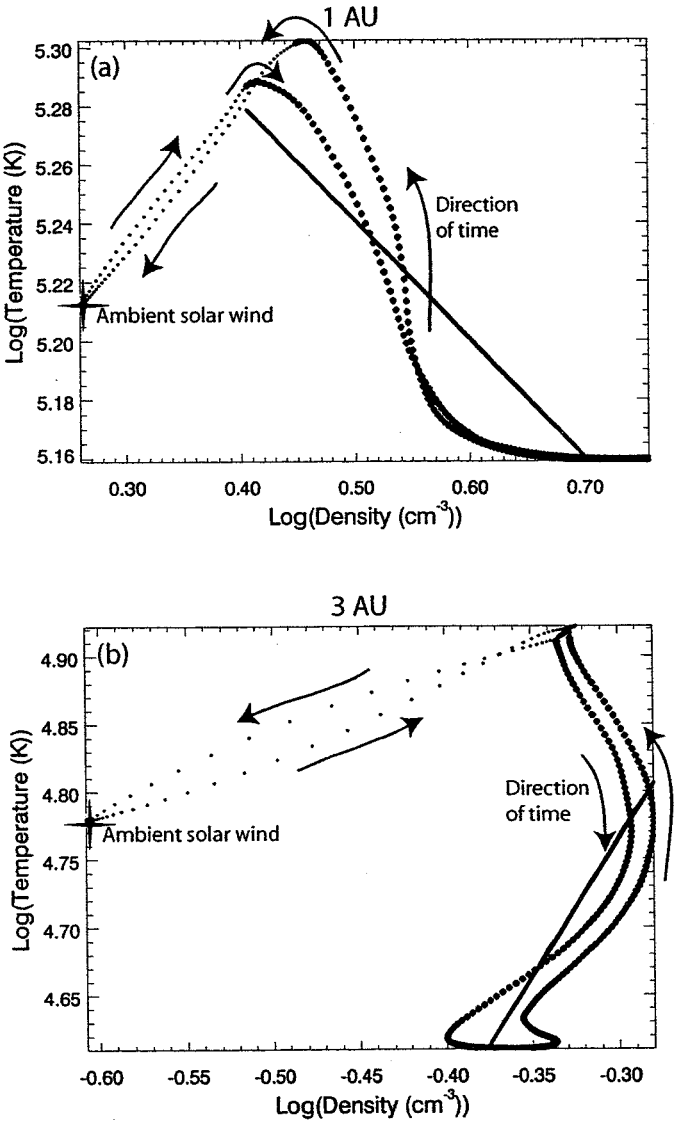
1 AU
(a)
Direction
of time
Ambient solar wind
Log(Temperature (K))
Log(Density (cm^{-3}))
5.30
5.28
5.26
5.24
5.22
5.20
5.18
5.16
0.30
0.40
0.50
0.60
0.70
3 AU
(b)
Direction
of time
Ambient solar wind
Log(Temperature (K))
Log(Density (cm^{-3}))
4.90
4.85
4.80
4.75
4.70
4.65
-0.60
-0.55
-0.50
-0.45
-0.40
-0.35
-0.30

Figure 5

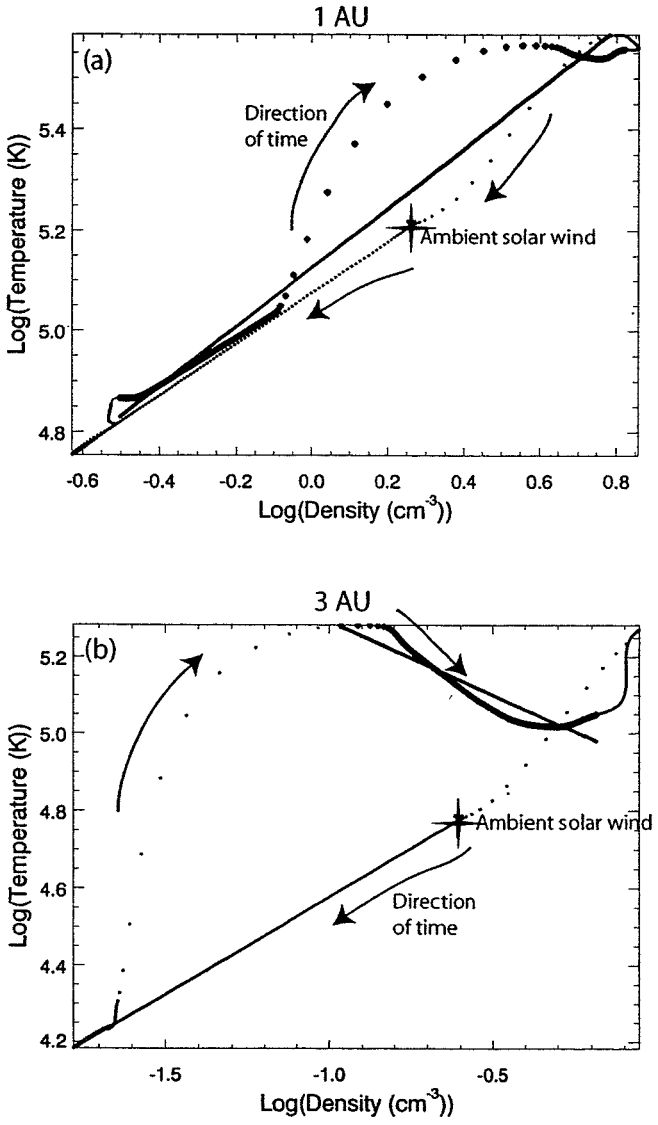
1 AU
(a)
Direction
of time
Ambient solar wind
Log(Temperature (K))
5.4
5.2
5.0
4.8
-0.6
-0.4
-0.2
0.0
0.2
0.4
0.6
0.8
Log(Density (cm^{-3}))
3 AU
(b)
Ambient solar wind
Direction
of time
Log(Temperature (K))
5.2
5.0
4.8
4.6
4.4
4.2
-1.5
-1.0
-0.5
Log(Density (cm^{-3}))

Figure 6

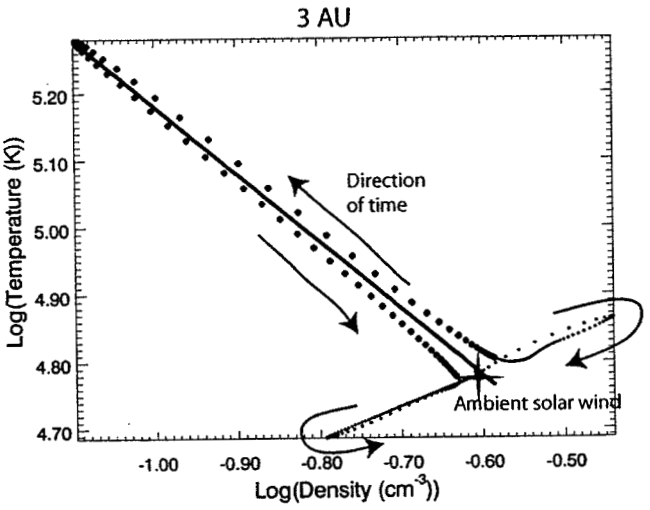
3 AU
5.20
5.10
5.00
4.90
4.80
4.70
Log(Temperature (K))
Direction
of time
Ambient solar wind
-1.00
-0.90
-0.80
-0.70
-0.60
-0.50
Log(Density (cm-3))

Figure 7

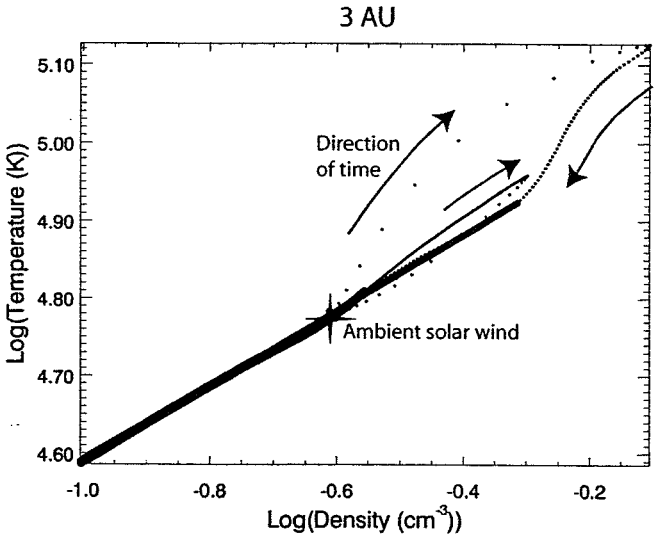
3 AU
5.10
5.00
4.90
4.80
4.70
4.60
Log(Temperature (K))
Direction
of time
Ambient solar wind
-1.0
-0.8
-0.6
-0.4
-0.2
Log(Density (cm-3))

Figure 8

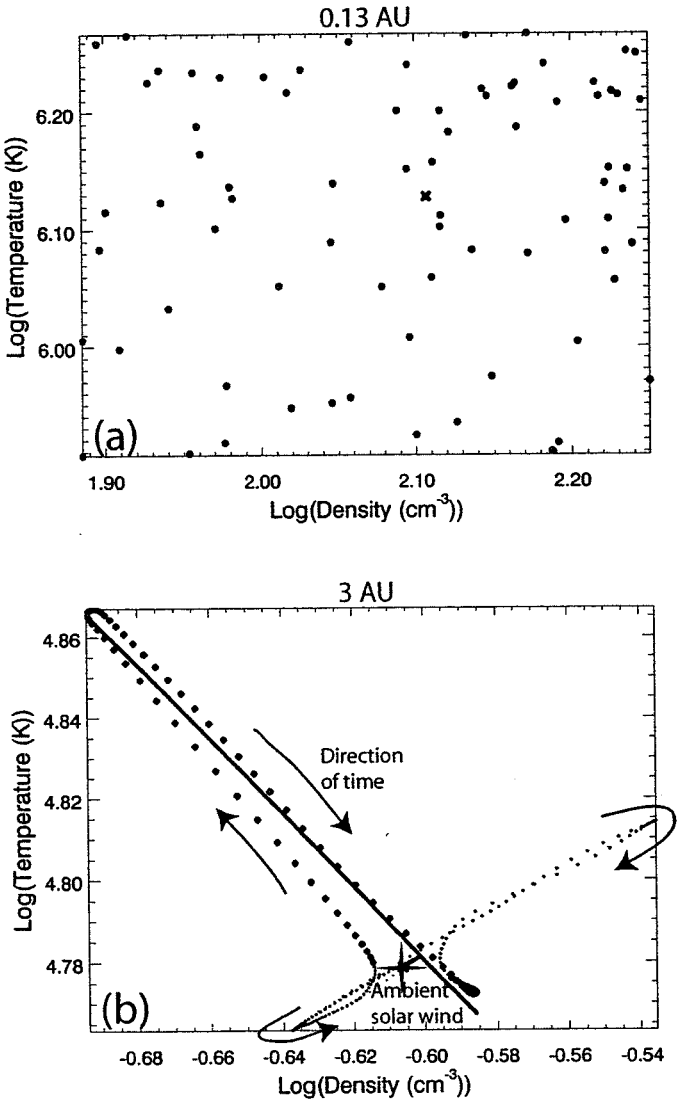
0.13 AU
Log(Temperature (K))
6.20
6.10
6.00
(a)
1.90
2.00
2.10
2.20
Log(Density (cm^{-3}))
3 AU
Log(Temperature (K))
4.86
4.84
4.82
4.80
4.78
Direction
of time
Ambient
solar wind
(b)
-0.68
-0.66
-0.64
-0.62
-0.60
-0.58
-0.56
-0.54
Log(Density (cm^{-3}))

Figure 9

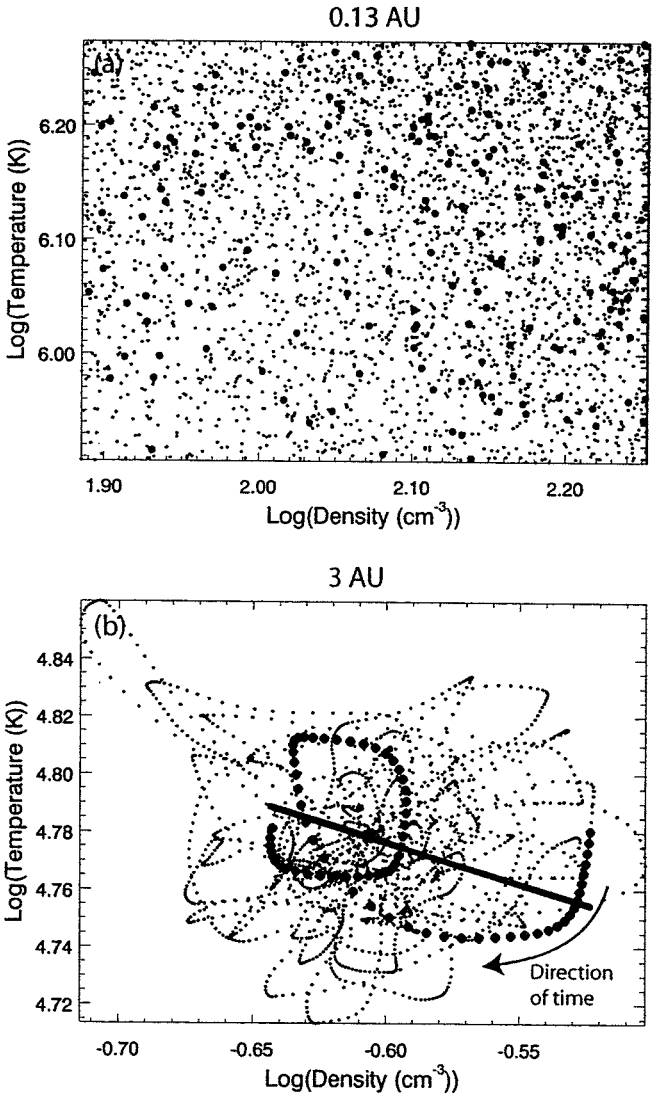
0.13 AU
(a)
6.20
6.10
6.00
Log(Temperature (K))
1.90
2.00
2.10
2.20
Log(Density (cm-3))
3 AU
(b).
4.84
4.82
4.80
4.78
4.76
4.74
4.72
Log(Temperature (K))
-0.70
-0.65
-0.60
-0.55
Log(Density (cm-3))
Direction
of time

Figure 10

Appendix 5

Reply to "Comment on the paper "On the determination of electron polytrope indices within coronal mass ejections in the solar wind""

J. T. Gosling, Pete Riley, and R. Skoug

Submitted to the *Journal of Geophysical Research*, July, 2000.

LA-UR-00-3943

Approved for public release; distribution is unlimited.

Title:	REPLY
Author(s):	JOHN GOSLING, NIS-1 PETE RILEY, SAIC RUTH SKOUG, NIS-1
Submitted to:	JOURNAL OF GEOPHYSICAL RESEARCH

Los Alamos
NATIONAL LABORATORY

Form 836 (8/00)

Reply

J. T. Gosling[1], P. Riley[2], and R. M. Skoug[1]

1. Los Alamos National Laboratory, Los Alamos, New Mexico

2. Science Applications International Corporation, San Diego, California

We strongly disagree with the essence of the *Osherovich* [this issue] (hereafter Osherovich) comment on one of our papers [*Gosling*, 1999]. The following paragraphs provide the basis of our disagreement and elaborate on why we believe that none of the concluding statements in his Comment are true. Our most important point is that one can apply the model developed by Osherovich and colleagues to real data obtained at a single point in space to determine the polytropic index within magnetic clouds if and only if the highly idealized assumptions of that model conform to physical reality. There is good reason to believe that those assumptions do not provide an accurate physical description of real magnetic clouds in the spherically expanding solar wind.

The polytropic equation that relates pressure, P, and mass density, ρ, in a parcel of solar wind plasma as a function of time and distance has the form

$$P\rho^{-\gamma} = \text{constant}, \qquad (1)$$

where γ is the polytropic index. When one also assumes an ideal gas, this takes the form

$$T = Sn^{\gamma-1}, \qquad (2)$$

where T is the temperature, n is the number density, and S is the entropy. Rigorously, to determine γ it is necessary to sample temperature and density within the same plasma parcel at different radial distances from the Sun. In practice, the requirement of sampling the same plasma parcel can be relaxed if different plasma parcels sampled at different heliocentric distances start with essentially the same entropy and the entropy remains constant with distance as, for example,

appears to be the case for protons in the high-speed wind at high heliographic latitudes near solar activity minimum [*Feldman et al.*, 1998].

Osherovich et al. [1993a] model magnetic clouds in the solar wind as cylindrical magnetic flux ropes with axially symmetric plasma and magnetic field properties that are invariant along extended cylindrical surfaces. In such a model the function $\Psi = rA_\phi$ is a constant on any cylindrical surface within the flux rope, where r is radial distance normal to the axis of the cylinder and A_ϕ is the azimuthal component of the vector magnetic potential (in cylindrical coordinates). As noted in his comment, Osherovich and colleagues also assume a polytropic relationship between gas pressure and mass density, an ideal gas equation of state, and uniform cylindrical expansion about the flux rope axis as a function of time. If such a model describes physical reality, then Osherovich is correct in stating that T and ρ on expanding cylindrical surfaces within the flux rope should be related to one another by

$$T = F(\Psi)\rho^{\gamma-1}, \qquad (3)$$

where $F(\Psi)$ is a constant for any given expanding cylindrical surface, but may vary from one surface to another. This equation simply states that all plasma parcels on an expanding cylindrical surface are equivalent in that they evolve in time in an identical fashion, as is required by the symmetry assumptions of the model. Since Osherovich and colleagues have assumed an ideal gas and a polytropic relationship between gas pressure and mass density, (2) must be satisfied as well, so that $F(\Psi)$ is directly related to entropy by

$$F(\Psi) = S(\Psi) / m^{\gamma-1}, \qquad (4)$$

where m is the average particle mass. They do not seem to have appreciated this simple connection between $F(\Psi)$ and entropy; their introduction of $F(\Psi)$ as something different from entropy has simply confused the issue. In reality, (3) reduces to (2) on expanding cylindrical surfaces and therefore does not depend explicitly upon a flux rope magnetic field topology; the essential assumptions are axial symmetry, invariant plasma properties along extended cylindrical

surfaces, an ideal gas, a polytropic relationship between P and ρ, and uniform cylindrical expansion. If a flux rope of this nature were to pass over a spacecraft, each expanding cylindrical surface would be crossed twice, so that one would obtain pairs of temperature and density measurements of essentially equivalent plasma parcels on each expanding cylindrical surface within the flux rope. From these paired measurements one could make a series of two-point determinations of both $F(\Psi)$ and γ, as Osherovich claims.

Spacecraft measurements indicate that electron temperature, T_e, and density, n_e, are often negatively correlated as a magnetic cloud passes over a spacecraft. Osherovich and colleagues [e.g., *Osherovich et al.*, 1993*a,b*, 1995, 1998, 1999; *Fainberg et al.*, 1996; *Farrugia et al.*, 1995, 1999; *Osherovich and Burlaga*, 1997] have used such measurements together with their model assumptions to infer that the electron polytropic index, γ_e, is less than 1.0 within magnetic clouds and that $F(\Psi)$ typically is roughly constant in a given flux rope; in addition, they infer the presence of multiple flux ropes in some magnetic clouds. For different flux ropes they find different values of $F(\Psi)$ and different values of γ_e (but always < 1.0). If these determinations of γ_e are valid, then T_e must increase as the clouds expand and $S(\Psi)$ must be nearly constant throughout a given flux rope.

We wish to emphasize that the technique used by Osherovich and colleagues to determine γ_e within magnetic clouds is valid if and only if their model assumptions accurately describe the physical properties of real magnetic clouds. If magnetic clouds are not axially symmetric with uniform properties along extended cylindrical surfaces and do not expand in a purely cylindrical sense, then one does not obtain a series of 2-point samplings of essentially equivalent plasma parcels as a cloud passes over a spacecraft. The onus is on Osherovich and colleagues to prove that their model assumptions conform to physical reality and apply to real magnetic clouds in the spherically expanding solar wind. In this regard, the observed negative correlation between T_e and n_e within magnetic clouds is not proof that their assumptions are valid or a demonstration either that γ_e is less than 1.0 in magnetic clouds or that S is constant throughout a given cloud. Negative correlations between temperature and density at a single point in the heliosphere can and do arise for other reasons [e. g., *Gosling*, 1999]. We think it is highly unlikely that real flux

ropes in the solar wind have axially symmetric and uniform properties along extended cylindrical surfaces, expand in a purely cylindrical sense, and have constant entropy throughout.

Osherovich notes that in their model the plasma density on a given expanding cylindrical surface must decrease with time as the flux rope expands. He also claims that the magnetic cloud observed by Ulysses on June 10, 1993 at 4.64 AU contained two separate flux ropes that passed Ulysses on June 10.00 - June 11.75 and June 11.75 - June 13.0, respectively. Figure 1 shows a plot of the proton density observed by Ulysses for these and the surrounding time intervals. Closest approach to the axis of the first flux rope or "tube" would have occurred approximately on June 10.88 and that of the second on June 12.38. It is immediately apparent that for many of the pairs of points equidistant in time on either side of closest approach to the tube axes, which would correspond roughly to the same expanding cylindrical surfaces in their model, the densities are not lower at the later times, in contrast to the model's assumption. The same is true if one uses the observed flow speed to convert time into a spatial distance. Clearly, these presumed separate flux rope tubes do not have uniform and axially symmetric plasma properties. Yet, the June 10, 1993 Ulysses event is often touted as a prime example supporting the model [e.g., *Fainberg et al.*, 1996; *Osherovich and Burlaga*, 1997; *Osherovich et al.*, 1999; *Osherovich*, this issue].

Making the further assumption that flux rope expansions are "self-similar", Osherovich and colleagues have found that expansion does not occur unless $\gamma_e < 1.0$ [e.g., *Osherovich et al.*, 1993*b*; *Osherovich*, this issue]. Since most clouds are observed to expand, he thus finds support for their model in their presumed experimental determinations of γ_e within magnetic clouds. But, as we have noted, those determinations of γ_e are themselves strongly dependent on the model assumptions. One cannot prove the validity of a model in this way. Further, flux rope expansion in the solar wind has been demonstrated in one-fluid MHD simulations where γ has explicitly been chosen to be 1.67 [*Vandas et al.*, 1996*a,b*], as well as in 3D analytical MHD calculations for values of γ ranging from 1.2 to 1.67 [*Chen and Garren*, 1993; *Chen*, 1996, 1997]. *Chen* [1996], who does not assume that flux ropes are axially symmetric cylinders, ascribes this difference in results to the difference between a 3D and a 2D calculation and Osherovich et al.'s neglect of the radial variation in pressure in the background solar wind in which real magnetic clouds are

embedded.

Our own one-fluid simulations have been concerned primarily with dynamic effects associated with coronal mass ejection, CME, expansions, such as the forward-reverse shock pairs associated with expansions driven by high internal CME pressures [*Gosling et al.*, 1994*a,b*, 1998; *Gosling and Riley*, 1996; *Riley et al.*, 1997]. Usually in these and similar simulations [e.g., *Odstrcil and Pizzo*, 1999*a,b*] it is assumed that $\gamma = 1.67$. However, as we have previously noted [e.g., *Gosling*, 1999], other choices of $\gamma > 1.0$ have only a minor effect on the overall dynamics of these expansions, which is where our primary interest lies in these particular simulations. We have never claimed that a choice of $\gamma = 1.67$ provides a reasonable estimate of electron temperature evolution within CMEs. Indeed, we believe that smaller (but > 1.0) values probably better describe the electron thermal evolution within expanding CMEs in the solar wind. Thus the comparison shown in Figure 1a by Osherovich, which shows predictions for $\gamma = 1.67$ and which Osherovich claims is what we would predict, is not what we would advocate for electrons within CMEs in the solar wind, be they magnetic clouds or otherwise. Moreover, in attempting to make the comparison seem as poor as possible Osherovich conveniently ignores the fact that electron temperatures within CMEs in the solar wind at 1 AU often are considerably greater than 1×10^5 K [*Gosling et al.*, 1987]. We find no basis for his claim that "...no polytropic index can accommodate the evolution of temperature in magnetic clouds, if Formula (4) is used." We also stand by our previous comments [*Gosling*, 1999] to the effect that there is no observational evidence to support the idea that electron temperatures within expanding magnetic clouds, or expanding CMEs in general, increase with increasing heliocentric distance at any distance from the Sun. Indeed, the evidence is to the contrary. For example, we have recently obtained widely separated (in heliocentric distance) 2-point measurements of the same magnetic cloud and found that both T_e and n_e decreased with increasing heliocentric distance despite the fact that at each spacecraft T_e and n_e were negatively correlated [*Skoug et al.*, 2000*b*].

In order to circumvent some of the difficulties associated with predictions of ever increasing values of electron temperature as a magnetic cloud expands, Osherovich now incorporates an electron heat flux term into the polytropic equation, where he seems to advocate that the only heat

flux that affects electron temperature within a flux rope is through the walls of the flux rope tube, transverse to the magnetic field. We fail to understand how electrons can carry a significant flow of heat transverse to the magnetic field in the essentially collisionless solar wind or how this new version of their model makes any more physical sense than the previous one.

Osherovich claims that the choice of $\gamma > 1.0$ in our simulations leads to a positive correlation between T and ρ at a fixed point in space, which he notes is contrary to electron observations within magnetic clouds. However, in many of our simulations we obtain neither a linear nor a positive correlation between log T and log ρ (or n) at a fixed point in space [*Riley et al.*, 2000]. The relationship between T and n at a fixed point depends on the nature of the initial perturbation at the inner boundary of the simulation and on heliocentric distance. We obtain a straight line with positive slope in log T vs. log n space at a fixed point in space only when the plasma introduced at the inner boundary is isentropic and remains unshocked as it propagates outward from the Sun. When both of these conditions are satisfied the slope of the log T vs. log n relationship at a single point does provide a direct measure of the value of γ used in the simulation.

In some of our simulations we obtain strong negative correlations between T and n at a single point in space [*Riley et al.*, 2000]. The upper panel of Figure 2 displays a random set of points in log T vs. log n space used to initialize a disturbance lasting 10 hours at 0.13 AU in a spherically symmetric, 1-dimensional, 1-fluid simulation in which $\gamma = 1.5$. The speed at 0.13 AU was held constant at 702 km s^{-1} and the random density/temperature disturbance was preceded and followed by extended intervals of constant density and temperature, and thus also constant entropy. The cross marks the value of density and temperature for this ambient surrounding wind. The simulation follows the evolution of the disturbance out into the heliosphere; the lower panel of Figure 2 shows the resulting log T vs. log n plot at 3.0 AU where the disturbance has evolved into a structure that is nearly in pressure balance. The cross in this panel denotes undisturbed ambient solar wind at 3 AU. All values of density and temperature are lower at 3.0 AU than at 0.13 AU owing to the spherical expansion of the solar wind and our choice of $\gamma > 1.0$. Points in the perturbed ambient wind (small dots) lie roughly along a straight line with positive slope (0.5), indicating that the perturbation to the surrounding, initially isentropic, ambient wind produced by

the initial disturbance was devoid of strong shocks. On the other hand, points within the original disturbance pulse (large dots) lie roughly along a line of negative slope (-0.908) even though γ for the entire simulation was 1.5. The negative slope is a consequence of non-isentropic structure in the initial disturbance and evolution toward pressure balance. Thus, negative correlations between density and temperature at a single point in space within a CME or magnetic cloud may simply reflect the presence of (non-isentropic) structure in the initial disturbance close to the Sun and the tendency for such structure to achieve pressure balance as it evolves outward [*Gosling*, 1999; *Riley et al.*, 2000; *Skoug et al.*, 2000*a*]. And, of course, one can not directly infer the value of γ from the log T vs. log n plot within the simulated CME in this case.

Finally, Osherovich and colleagues give the impression that negative correlations between T_e and n_e are not observed in the solar wind except within magnetic clouds. However, recent work [*Skoug et al.*, 2000*a*] demonstrates that negative correlations between T_e and n_e are common in much of the solar wind, including within CMEs in the solar wind that are not magnetic clouds. This is consistent with previous studies of solar wind thermal core electrons [*Phillips and Gosling*, 1990; *Hammond et al.*, 1996]. That is, the negative T_e-n_e correlation in the solar wind does not depend on the presence of a magnetic structure with a flux rope topology. It has also been demonstrated that at 1 AU halo electrons do not contribute more to the total pressure in magnetic clouds than they do in other types of solar wind of comparable density [*Skoug et al.*, 2000*a*], contrary to statements by Osherovich.

To summarize, Osherovich's claim that essentially two-point, rather than single-point, measurements of T_e and n_e are made as a magnetic cloud passes over a spacecraft is valid if and only if the the highly idealized symmetry and uniformity assumptions of their model correspond to reality. If those assumptions are not physically correct then such measurements reveal nothing about the value of γ_e within magnetic clouds. It is up to Osherovich and his colleagues to show that their assumptions conform to physical reality for real magnetic clouds in the spherically expanding solar wind, but we have provided solid evidence that they do not. We have also emphasized: (1) Their $F(\Psi)$ is simply related to entropy. (2) A value of γ_e less than 1.0 is not required for flux rope expansion in the solar wind. (3) T and ρ are often not positively correlated

in simulations where $\gamma > 1.0$. (4) Strong negative correlations between T_e and n_e at a single point in space can arise from non-isentropic structure within magnetic clouds and the solar wind in general even when $\gamma_e > 1.0$. (5) Negative correlations between T_e and n_e are observed in much of the non-magnetic cloud solar wind, making it unlikely that those correlations are related to the special magnetic topology of magnetic clouds or are a consequence of $\gamma_e < 1.0$. (6) Available evidence indicates that electron temperatures within magnetic clouds, and within CMEs in general, decline as those disturbances expand out into the heliosphere. (7) If a polytrope equation adequately describes electron evolution, the polytropic index is greater than 1.0 in magnetic clouds, in non-cloud CMEs, and in the solar wind in general.

Acknowledgments. The authors have profited from discussions on this topic with J. Chen and M. Thomsen. Work at Los Alamos was performed under the auspices of the U. S. Department of Energy with support from NASA and the Ulysses project. Work at SAIC was supported by NASA grant NASW-98007 and contract NAS4-96081.

References

Chen, J., Theory of prominence eruption and propagation: Interplanetary consequences, *J. Geophys. Res., 101*, 27,499, 1996.

Chen, J., Coronal mass ejections: Causes and consequences, a theoretical view, in *Coronal Mass Ejections, Geophysical Monogr. Ser.*, Vol. 99, edited, N. Crooker, J. A. Joselyn, and J. Feynman, Amer. Geophys. Union, 9, pp. 65-81, 1997.

Chen, J., and D. A. Garren, Interplanetary magnetic clouds: Topology and driving mechanism, *Geophys. Res. Lett., 20*, 2319, 1993.

Fainberg, J., V. A. Osherovich, R. G. Stone, R. J. MacDowall, and A. Balogh, Ulysses observations of electron and proton components in a magnetic cloud and related wave activity, in *Solar Wind Eight, Amer. Instit. Phys., Conf. Proceed. 382*, edited by D. Winterhalter, J. T. Gosling, S. R. Habbal, W. S. Kurth and M. Neugebauer, New York, pp. 554-557, 1996.

Farrugia, C. F., V. A. Osherovich, and L. F. Burlaga, The magnetic flux rope versus the spheromak as models for interplanetary magnetic clouds, *J. Geophys. Res., 100*, 12,293, 1995.

Farrugia, C. F., V. A. Osherovich, and J. Fainberg, Tensor nature of the gas pressure and measurements of the polytropic indices for magnetic clouds: A case study, in *Solar Wind Nine, Amer. Instit. Phys., Conf. Proceed. 471*, edited b S. R. Habbal, R. Esser, J. V. Hollweg, and P. A. Isenberg, New York, pp. 499-502, 1999.

Feldman, W. C., B. L. Barraclough, J. T. Gosling, D. J. McComas, P. Riley, B. E. Goldstein, and A. Balogh, Ion energy equation for the high-speed solar wind: Ulysses observations, *J. Geophys. Res., 103*, 14,547, 1998.

Gosling, J. T., On the determination of electron polytrope indices within coronal mass ejections in

the solar wind, *J. Geophys. Res., 104*, 19,851, 1999.

Gosling, J. T., and P. Riley, The acceleration of slow coronal mass ejections in the high-speed solar wind, *Geophys. Res., Lett., 23,* 2867, 1996.

Gosling, J. T., D. N. Baker, S. J. Bame, W. C. Feldman, R. D. Zwickl, and E. J. Smith, Bidirectional solar wind electron heat flux events, *J. Geophys. Res., 92,* 8519, 1987.

Gosling, J. T., S. J. Bame, D. J. McComas, J. L. Phillips, E. E. Scime, V. J. Pizzo, B. E. Goldstein, and A. Balogh, A forward-reverse shock pair in the solar wind driven by over-expansion of a coronal mass ejection: Ulysses observations, *Geophys. Res. Lett., 21,* 237, 1994*a.*

Gosling, J. T., D. J. McComas, J. L. Phillips, L. A. Weiss, V. J. Pizzo, B. E. Goldstein, and R. J. Forsyth, A new class of forward-reverse shock pairs in the solar wind, *Geophys. Res. Lett., 21, 2271,* 1994*b.*

Gosling, J. T., P. Riley, D. J. McComas, and V. J. Pizzo, Over-expanding coronal mass ejections at high heliographic latitudes: Observations and simulations, *J. Geophys. Res., 103,* 1941, 1998.

Hammond, C. M., J. L. Phillips, G. K. Crawford, and A. Balogh, The relationship between electron density and temperature inside coronal mass ejections, in *Solar Wind Eight, Amer. Instit. Phys., Conf. Proceed. 382*, edited by D. Winterhalter, J. T. Gosling, S. R. Habbal, W. S. Kurth and M. Neugebauer, New York, pp. 558-561, 1996.

Odstrcil, D., and V. J. Pizzo, Three-dimensional propagation of coronal mass ejections (CMEs) in a structured solar wind flow 1. CME launched within the streamer belt, *J. Geophys. Res., 104,* 483, 1999*a.*

Odstrcil, D., and V. J. Pizzo, Three-dimensional propagation of coronal mass ejections (CMEs) in a structured solar wind flow 2. CME launched adjacent to the streamer belt, *J. Geophys. Res., 104,* 493, 1999*b*.

Osherovich, V., Comment on the paper "On the determination of electron polytrope indices within coronal mass ejections in the solar wind" by J. T. Gosling, this issue.

Osherovich, V., and L. F. Burlaga, Magnetic clouds, in *Coronal Mass Ejections, Geophysical Monogr. Ser.*, Vol. 99, edited, N. Crooker, J. A. Joselyn, and J. Feynman, Amer. Geophys. Union, 9, pp. 157-168, 1997.

Osherovich, V. A., C. J. Farrugia, L. F. Burlaga, R. P. Lepping, J. Fainberg, and R. G. Stone, Polytropic relationship in interplanetary magnetic clouds, *J. Geophys. Res., 98,* 15,331, 1993*a*.

Osherovich, V. A., C. J. Farrugia, and L. F. Burlaga, Dynamics of aging magnetic clouds, *Adv. Space Res., 13(6),* 57, 1993*b*.

Osherovich, V. A., C. J. Farrugia, and L. F. Burlaga, Nonlinear evolution of magnetic flux ropes 2. Finite beta plasma, *J. Geophys. Res., 100,* 12,307, 1995.

Osherovich, V. A., J. Fainberg, R. G. Stone, R. Fitzenreiter, and A. F. Vinas, Measurements of polytropic index in the January 10-11, 1997 magnetic cloud observed by Wind, *Geophys. Res. Lett., 25,* 3003, 1998.

Osherovich, V. A., J. Fainberg, and R. G. Stone, Multi-tube model for interplanetary magnetic clouds, *Geophys. Res. Lett., 26,* 401, 1999.

Phillips, J. L., and J. T. Gosling, Radial evolution of solar wind thermal electron distributions due to expansion and collisions, *J. Geophys. Res., 95,* 4217, 1990.

Riley, P., J. T. Gosling, and V. J. Pizzo, A two-dimensional simulation of the radial and latitudinal evolution of a solar wind disturbance driven by a fast, high-pressure coronal mass ejection, *J. Geophys. Res., 102,* 14,677, 1997.

Riley, P., J. T. Gosling, and V. J. Pizzo, Investigation of the polytropic relationship between density and temperature within interplanetary coronal mass ejections using numerical simulations, *J. Geophys. Res.*, submitted, 2000.

Skoug, R. M., W. C. Feldman, J. T. Gosling, D. J. McComas, and C. W. Smith, Solar wind electron characteristics inside and outside coronal mass ejections, *J. Geophys. Res.*, in press, 2000*a.*

Skoug, R. M., W. C. Feldman, J. T. Gosling, D. J. McComas, D. B. Reisenfeld, C. W. Smith, R. P. Lepping, and A. Balogh, Radial variation of solar wind electrons inside a magnetic cloud observed at 1 and 5 AU, *J. Geophys. Res.*, in press, 2000*b.*

Vandas, M., S. Fischer, P. Pelant, M. Dryer, Z. Smith, and T. Detman, MHD simulation of the propagation of loop-like and bubble-like magnetic clouds, in *Solar Wind Eight, Amer. Instit. Phys., Conf. Proceed. 382*, edited by D. Winterhalter, J. T. Gosling, S. R. Habbal, W. S. Kurth and M. Neugebauer, New York, pp. 556-569, 1996*a.*

Vandas, M., S. Fischer, M. Dryer, Z. Smith, and T. Detman, Parametric study of loop-like magnetic cloud propagation, *J. Geophys. Res., 10*1, 15,645, 1996*b.*

Figure Captions

Figure 1. Solar wind density measured by Ulysses at 4.64 AU and S32.5° during passage of a disturbance driven by an overexpanding CME that was also a magnetic cloud. The two separate, but adjacent, flux ropes within the CME/cloud identified by Osherovich and colleagues are indicated by the solid vertical lines. Dashed vertical lines indicate closest approach to the presumed axes of those flux ropes.

Figure 2. (**a**) Density-temperature points used to initialize a 10-hour disturbance in the solar wind at 0.13 AU in a one-dimensional (radial), one-fluid simulation. The cross marks the value of density and temperature in the surrounding ambient solar wind at 0.13 AU. (**b**) The resulting paired values of density and temperature at 3.0 AU. The solid curve is the best-fit straight line to plasma parcels that originated within the 10-hour disturbance at 0.13 AU. See text for full explanation. Adapted from *Riley et al.* [2000].

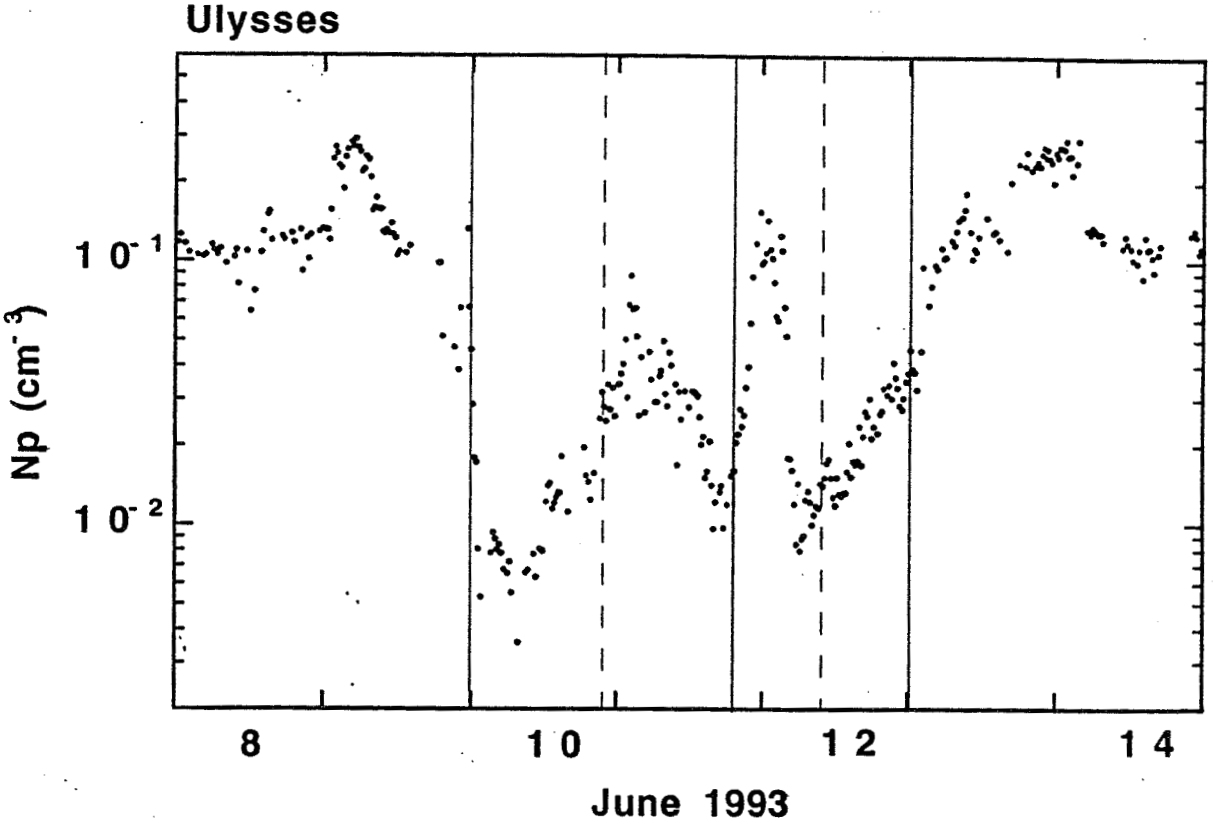

Figure 1.

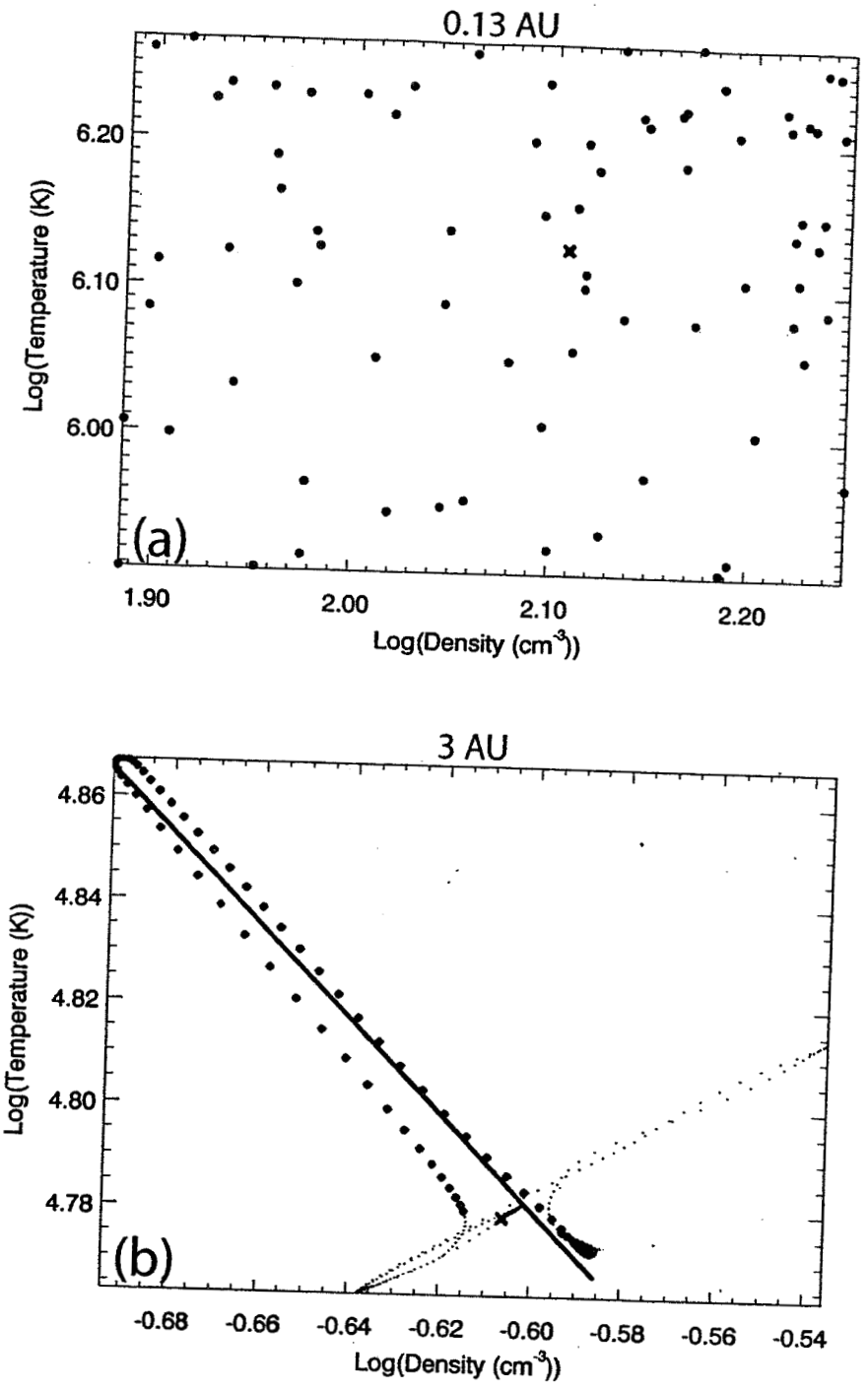
0.13 AU
6.20
6.10
6.00
Log(Temperature (K))
(a)
1.90
2.00
2.10
2.20
Log(Density (cm^{-3}))
3 AU
4.86
4.84
4.82
4.80
4.78
Log(Temperature (K))
(b)
-0.68
-0.66
-0.64
-0.62
-0.60
-0.58
-0.56
-0.54
Log(Density (cm^{-3}))

Figure 2.

Appendix 6

An unusual coronal mass ejection: First solar wind electron, proton, alpha monitor (SWEPAM) results from the Advanced Composition Explorer

D. J. McComas, S. J. Bame, P. L. Barker, D. M. Delapp, W. C. Feldman, J. T. Gosling, E. Santiago, R. M. Skoug, R. L. Tokar, P. Riley, J. L. Phillips, and J. W. Griffee

Geophysical Research Letters, 25, 4289, 1998.

GEOPHYSICAL RESEARCH LETTERS, VOL. 25, NO. 23, PAGES 4289-4292, DECEMBER 1, 1998

An unusual coronal mass ejection: First Solar Wind Electron, Proton, Alpha Monitor (SWEPAM) results from the Advanced Composition Explorer

D.J. McComas[1], S.J. Bame[1], P.L. Barker[1], D.M. Delapp[1], W.C. Feldman[1], J.T. Gosling[1], E. Santiago[1], R.M. Skoug[1], R.L. Tokar[1], P. Riley[2], J.L. Phillips[3], J.W. Griffee[4]

Abstract. This paper reports the first scientific results from the Solar Wind Electron Proton Alpha Monitor (SWEPAM) instrument on board the Advanced Composition Explorer (ACE) spacecraft. We analyzed a coronal mass ejection (CME) observed in the solar wind using data from early February, 1998. This event displayed several of the common signatures of CMEs, such as counterstreaming halo electrons and depressed ion and electron temperatures, as well as some unusual features. During a portion of the CME traversal, SWEPAM measured a very large helium to proton abundance ratio. Other heavy ions, with a set of ionization states consistent with normal (1-2 x 10^6 K) coronal temperatures, were proportionately enhanced at this time. These observations suggest a source for at least some of the CME material, where heavy ions are initially concentrated relative to hydrogen and then accelerated up into the solar wind, independent of their mass and first ionization potential.

Introduction

The Advanced Composition Explorer (ACE) was launched on 25 August 1997 toward its orbit about the Sun-Earth libration point, L1, situated ~1.5x10^6 km sunward of the Earth. ACE carries a magnetometer and a compliment of instruments appropriate for examining the composition of matter from solar wind ions with energies <1 keV through galactic cosmic rays with energies of hundreds of MeV/nucleon [Stone, 1998]. As a part of that instrumentation, the Solar Wind Electron Proton Alpha Monitor (SWEPAM) continuously measures solar wind electrons and ions [McComas et al., 1998].

SWEPAM measures the detailed solar wind electron and ion distributions, providing direct measurements of solar wind phenomena such as coronal mass ejections and interplanetary shocks. In addition to being interesting in their own right, these observations provide the solar wind context for the measurements of elemental and isotopic composition made by other ACE instruments. Because of ACE's position upstream of the Earth, SWEPAM measurements are also ideally suited for multi-spacecraft heliospheric and magnetospheric studies. Finally, SWEPAM provides a subset of the ion observations to NOAA for real-time space weather monitoring purposes.

[1]*Los Alamos National Laboratory, Los Alamos NM.*
[2]*Scibernet Inc., San Diego CA.*
[3]*Johnson Space Center, Houston TX.*
[4]*Sandia National Laboratories, Albuquerque NM.*

Paper number 1998GL900174.
0094-8276/98/1998GL900174$05.00

The SWEPAM experiment comprises two completely independent sensors: one for electrons and one for ions. Both are based on spherical section electrostatic analyzers followed by sets of channel electron multiplier detectors. These sensors were first developed as spare units for the solar wind experiment on the Ulysses spacecraft and were refurbished, modified, and updated for the ACE mission. Enhancements from their original form include a factor of 16 increase in the sensitivity for high energy halo electrons and an increased sensitivity for solar wind ions (especially useful for observing heavy ions). New control electronics and programming provide 64 second time resolution for full 3-D measurements of the electron and ion distribution functions. Details of the ACE SWEPAM instruments are given by McComas et al. [1998].

Coronal mass ejections (CMEs) are transient eruptions of material from the solar atmosphere and are commonly observed in coronagraph images as rising, bright, and hence relatively dense, loops of material and magnetic flux which subsequently join in the solar wind flow. In interplanetary space, such loops can often be inferred through the signature of counterstreaming suprathermal electrons, which may indicate magnetic connection back to the hot corona in both directions along the local magnetic field [Gosling et al., 1987; Gosling, 1990]. While we believe that the presence of counterstreaming suprathermal electrons is the best single indicator of a CME in the solar wind near 1 AU, many other phenomena have also been identified with CMEs. These include an enhanced helium abundance that is often characterized by large temporal and/or spatial variations, unusually low ion and/or electron temperatures, low plasma beta, charge-state distributions of heavy ions that indicate unusually high and/or low coronal "freezing-in" temperatures, and counterstreaming suprathermal ions (see, for example, reviews by Gosling [1990], Neugebauer and Goldstein [1997], Goldstein et al. [1998], and references therein). In addition, an important subset of all CMEs in the solar wind, called magnetic clouds, is characterized by large, smooth rotations of the interplanetary magnetic field (IMF) together with an increase in the magnetic field magnitude and decrease in the field variance [Klein and Burlaga, 1982; Burlaga et al., 1998]. Not all of these signatures are associated with all CMEs or even all parts of a given CME.

Observations

Plasma moments from 3-6 February 1998, are displayed in Figure 1. From top to bottom the figure shows the solar wind speed, proton density, electron and proton temperatures, and ratio of $^4He^{2+}$ to proton density. The vertical lines at 2:10 on 4 February and 23:10 on 5 February indicate the likely spacecraft entrance into and exit from the CME, as identified by

"Page missing from available version"

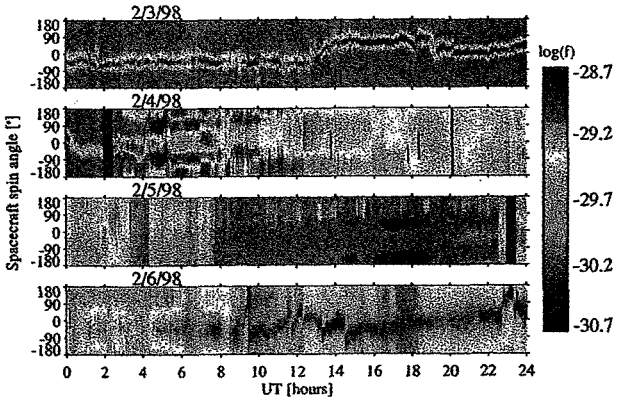

Figure 2. Color-coded log of the electron distribution function [$s^3 cm^{-6}$] for energies from 142-373 eV, as a function of spacecraft spin angle, for 3-6 February 1998. The spacecraft spin axis points ~11° away from the Sun at this time; 0° indicates the spin phase when the sensor looks nearest the Sun.

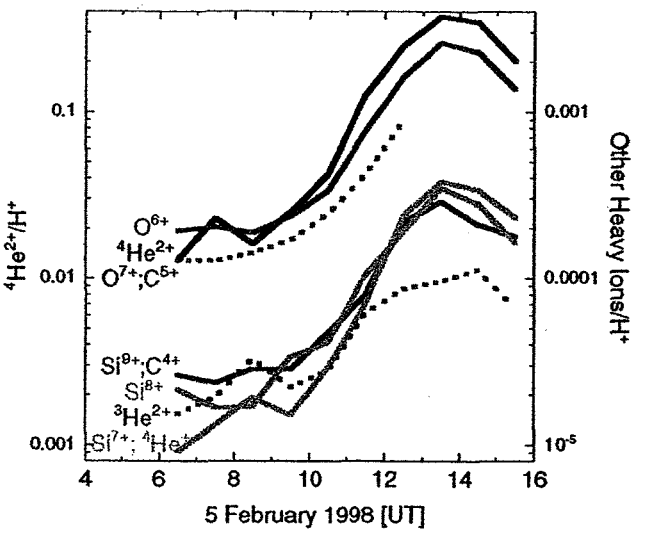

Figure 4. Abundances of heavy ions relative to H^+ for 6:00-16:00 UT on 5 February 1998. Note that the scale for alpha particles (left side, black curve) is 100x larger than for the other ions (right side scale).

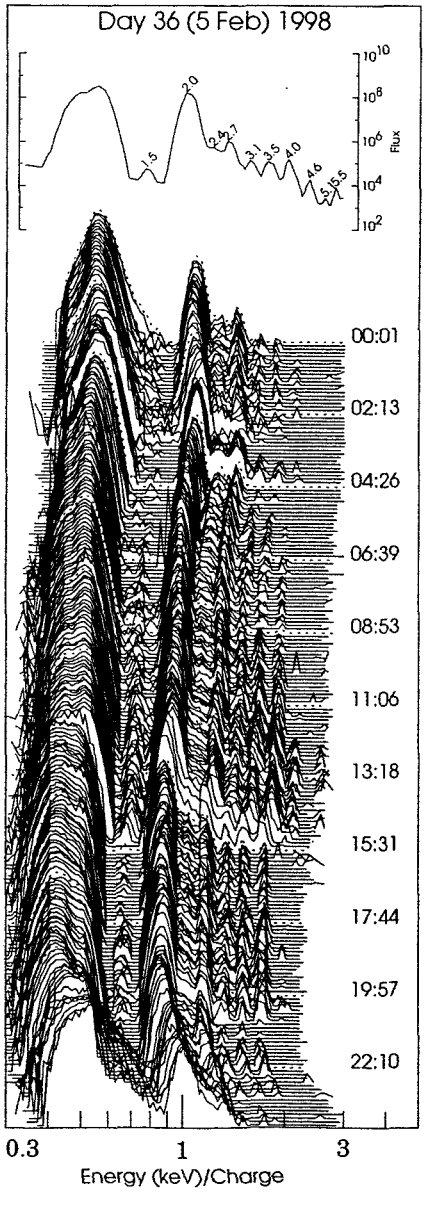

While fluxes of heavy ions are highly variable on 5 February, all species appear to come and go together. In order to quantify this variability, we scaled the ion density ratios from the peak flux values. This scaling assumes that all of the ions have the same thermal speed which is expected since the kinetic temperatures of heavy ions are proportional to their masses [von Steiger et al., 1995a]. Figure 4 displays one-hour averages of the ratios of heavy ion densities to proton density from 6:00-16:00 UT. This interval was chosen because solar wind speed was relatively constant, which makes the summing of E/q spectra less complicated and more accurate. The $^3He^{2+}$ and $O^{7+};C^{5+}$ peaks are overlapped with larger, adjacent peaks, and thus are less certain (dashed lines). The remaining heavy ion peaks all appear to be well resolved and display consistent variations (within a factor of 2, roughly the accuracy of this scaling) over a factor of 20 change during this interval, from roughly half to ten times their typical solar wind abundances [e.g., Anders and Grevesse, 1989]. The coherent variation of abundances for all of these ions suggests that they originated in a source region in the corona, which was characterized by a normal 1-2 x 10^6 K temperature, but where large concentrations of heavy ions, relative to protons, occurred.

Discussion

In an effort to identify the solar source of the CME described in this study, we examined Yohkoh, SOHO, and ground-based soft X-ray, Hα, and He-304 observations for the interval from 27-31 January, which should include the time that the CME left

Figure 3. Ion flux [cm^{-2} s^{-1} sr^{-1}] spectra, as a function of E/q, for 5 February 1998. The top spectrum is summed over the 54 spectra from 14:00-15:00 UT and labeled as mass/charge peaks. The remaining spectra are each summed over 6 consecutive 64 s spectra and are plotted on the same scale as is given above. Times on the right correspond to the adjacent dashed curves.

Appendix 7

A prolonged He+ enhancement within a coronal mass ejection in the solar wind

R. Skoug, S. J. Bame, W. C. Feldman, J. T. Gosling, D. J. McComas, J. T. Steinberg, R. L. Tokar, P. Riley, L. F. Burlaga, N. F. Ness, and C. W. Smith

Geophysical Research Letters, 26, 161, 1999.

GEOPHYSICAL RESEARCH LETTERS, VOL. 26, NO.2, PAGES 161-164, JANUARY 15, 1999

A prolonged He^+ enhancement within a coronal mass ejection in the solar wind

R. M. Skoug,[1] S. J. Bame,[1] W. C. Feldman,[1] J. T. Gosling,[1]
D. J. McComas,[1] J. T. Steinberg,[1] R. L. Tokar,[1] P. Riley,[2] L. F. Burlaga,[3]
N. F. Ness,[4] and C. W. Smith[4]

Abstract. A coronal mass ejection and magnetic cloud containing an unusually large enhancement of He^+ was observed in the solar wind by the plasma and magnetic field instruments on the Advanced Composition Explorer (ACE) spacecraft on May 2–4, 1998. The He^+/He^{++} ratio during this event exceeded 0.5% for a period of more than 24 hours, and reached values as high as 100%. The high He^+/He^{++} ratio indicates the presence of prominence material, and in fact a disappearing filament and prominence were observed at the Sun in association with this event. The prolonged observation of He^+ indicates that prominence material extended through much of this CME, the first such observation in a CME in the solar wind.

Introduction

Coronal mass ejections (CMEs) are transient events in which large quantities of matter are ejected from the Sun [*Gosling et al.,* 1974]. They typically originate in closed field regions in the solar corona, often in association with other forms of solar activity such as eruptive prominences. CMEs in the solar wind are identified by several characteristics, including counterstreaming halo electrons, enhanced helium abundance, low proton and electron temperatures, a strong magnetic field and low field variance [e.g. *Gosling,* 1990]. However, individual CMEs vary a great deal from one another, and a given CME may not include all of these features. Approximately one-third of CMEs in the solar wind are also magnetic clouds [*Gosling,* 1990], characterized by a flux rope geometry (observed as a large, smooth rotation in the magnetic field), a strong magnetic field and a low proton temperature [*Burlaga et al.,* 1981].

The solar wind (and CME) He^+/He^{++} ratio is typically 10^{-6} [*Kozlovsky,* 1968], corresponding to a coronal freezing-in temperature of $\approx 10^6$ K. On rare occasions, however, CMEs in the solar wind have been observed with significant He^+, from 0.1–30% of the He^{++} density. Four such events occurred in 1977 [*Schwenn et al.,* 1980; *Gosling et al.,* 1980; *Zwickl et al.,* 1982], and one during a magnetic cloud in 1997 [*Burlaga et al.,* 1998], all during the rising portion of the solar cycle. The presence of He^+ suggests that this material originated at a much lower temperature in the solar atmosphere, presumably from a solar prominence [e.g. *Schwenn et al.,* 1980; *Gosling et al.,* 1980]. Indeed, prominence disappearances were associated with the events of *Gosling et al.* [1980] and *Burlaga et al.* [1998]. In this paper, we present observations of a CME and magnetic cloud with an unusually high He^+/He^{++} ratio using data from the Solar Wind Electron Proton Alpha Monitor (SWEPAM) [*McComas et al.,* 1998a,b] and Magnetic Field Experiment (MAG) [*Smith et al.,* 1998] instruments on the Advanced Composition Explorer (ACE) satellite. These high time resolution data provide a global overview of the event and show time variations of the He charge state. Details of the ion composition are presented in the accompanying paper by *Gloeckler et al.* [1998]. This event is unique in that He^+ was observed over a prolonged interval, indicating that prominence material occupied a large fraction of the CME.

Observations

In early May, 1998, ACE was in a halo orbit about the L1 point, at (228,−33,−16) R_E GSE. Figure 1 shows the plasma and magnetic field parameters from May 1–4, 1998. The plasma parameters were calculated by integrating the measured ion distribution over velocity space, and are shown with 64 second time resolution. Field data are plotted with 16 second time resolution.

Early on May 3, the plasma was very cold ($\approx 10^4$ K) and quite dense (10–60 cm^{-3}). This extremely unusual combination of conditions caused the proton fluxes to exceed the dead time limited counting capability of SWEPAM for several hours. At these times (off and on from 0–17 UT), when inaccurate proton densities were calculated from SWEPAM, densities from the SWE instrument on the WIND spacecraft [*Ogilvie et al.,* 1995], also located near L1, have been used. Densities calculated from the two spacecraft in general agree well, within ≈15% [*McComas et al.,* 1998b]. Helium densities at this time are not affected by dead time effects, because of the lower He fluxes and counting rates.

[1]Los Alamos National Laboratory, Los Alamos, NM
[2]SciberNet, Inc., San Diego, CA
[3]NASA Goddard Space Flight Center, Greenbelt, MD
[4]Univ. of Delaware-Bartol Research Inst., Newark, DE

Paper number 1998GL900207.
0094-8276/98/1998GL900207$05.00

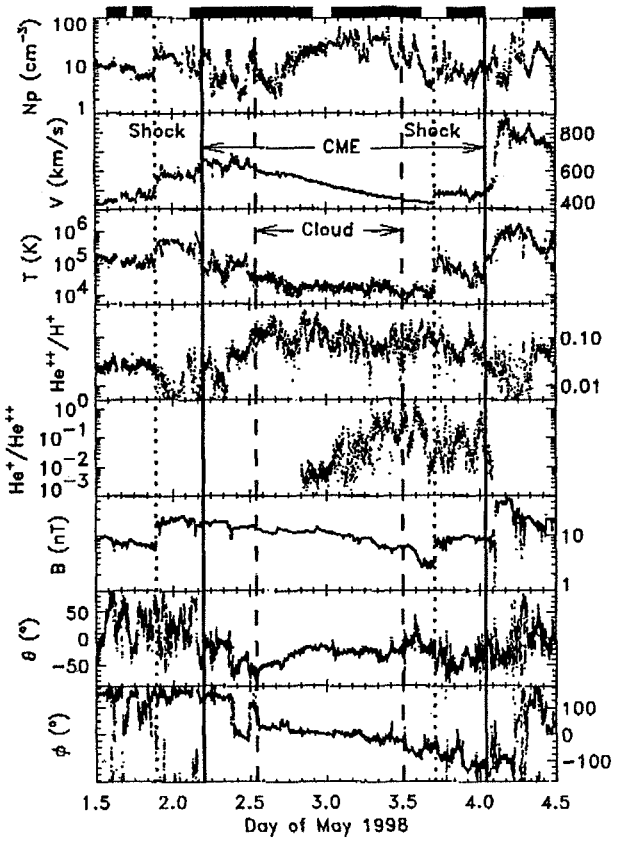

Figure 1. Solar wind plasma and magnetic field parameters for May 1–4, 1998. From top to bottom, panels show proton density (cm^{-3}), speed (km s^{-1}), and temperature (K), He^{++}/H^+ and He^+/He^{++} density ratios, and magnetic field magnitude and elevation (θ) and azimuthal (ϕ) angles in GSE coordinates. The CME is indicated by solid vertical lines, the magnetic cloud by dashed vertical lines, and shocks by dotted vertical lines. Solid bars at the top of the figure indicate periods of counterstreaming halo electrons (70–1370 eV).

Figure 1 shows a series of events, including multiple shocks and CMEs. A forward shock was observed at 2123 UT on May 1 (first dotted line). Bidirectional electrons (black bars) were seen prior to this shock, in association with an earlier CME event. The May 1 shock was followed by a clear CME (solid lines), with counterstreaming electrons, a depressed proton temperature, and an increased He^{++}/H^+ ratio beginning between 3–5 UT on May 2. A further temperature decrease and increase in He^{++}/H^+ ratio were observed at 12 UT. This CME was expanding, as indicated by the decreasing speed from front to rear. The He^{++}/H^+ ratio reached extremely high levels during the CME, with an average value of 8%, and individual points as high as 30%.

Magnetic field rotations characteristic of a magnetic cloud were observed from 13 UT on May 2 to 12 UT on May 3 (dashed lines). The field angle rotated by ≈65° during this event, including rotations both in and perpendicular to the ecliptic plane. The cloud also displayed a strong magnetic field with low variance. Counterstreaming halo electrons were observed during much of the CME, indicating that most of the CME had a closed magnetic field topology. The periods of unidirectional electron flow in this CME are common, indicating open field lines within the CME [*Gosling et al.*, 1995].

A second forward shock (second dotted line) was observed at 17 UT on May 3, propagating into the back of the CME, and large increases in the plasma speed, temperature, and field strength were seen at ≈0230 UT on May 4. The latter event was not a shock, since the variations occurred over an extended period. We identify the temperature increase, decrease in He^{++}/H^+ ratio, and cessation of counterstreaming electron flow at 1 UT on May 4 as the end of the CME.

In many ways, the May 2–4 event fits the classical picture of a CME and magnetic cloud in the solar wind, as defined in the Introduction. However, one anomalous feature was observed: large fluxes of He^+ over an extended time. Significant He^+ (>0.1% of He^{++}) was seen beginning at 19 UT on May 2, and the He^+/He^{++} ratio was elevated above 0.5% for a period of over 24 hours, from 0 UT on May 3 through 1 UT on May 4. The He^+/He^{++} ratio reached a maximum value of ≈100% in individual 64 second samples, and a maximum hourly average of 45%, from 12–13 UT. The He^+/He^{++} ratio was quite variable, with fluctuations by a factor of 2–10 on time scales of a few minutes. He^+ was present both before and after the May 3 shock, with an increased kinetic temperature following the shock. After the May 4 discontinuity, He^+ cannot be distinguished in the spectra due to the high plasma speed and temperature. We are thus unable to specify the end of the He^+ event.

Figure 2 shows stacked SWEPAM ion flux spectra from 15 UT on May 2 to 7 UT on May 4, with ion flux plotted as a function of energy-per-charge (E/q) and time. Data were collected at angles within ≈30° of the solar wind beam, and have been summed over all angles and averaged over 20 64-second measurements. Since all solar wind ions travel with approximately the same bulk speed, ions with different mass-per-charge (m/q) ratios appear in the spectrum at different locations in E/q. When the distribution is cold, as in this event, different m/q states are well-resolved, and SWEPAM can measure the solar wind composition. To display the spectral peaks more clearly, the top portion of Figure 2 shows a one hour averaged spectrum. Peaks are labeled by E/q ratio relative to the proton peak (E/q=1).

The lowest E/q peaks in the spectra are the solar wind protons, starting at E/q≈1.8 keV/q at 15 UT on May 2. He^{++} is observed at E/q=2 relative to the proton peak. In contrast to typical solar wind measurements, the spectra also show large, well-defined peaks at E/q=4 relative to protons, which we identify as He^+. This peak is seen from ≈19 UT on May 2 through ≈1 UT on May 4, making this the longest reported He^+ enhancement. Part of this increased length may be due to the increased sensitivity of SWEPAM over many early solar wind instruments, allowing detection of very low He^+ levels. Although a peak at E/q=4 could

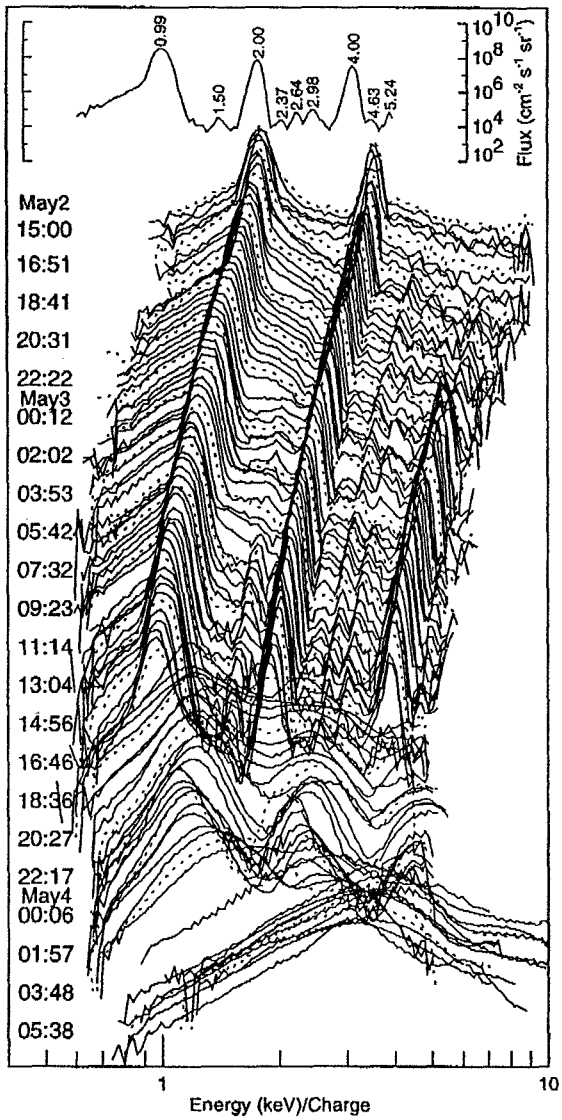

Figure 2. Ion flux spectra ($cm^{-2}s^{-1}sr^{-1}$) as a function of energy-per-charge (keV/q) and time (top to bottom) for May 2–4, 1998. Time labels are given for every fifth spectrum (dashed lines). The top panel shows a one hour averaged flux spectrum from 10–11 UT on May 3. Peaks are labeled by E/q value relative to protons.

be produced by several solar wind ions (e.g. O^{+4}, C^{+3}, Si^{+7}), and may include small contributions from these species, the large amplitude of the E/q=4 peak strongly suggests this peak is almost entirely due to He^+, rather than a less abundant element. Observations of significant He^+ by the Solar Wind Ion Composition Spectrometer (SWICS) instrument on ACE support this conclusion [*Gloeckler et al.*, 1998]. The SWEPAM and SWICS He densities in general show good agreement, although there are some quantitative differences in the He^+ density due to complicated instrument efficiency factors. In addition to the three main peaks, smaller peaks can be distinguished at other E/q ratios, including 1.5 ($^3He^{++}$), 2.67 (O^{+6}), 2.37 (Si^{+12}, O^{+7}, or C^{+5}), and 3.0 (C^{+4} or Si^{+9}). The fluxes of these ions are 2–3 orders of magnitude lower than the He^+ flux.

The May 2 4 event was associated with a halo CME observed at the Sun by the LASCO C2 coronagraph on SOHO starting at 1658 UT on May 29. Prominence material was observed by LASCO starting at 1931 UT [*C. St. Cyr, personal communication*, 1998]. The event was also observed by the SOHO/EIT instrument, which recorded a filament disappearance and an eruption on the disk with onset at ≈1610 UT [*B. J. Thompson, personal communication*, 1998]. LASCO observed a second halo CME on May 2, which may be associated with the May 3 shock and May 4 discontinuity in the ACE data [*C. St. Cyr, personal communication*, 1998].

Discussion

Although significant amounts of He^+ have been observed in the solar wind on only a few occasions, all nominally within CMEs, it is notable that each event has been quite different, suggesting that complex processes control the ionization state. The event presented here is unique in that the He^+ enhancement was both very large and persisted for an extended time, more than 24 hours, over the latter half of the CME. In comparison, *Schwenn et al.* [1980] observed a He^+/He^{++} ratio of 3–10% for ≈2 hours at the beginning of a CME and again for 5 hours near the middle of the CME, and *Gosling et al.* [1980] reported He^+/He^{++} ratios of 30% for ≈1 hour early in a CME. *Burlaga et al.*, [1998] measured a He^+/He^{++} ratio of 1% only near the end of a magnetic cloud, for ≈2.5 hours.

The He^+ observed within a large portion of the May, 1998 CME is most easily explained as prominence material incompletely ionized as it passed outward through the corona. The observation of prominence material by SOHO at the time of this CME supports this interpretation, but the question of how such an extended interval of He^+ enhancement is produced remains unanswered. Solar coronagraph observations of a CME containing prominence material throughout a large portion of its volume are not without precedent [*Hundhausen*, 1988]. In addition, the observation presented here shows that, on occasion, low charge state prominence material can comprise a large fraction of a CME in the solar wind.

We have attempted to relate the He^+ observations to other features of the CME, but find little correlation. The He^+ enhancement occurred during a high density period, but was not directly correlated with variations in the H^+ or He^{++} densities. Although the He^+ enhancement was observed during a magnetic cloud and CME, it was not directly correlated with a specific magnetic field configuration or with the changes in topology indicated by counterstreaming electrons. These results contrast with the *Burlaga et al.*, [1998] observation of a narrow region of He^+ at the back of a magnetic flux rope in association with very high H^+ and He^{++} densities, a result they explained by the difference in density between the solar corona and a filament.

In one suggested model for a CME, prominence material is assumed to be a thin sheet inside a magnetic flux rope cavity at the back of the CME [e.g. *Low and Hundhausen,* 1995]. This picture is consistent with the *Burlaga et al.* [1998] observation, but does not easily explain the extended He^+ observation presented here. The extension of the He^+ enhancement beyond the back of the cloud indicates that the flux rope topology of the cloud is not responsible for maintaining the low ionization state. Instead, the geometry appears to be more complex, with prominence material extending throughout much of the CME.

The E/q spectra for this event also reveal a complex picture. Although the presence of He^+ suggests a low ionization temperature, the distribution of oxygen charge states (Figure 2), with O^{+6} (E/q=2.7) more abundant than O^{+5} (E/q=3.2) or O^{+7} (E/q=2.3), suggests a normal oxygen ionization temperature ($\approx 10^6$ K). This CME thus appears to contain a mixture of hot and cold plasmas. Measurements by SWICS of both cold and hot ion charge states also indicate a mixture of plasmas [*Gloeckler et al.,* 1998], and mixtures were also seen in previous He^+ events [e.g. *Gosling et al.,* 1980]. Mixed ionization states may be explained by partial ionization of prominence material by the solar corona, since the ionization rate is different for different elements. A recent model [*Neukomm and Bochsler,* 1996] predicts that magnetically confined plasmoids may develop a mixture of hot and cold charge states as they travel out from the Sun. Mixing may also occur after the ionization state is frozen in, as changing magnetic topologies bring together plasmas with different ionization states.

Solar prominence eruptions are often associated with CMEs observed in the solar corona [*Gosling et al.,* 1974]. It is thus curious that solar wind He^+ enhancements are so uncommon. Despite nearly continuous solar wind measurements since 1971, the event discussed here is only the sixth reported. This rarity suggests that prominence material is usually completely ionized during transit through the corona. It is thus possible that prominence material is regularly observed in CMEs at 1 AU, but is not recognized as such because it is no longer distinguishable as ionizationally cold.

Acknowledgments. We thank Chris St. Cyr and Barbara Thompson for information about SOHO/LASCO and EIT observations, and Ed Santiago and Dot Delapp for developing SWEPAM data processing algorithms. Work at Los Alamos was performed under the auspices of the U. S. Department of Energy with financial support from the NASA ACE program. CWS and NFN acknowledge partial support from the Caltech ACE project office. Work by JTS while at MIT was supported by the NASA WIND program.

References

Burlaga, L., E. Sittler, F. Mariani, and R. Schwenn, Magnetic loop behind an interplanetary shock: Voyager, Helios, and IMP 8 observations, *J. Geophys. Res., 86,* 6673, 1981.

Burlaga, L., et al., A magnetic cloud containing prominence material: January 1997, *J. Geophys. Res., 103,* 277, 1998.

Gloeckler, G., et al., Unusual composition of the solar wind in the 2-3 May 1998 CME observed with SWICS on ACE, *Geophys. Res. Lett., this issue,* 1998.

Gosling, J. T., Coronal mass ejections and magnetic flux ropes in interplanetary space, in *Physics of Magnetic Flux Ropes,* edited by C. T. Russell, E. R. Priest, and L. C. Lee, pp. 343, AGU, Washington, D. C., 1990.

Gosling, J. T., et al., Mass ejections from the Sun: A view from Skylab, *J. Geophys. Res., 79,* 4581, 1974.

Gosling, J. T., et al., Observations of large fluxes of He^+ in the solar wind following an interplanetary shock, *J. Geophys. Res., 85,* 3431, 1980.

Gosling, J., J. Birn, and M. Hesse, Three-dimensional magnetic reconnection and the magnetic topology of coronal mass ejection events, *Geophys. Res. Lett., 22,* 869, 1995.

Hundhausen, A. J., The origin and propagation of coronal mass ejections, in *Proceedings of the Sixth International Solar Wind Conference,* edited by V. J. Pizzo, T. Holzer, and D. Sime, pp. 181, NCAR, Boulder, CO, 1988.

Kozlovsky, B.-Z., The stages of ionization of oxygen and helium in the solar wind, *Solar Phys., 5,* 410, 1968.

Low, B. C. and J. R. Hundhausen, Magnetostatic structures of the solar corona II. The magnetic topology of quiescent prominences, *Astrophys. J., 443,* 818, 1995.

McComas, D. J., et al., Solar Wind Electron Proton Alpha Monitor (SWEPAM) for the Advanced Composition Explorer, *Space Sci. Rev., in press,* 1998a.

McComas, D. J., et al., An unusual coronal mass ejection: First Solar Wind Electron, Proton, Alpha Monitor (SWEPAM) results from the Advanced Composition Explorer, *Geophys. Res. Lett., in press,* 1998b.

Neukomm, R. O. and P. Bochsler, Diagnostics of closed magnetic structures in the solar corona using charge states of helium and of minor ions, *Astrophys. J., 465,* 462, 1996.

Ogilvie, K. W., et al., SWE, A comprehensive plasma instrument for the WIND spacecraft, *Space Sci. Rev., 71,* 55, 1995.

Schwenn, R., H. Rosenbauer, and K.-H. Mühlhäuser, Singly-ionized helium in the driver gas of an interplanetary shock wave, *Geophys. Res. Lett., 7,* 201, 1980.

Smith, C. W., et al., The ACE magnetic fields experiment, *Space Sci. Rev., in press,* 1998.

Zwickl, R. D., et al., He^+ and other unusual ions in the solar wind: A systematic search covering 1972-1980, *J. Geophys. Res., 87,* 7379, 1982.

S. J. Bame, W. C. Feldman, J. T. Gosling, D. J. McComas, R. M. Skoug, J. T. Steinberg, and R. L. Tokar, MS D466, Los Alamos National Laboratory, Los Alamos, NM 87545 (e-mail: rskoug@lanl.gov)

P. Riley, SciberNet, Inc., 5414 Oberlin Dr., Suite 251, San Diego, CA 92121

L. F. Burlaga, NASA Goddard Space Flight Center, Greenbelt, MD 20771

N. F. Ness, C. W. Smith, University of Delaware-Bartol Research Institute, Newark, DE 19716

(Received September 1, 1998; revised October 26, 1998; accepted October 29, 1998.)

Appendix 8

Combined Ulysses solar wind and SOHO coronal observations of several west limb coronal mass ejections

O. Funsten, J. T. Gosling, P. Riley, O. C. St. Cyr, R. J. Forsyth, R. A. Howard, and R. Schwenn

Journal of Geophysical Research, 104, 6679, 1999.

JOURNAL OF GEOPHYSICAL RESEARCH, VOL. 104, NO. A4, PAGES 6679–6689, APRIL 1, 1999

Combined Ulysses solar wind and SOHO coronal observations of several west limb coronal mass ejections

H. O. Funsten,[1] J. T. Gosling,[1] P. Riley,[2] O. C. St. Cyr,[3] R. J. Forsyth,[4]
R. A. Howard,[5] and R. Schwenn[6]

Abstract. From October 1996 to January 1997, Ulysses was situated roughly above the west limb of the Sun as observed from Earth at a heliocentric distance of about 4.6 AU and a latitude of about 25^0. This presents the first opportunity to compare Solar and Heliospheric Observatory (SOHO) limb observations of coronal mass ejections (CMEs) directly with their solar wind counterparts far from the Sun using the Ulysses data. During this interval, large eruptive events were observed above the west limb of the Sun by the Large Angle Spectrometric Coronagraph (LASCO) on SOHO on October 5, November 28, and December 21-25, 1996. Using the combined plasma and magnetic field data from Ulysses, the October 5 event was clearly identified by several distinguishing signatures as a CME. The November 28 event was also identified as a CME that trailed fast ambient solar wind, although it was identified only by an extended interval of counterstreaming suprathermal electrons. The December 21 event was apparently characterized by a 6-day interval of nearly radial field and a plasma rarefaction. For the numerous eruptive events observed by the LASCO coronagraph during December 23-25, Ulysses showed no distinct, individual CMEs, perhaps because of intermingling of two or more of the eruptive events. By mapping the Ulysses observations back in time to the Sun assuming a constant flow speed, we have identified intervals of plasma that were accelerated or decelerated between the LASCO and Ulysses observations.

1. Introduction

Coronal mass ejections (CMEs) are eruptions of large quantities of material from closed magnetic field regions in the solar atmosphere into interplanetary space (e.g., *Gosling et al.* [1991]). The characteristics of CMEs close to the Sun have been studied using the Skylab, Solwind, SMM, and Solar and Heliospheric Observatory (SOHO) coronagraphs. These studies show that frequency of occurrence of CMEs varies by over an order of magnitude over the 11-year solar activity cycle (e.g., *Webb and Howard,* [1994]), CMEs generally result from the reconfiguration of a magnetic field structure surrounding eruptive prominences [*St. Cyr and Webb*, 1991], ejection masses lie within a range of 10^{15} to 10^{16} g (e.g., *Hundhausen* [1993] and *Jackson and Howard* [1993]), and leading edge speeds close to the Sun vary over a wide range from less than 50 km s^{-1} to more than 2000 km s^{-1} [*Gosling et al.*, 1976; *Howard et al.*, 1985; *Hundhausen et al.*, 1994].

In interplanetary space, CMEs can be identified by any of several plasma signatures (see, for example, reviews by *Gosling* [1990, 1996] and *Neugebauer and Goldstein* [1997]), including counterstreaming suprathermal electrons [*Bame et al.*, 1981; *Gosling et al.*, 1987], bidirectional energetic protons [*Palmer et al.*, 1978; *Richardson and Reames,* 1993], anomalously low proton and electron temperatures [*Gosling et al.*, 1973; *Montgomery et al.*, 1974], and high helium abundances [*Borrini et al.*, 1982]. The faster CMEs drive shocks that propagate into the ambient solar wind [*Sheely et al,* 1985; *Cane et al.*, 1987], and CMEs at large heliocentric distances often have a low plasma density caused by expansion [*Gosling et al.*, 1998]. Magnetic field signatures of CMEs include strong, quiet magnetic fields [*Burlaga and King,* 1979; *Burlaga et al.*, 1981] and the smooth field rotations characteristic of magnetic clouds [*Burlaga et al.*, 1981; *Lepping et al.*, 1990].

Ulysses was launched on October 6, 1990 and used a Jupiter swingby to attain a nearly polar orbit around the Sun with a nearly fixed longitude in an inertial reference frame. With this orbit the longitude of Ulysses relative to Earth increases by slightly more than 1^0 per day, and Ulysses is situated above the east and west limbs of the Sun once each year. Such times provide a unique opportunity to study CMEs previously observed close to the Sun by SOHO. Previous studies of CMEs observed both on the limb and in the solar wind include those of *Sheeley et al.* [1985] (Solwind and Helios) and *Richardson et al.* [1994] (SMM and ICE).

The purpose of the present paper is to compare the SOHO observations of three CME events observed above the west limb of the Sun with Ulysses magnetic field and plasma observations of the same events far from the Sun. During the

[1] Los Alamos National Laboratory, Los Alamos, New Mexico.
[2] Science Applications International Corporation, San Diego, California.
[3] Computational Physics, Inc., Naval Research Laboratory, Washington, D.C.
[4] The Blacklett Laboratory, Imperial College, London.
[5] Naval Research Laboratory, Washington, D.C.
[6] Max Planck Institut für Aeronomie, Lindau, Germany.

Paper number 1998JA900088.
0148-0227/99/1998JA900088$09.00

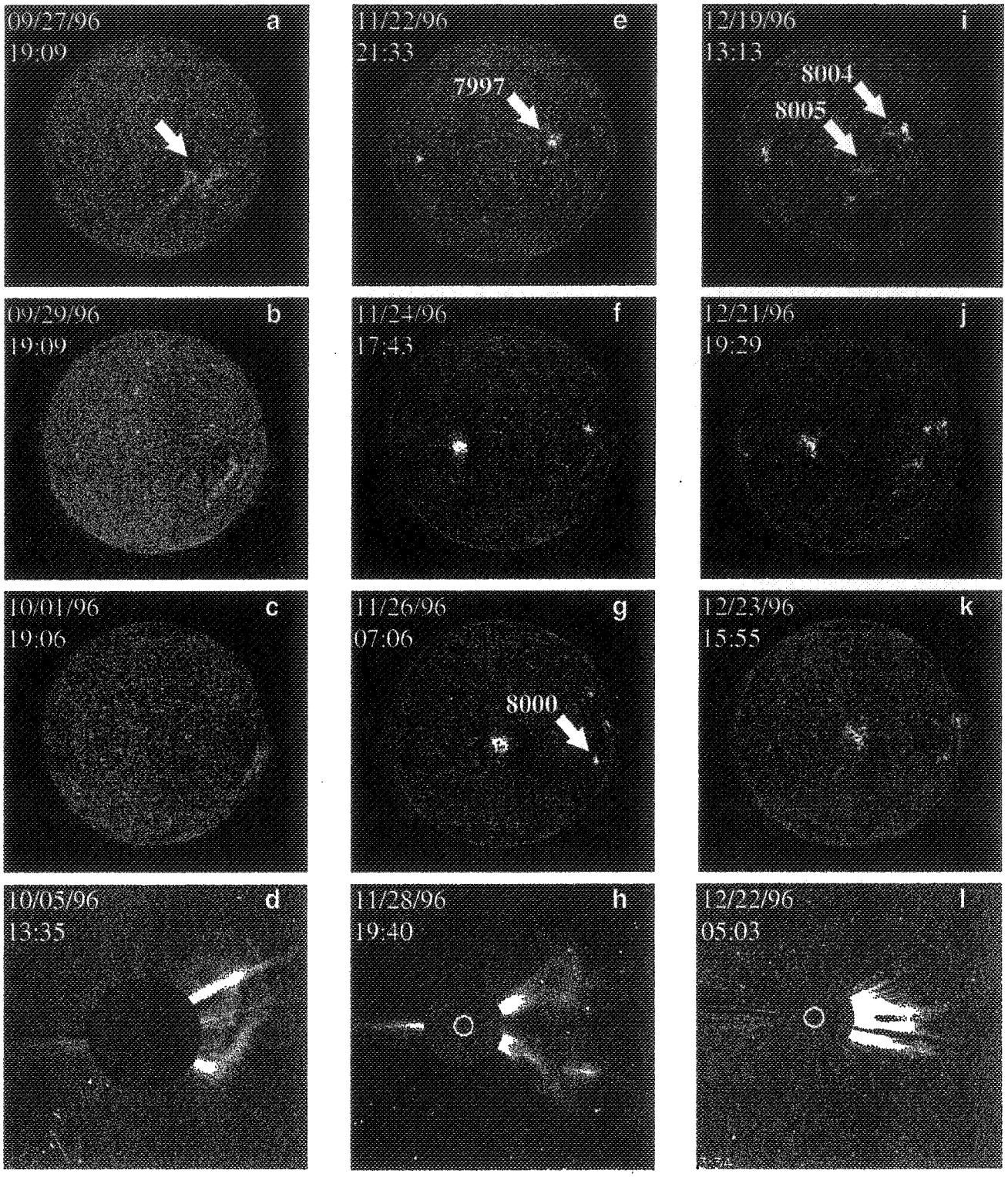

Plate 1. Full solar disk images using the extreme ultraviolet imaging telescope (EIT) (304 Å HII) in Plates 1a-1c, 1e-1g, and 1i-1k show the rotation of active regions toward the west limb at times before the October 5, November 28, and December 21-25 west limb coronal mass ejections (CMEs), respectively. Plates 1d, 1h, and 1l show a Large Angle Spectrometric Coronagraph (LASCO) image of each of the events. The CMEs observed by both SOHO and Ulysses originated from a single band of active longitudes that was first observed in July 1996 and persisted through December 1996. NOAA active regions AR 7997, AR 8000, AR 8004, and AR 8005 are noted in the panels.

latter part of 1996, which was near solar activity minimum, CME events were much less frequent than at solar maximum and were concentrated at low latitudes. In October 1996, Ulysses was traveling southward at a latitude of 30°N and had not detected any CMEs during the previous ~1.5 years as it had traversed the northern hemisphere [*Gosling et al.*, 1997]. The relative infrequency of CME events as Ulysses entered the northern edge of the band of solar wind variability late in 1996 enabled relatively unambiguous association of events isolated in time observed by Ulysses at ~4.5 AU to events observed at the Sun by SOHO.

The SOHO data provided the time that the CME was first observed close to the Sun and its speed close to the Sun in the plane of the sky. The Ulysses observations provided detailed in situ measurements of the ambient solar wind parameters preceding and following the CME in addition to the internal properties of the CME far from the Sun. Using both SOHO and Ulysses observations, we study the evolution of the CMEs from their departure from the Sun to Ulysses.

2. Observations

Solar coronagraph images were obtained from the Large Angle Spectrometric Coronagraph (LASCO) experiment on SOHO [*Brueckner et al.*, 1995]. In particular, we used images from the C2 and C3 white light optical systems, which have overlapping fields of view of 1.5-6 R_S and 3.5-30 R_S, respectively, where R_S is the solar radius. The pylon supporting the occultation disk is located at the southeast quadrant of the field of view, enabling unobstructed viewing of events emitted above the west limb of the Sun as viewed from Earth. LASCO images for each of the events studied in this paper are shown in Plates 1d, 1h, and 1l.

Because coronagraphs observe CMEs projected into the plane of the sky, they cannot uniquely determine the central longitude of an event (see *Hundhausen* [1993, Appendix B] for the projection geometry). A radial structure emitted either behind or in front of the limb of the Sun would therefore have an apparent latitude as viewed by SOHO that is higher than its actual latitude and an apparent speed that is less than its actual speed.

The Ulysses payload includes solar wind ion and electron instruments that measure 3-dimensional particle distributions over an energy-per-charge range of 0.257-35.0 keV/charge for ions and an energy range of 0.81-862 eV for electrons [*Bame et al.*, 1992]. From October 1996 to January 1997, Ulysses observed one CME in October, one CME in December, and several possible CME-like episodes in January. As will be shown later, we extrapolate the events observed at Ulysses back in time to the Sun. For each of these events, the extrapolated time that the CME left the Sun lies within 1.5 days of a prominent eruptive event observed by LASCO near the west limb. These solar events occurred on October 5, November 28, and December 20-25, 1996 (see Plate 1). When Ulysses observed these events, it was located at radial distances ranging from 4.44 AU to 4.73 AU and latitudes ranging from 31.5°N to 25.6°N.

The CMEs observed by LASCO and Ulysses were associated with a single band of active longitudes on the Sun. Plate 1 shows full-disk images using the He II (304 Å) emission line obtained from the extreme ultraviolet imaging telescope (EIT) on SOHO [*Delaboudinière et al.*, 1996]. These images show the regions of activity at several points in time preceding the October 5 (Plates 1a-1c), November 28 (Plates 1e-1g), and December 20 (Plates 1i-1k) events.

2.1. October 5, 1996, Event

The first LASCO observations of the October 5, 1996, west limb event occurred at 1040 UT at a heliocentric distance of 2.5 R_S. Plate 1d shows a LASCO C2 coronagraph image of the CME at 1335 UT on October 5. The CME came from a region of activity, shown by the arrow in Plate 1a. The rotation of this active region toward the west limb is illustrated in Plates 1b and 1c. By the time that the CME is first observed by LASCO on October 5, this region of activity has rotated beyond the west limb.

Figure 1a shows the apparent heliocentric distance and apparent latitude for several points in time derived using images from the LASCO C2 and C3 coronagraphs. At the time that this CME was emitted from the Sun, Ulysses was 50° behind the west limb at a radial distance of 4.44 AU. The dashed line in Figure 1a shows the apparent latitude of Ulysses in the plane of the sky as viewed from near Earth at the time that the CME was first detected at Ulysses. The 35.2°N apparent latitude and the actual Ulysses latitude of 24.4°N differ by 10.8°.

Figure 1b shows the radial height of the CME leading edge at an apparent latitude of 35°N above the west limb of the Sun as a function of time. After the leading edge reaches an apparent height of ~7 R_S, it maintains a constant speed of ~650 km s^{-1} at the apparent latitude of Ulysses. This speed corresponds to the slope of the solid line, which is a linear fit to the data after 1200 UT.

Figure 2 shows 2.5-min averages of the magnetic field polar angle θ (line) and azimuthal angle ϕ (dots), magnetic field strength B, proton density n_p, bulk flow speed v, proton temperature T_p, proton pressure P, and helium-to-hydrogen abundance ratio He^{++}/H^+ observed by Ulysses and associated with the October 5 west limb event observed by LASCO. Typical solar wind parameters at 4.5 AU include $n_p \approx 0.3$ cm^{-3}, $v \approx 400$ km s^{-1}, and a He^{++}/H^+ ratio of ~4%. Periods of counterstreaming suprathermal electrons, observed in the two energy passbands covering 30-172 eV, are shown at the top of Figure 2. The magnetic field is defined in the spacecraft radial-tangential-normal (RTN) coordinate system, where θ is the polar angle relative to the radial direction toward the Sun and ϕ is the azimuthal angle.

The CME was preceded by a forward shock on October 13 that was driven by the expanding CME. While several identifying signatures can be used for CME identification [*Goldstein et al.*, 1998], we have identified the CME material using the prolonged intervals of counterstreaming suprathermal electrons extended for a week (see *Gosling et al.* [1998] for a preliminary discussion of this CME). Within the CME, Ulysses also observed enhanced helium abundances and unusually low proton temperatures. The flow speed decreased from 800 km s^{-1} to 550 km s^{-1} from the front to the rear of the CME, indicating that the CME was still expanding at 4.5 AU (for other studies of expanding CMEs, see *Farrugia et al.* [1993], *Burlaga* [1995], *Chen and Garren* [1993], and *Gosling et al.* [1998]). The declining speed and minimum in the proton density, temperature, and pressure at the center of the CME clearly show rarefaction of the material within the CME. Note that the forward shock that passed

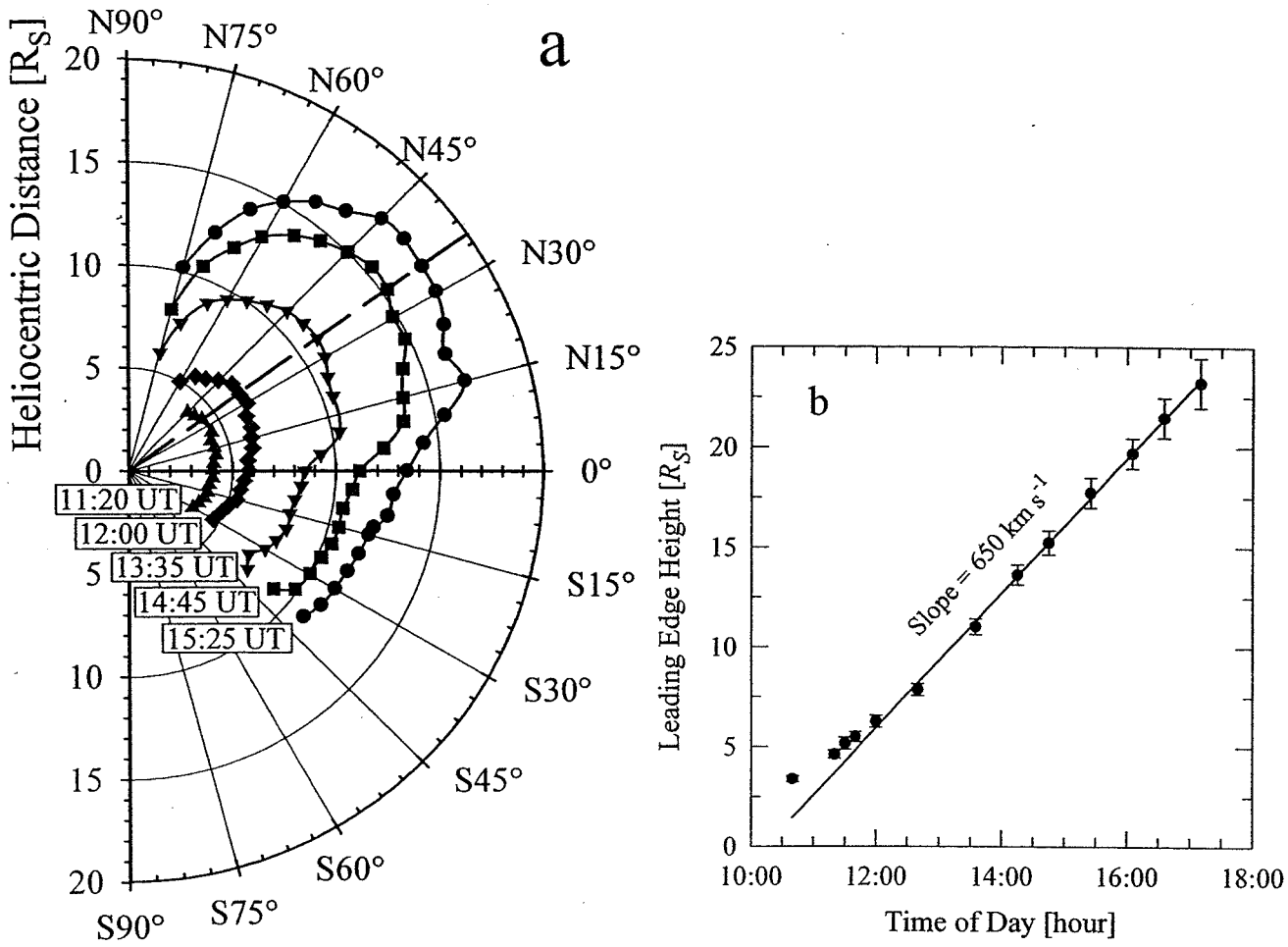

Figure 1. LASCO observations of the October 5, 1996, CME: (a) Latitude profiles of the leading edge are shown at several points in time, where the Ulysses latitude projected onto the plane of the sky (35.2°N) is shown in the dashed line. (b) The CME leading edge height is shown as a function of time. The leading edge maintains a constant speed after reaching a height of ~7 R_S. The slope of the line fitted to the data corresponds to a leading edge speed of 650 km s^{-1} near the Ulysses latitude.

Ulysses on October 19, whose origin was not identified, was propagating through the rarefied material. Additionally, a nearly radial magnetic field directed antisunward was observed from late October 16 through October 19. On the basis of the bulk flow speed and the length of time Ulysses observed the CME, the radial thickness of the CME along the line of passage through the spacecraft at a heliocentric distance of 4.4 AU was ~2.5 AU.

We are particularly interested in the evolution of the CME plasma as it traveled from the Sun to Ulysses. While no measurements exist between the SOHO and Ulysses observations, we can infer several characteristics of this evolution using the time t_{SOHO} when the leading edge was first observed by SOHO, the speed v_{SOHO} near the Sun from SOHO observations, and the plasma properties at Ulysses.

Using the Ulysses plasma observations alone, we calculate the time t_C that the CME plasma left the Sun using

$$t_C = t_U - r_U / v_U, \quad (1)$$

where t_U, r_U, and v_U are the time of observation, heliocentric distance and the flow speed of plasma at Ulysses. Equation (1) assumes no net acceleration or deceleration of the CME throughout its transit. If a CME accelerates from the Sun to Ulysses, then its speed v_U at Ulysses will be greater than that at the Sun. The calculated time t_C at which the CME left the Sun using Equation (1) will therefore be later than t_{SOHO}. Alternately, if the CME decelerates between the Sun and Ulysses, then t_C will lie earlier than t_{SOHO}. Figure 2 (bottom) shows t_C as a function of the Ulysses observation time. The dotted line in Figure 2 corresponds to the time t_{SOHO} that the CME leading edge was first observed by SOHO. Inspection of this diagram indicates whether plasma within the event has been accelerated (t_C later than t_{SOHO}) or decelerated (t_C earlier than t_{SOHO}).

At the front of the CME, t_C lies at an earlier time than t_{SOHO}, indicating that this plasma has decelerated between the Sun and Ulysses. We expect this deceleration at the front of the CME since it is expanding into the slower solar wind ahead and driving a pressure wave. From October 16 through late October 19, t_C lies within 0.5 day of t_{SOHO}. If we assume that the CME plasma departed the Sun within a time close to t_{SOHO}, then this plasma has apparently undergone little or no net

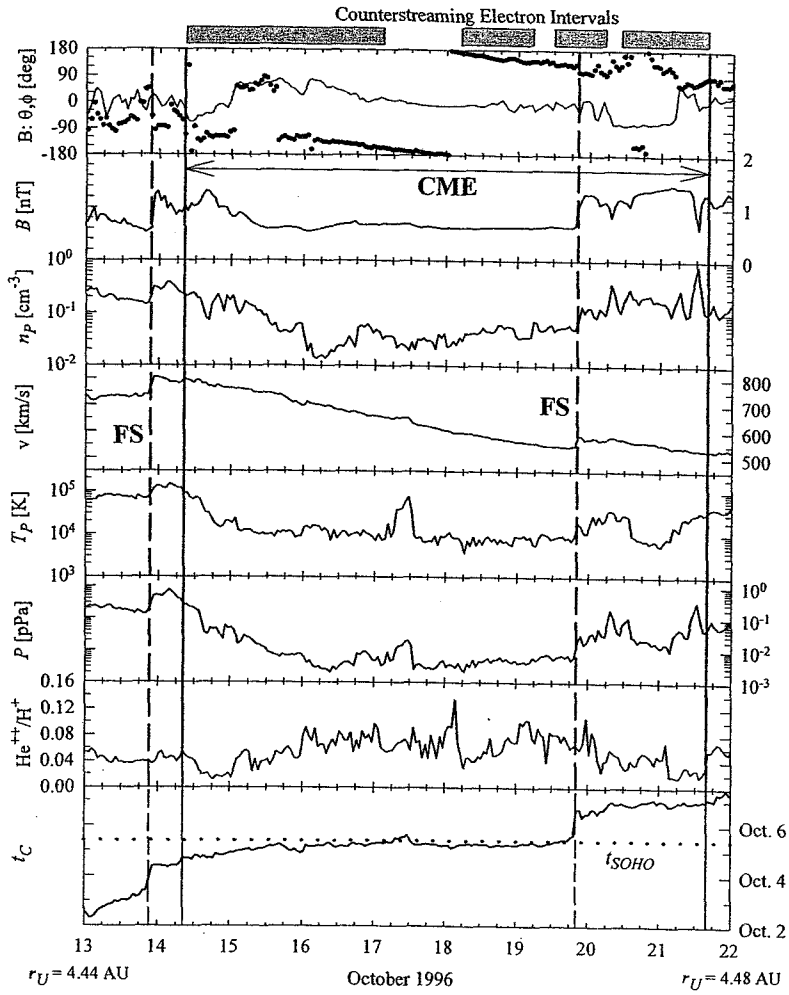

Figure 2. Ulysses magnetic field and plasma data for the CME associated with the October 5 event observed by SOHO. The panels show the magnetic field vector in the RTN coordinate system (polar angle θ and azimuthal angle ϕ), magnetic field strength B, proton density n_P, bulk solar wind flow speed v, proton temperature T_P, proton pressure P, and the ratio He^{++}/H^+ of helium to hydrogen abundances. The solid lines define the CME, which was identified by counterstreaming electrons, a modest magnetic field rotation, high helium abundance, and an anomalously low proton temperature. The forward shock (FS) observed on October 13 is associated with the CME. The origin of the forward shock on October 19 is not known. The bottom diagram shows the time t_C that the CME left the Sun calculated using the flow speed at Ulysses versus the actual time of observation at Ulysses. The dotted horizontal line in the bottom diagram indicates the time t_{SOHO} that LASCO first observed the event.

acceleration during its transit from the Sun to Ulysses. From October 19 to October 21, t_C lies later in time than t_{SOHO}, indicating acceleration of this plasma by the forward shock observed at Ulysses on October 19.

A large discrepancy exists between the apparent leading edge speed of 650 km s^{-1} observed near the Sun by LASCO and the leading edge speed of 800 km s^{-1} observed at ~4.4 AU by Ulysses. Furthermore, Figure 2 (bottom) suggests that the leading edge has decelerated between the Sun and Ulysses. We resolve these apparent contradictions by considering both the longitude of emission and deceleration of the CME as it traveled in interplanetary space to Ulysses.

The calculated speed v_C of the leading edge at the Sun is based on the transit time $t_U - t_{SOHO}$ of the CME from the Sun to Ulysses according to

$$v_C = 2\langle v \rangle - v_U = \frac{2\, r_U}{t_U - t_{SOHO}} - v_U \,, \qquad (2)$$

where $\langle v \rangle$ is the average speed of the CME leading edge between the Sun and Ulysses. Equation (2) assumes that acceleration of the leading edge is constant from the Sun to Ulysses. We note that this assumption does not necessarily reflect either the spatial scale of deceleration or the fact that most deceleration should occur close to the Sun where the pressure gradients between a CME and the ambient wind are probably largest.

Using v_U = 800 km s^{-1} and a transit time of 8.9 days, we obtain v_C = 935 km s^{-1}, which is significantly greater than the apparent leading edge speed v_{SOHO} = 650 km s^{-1}. Therefore the

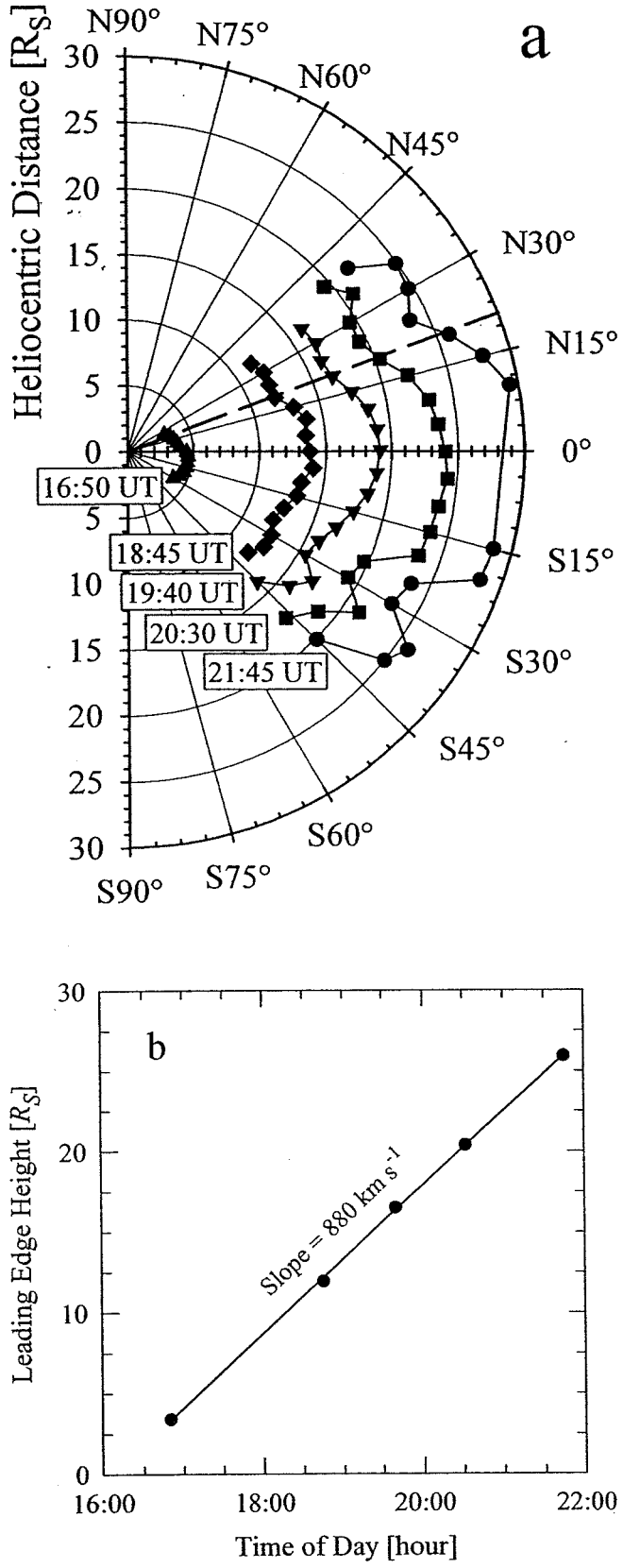

Figure 3. LASCO observations of the November 28, 1996, CME: (a) Latitude profiles of the leading edge are shown at several points in time, where the Ulysses latitude projected onto the plane of the sky (20.6°N) is shown in the dashed line. (b) The CME leading edge height is shown as a function of time. The slope of the line fitted to the data corresponds to a leading edge speed of 819 km s^{-1} near the Ulysses latitude.

leading edge as observed by SOHO must have been at a longitude significantly out of the plane of the sky.

By comparing the calculated speed v_C of the leading edge at the Sun and the its apparent speed v_{SOHO} observed by SOHO, we can infer the longitudinal angle ϕ_C of the observed leading edge relative to west limb of the Sun using

$$\phi_C = \cos^{-1}\left(\frac{v_{SOHO}}{v_C}\right). \quad (3)$$

General agreement of this calculated longitude with the Ulysses longitude provides a self-consistent verification of the Equations (2) and (3) and validates the assumption that the CME deceleration is roughly constant from the Sun to Ulysses.

Using v_C = 935 km s^{-1} and v_{SOHO} = 650 km s^{-1}, we calculate that the leading edge of the central section of the CME as observed by SOHO was directed at a longitudinal angle of ϕ_C = 46° behind the west limb of the Sun. This is quite close to the Ulysses longitude of 49° behind the west limb, so we conclude that the CME leading edge observed by SOHO was generally directed toward Ulysses.

As shown in Plates 1a-1c, a single band of active longitudes was clearly observed as it progressed toward the west limb. This region first appeared in July 1996 (NOAA AR 7978) and persisted through December 1996 (it can be seen in subsequent Plates 1e-1f and 1i-1j). All of the CMEs described in this paper are loosely associated with this single band of active longitudes.

Preceding the October 5 event, the time of central meridian passage of this large-scale region of activity was early September 26, and it had rotated to ~34° behind the west limb by the time the October 5 event was first observed by SOHO. A CME was observed on September 25 near the central meridian longitude and originated from the eruption of a structure within this active region and along a nearly north-south filament channel extending from the active region down to the south polar crown filament [*Schmieder et al.*, 1997]. While events behind the limb of the Sun are generally difficult to observe, *Watari et al.* [1997] identified this active region as the origin of the October 5 CME, and at least part of the eruptive structure was estimated to be ~2 days, or ~28°, behind the west limb when the CME was first observed. This is 20° closer in longitude to the west limb than the longitude calculated using Equation (3). Furthermore, this event was also detected in the low corona in emission lines of FeXIV by the LASCO C1 coronagraph, indicating that at least part of the CME was located near the plane of the sky. However, the study by *Schmieder et al.* [1997] demonstrated that an extended band of longitudes was involved in the September 25 CME, and we believe this is the case for the October 5 event.

2.2. November 28, 1996, Event

Plates 1f-1h show the rotation of NOAA AR7997 (5°N) toward the west limb and the emergence of NOAA AR8000 (14°S). The November 28 CME originated near these active regions, which also produced a C-level X-ray flare. EIT also observed post-CME loops within this area of activity.

The west limb CME event of November 28, 1996, which was first observed by LASCO at 1650 UT, had an apparent span of 90° in latitude as shown in Plate 1h. Figure 3a shows the apparent heliocentric distances and latitudes of the leading

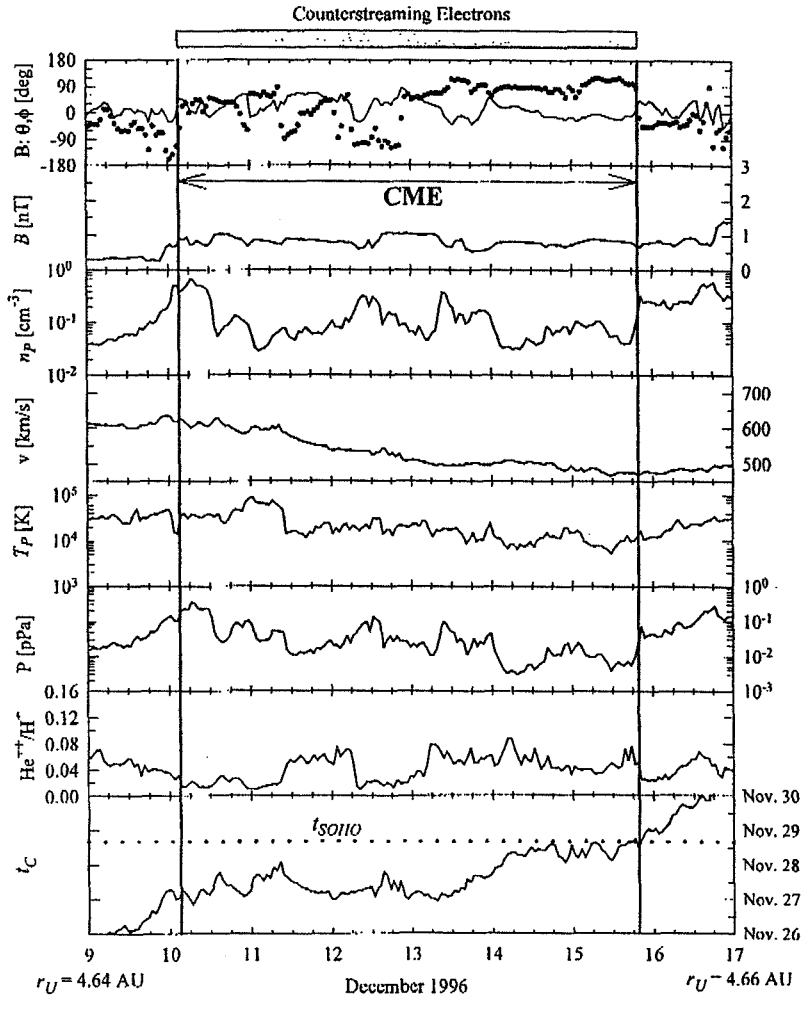

Figure 4. Ulysses magnetic field and plasma data for the CME associated with the November 28 event observed by SOHO. The solid lines define the CME, which was identified primarily by the extended interval of counterstreaming electrons. The bottom diagram shows the calculated time t_C that the CME left the Sun versus the actual time of observation at Ulysses. The dotted horizontal line in the bottom diagram indicates the time t_{SOHO} that LASCO first observed the event. While the CME as observed by LASCO was spectacular at the Sun, it likely would not have been identified as a CME at Ulysses without the counterstreaming electron signature.

edge of the CME at several times on November 28. The latitude of Ulysses when it first observed the CME was 20.5°N, and the projection of this latitude onto the plane of the sky as viewed from Earth was 20.6°N, which is shown as the dashed line in Figure 3a. From the sequential images of the CME leading edge at a latitude of 20°N shown in Figure 3b, we derive a constant leading edge speed of the CME equal to 819 km s^{-1} projected onto the plane of the sky.

Figure 4 shows magnetic field and plasma data measured at Ulysses at 4.65 AU and 27°N and apparently associated with the November 28 west limb event observed by SOHO. The CME material was identified by a period of counterstreaming suprathermal electrons spanning more than 5 days. Changes in the magnetic field direction were observed within the CME, although a smooth field rotation characteristic of a flux rope was not. The flow speed in the CME decreased from 600 km s^{-1} to ~475 km s^{-1} from front to rear, indicating that this CME was still expanding as it passed the spacecraft. The radial thickness of the CME at 4.6 AU was ~1.7 AU. No forward or reverse waves or shocks were observed in association with this event.

While it was an exquisite eruption at the Sun as viewed from SOHO (see the cover of *Eos Trans. AGU, 78*(17), Spring Meet. Suppl., 1997), the CME as observed in the plasma and magnetic field data was relatively benign. Ulysses observed no significant enhancement in the helium abundance, minimal compression of the leading edge plasma, a weak magnetic field rotation, and only a small increase in magnetic field strength. Indeed, this event likely would not have been identified as a CME without the counterstreaming electron measurements.

In Figure 4 (bottom), the calculated time t_C that various portions of the CME left the Sun based on Ulysses observations during December 10-16 lies within ~1.5 days of the onset of the November 28 event observed by SOHO. The net deceleration of the front half of the CME was nearly uniform, although the origin of this deceleration is not clear since this CME did not drive a large pressure wave. Only the

rear quarter of the CME appeared to have no net acceleration or deceleration.

The apparent leading edge speed v_{SOHO} = 880 km s^{-1} observed by SOHO near the Sun was significantly greater than the flow speed v_U = 620 km s^{-1} observed at Ulysses. From Equation (2) the calculated speed of the CME at the Sun was v_C = 789 km s^{-1}, which is ~10% slower than v_{SOHO}. As inferred from the bottom diagram in Figure 4, the leading edge of the CME decelerated by ~20% in interplanetary space. Since $v_C < v_{SOHO}$, we cannot use Equation (3) to estimate the initial CME longitude, although we can reasonably infer that the central part of the November 28 CME was located at a longitude nearly in the plane of the sky as observed by SOHO.

2.3. December 21-25, 1996, Events

During the interval of December 21-25, LASCO observed a rapid and complex series of eruptive solar events. The LASCO C3 coronagraph first observed a CME event at 2130 UT on December 21 (see Plate 1l). EIT observations indicate that this CME, which can be described as a ragged loop with a trailing core, was associated with a primarily NW-SE filament channel that was also associated with the September 25 CME. Then, during December 23-25, a series of eruptive events starting at 2020 UT on December 23 were observed. These have been associated with NOAA AR 8005 (shown in Plate 1i), which first appeared as AR 8000 on the previous Carrington rotation (shown in Plate 1g) [*Dere et al.*, 1997].

Figure 5a shows the apparent heliospheric distances and latitudes of the leading edge of the December 21 CME at several points in time. The heliographic latitude of Ulysses when it first observed the CME was 18.9°N, and the projection of this latitude onto the plane of the sky as viewed from Earth was 20.9°N, which is shown as the dashed line in Figure 5. In contrast to the October 5 and November 28 events, the leading edge profiles of the December 21 event indicate that Ulysses was located near the northern edge of the CME.

A plot of the leading edge height as a function of time, illustrated in Figure 5b, shows that the leading edge speed was 332 km s^{-1} at 10.3°N and 415 km s^{-1} at 5.2°N, and we expect that the leading edge speed at the apparent Ulysses latitude was slower than at 10.3°N. The fastest apparent leading edge speed of this event was ~455 km s^{-1} at both 10°S and 15°S, which is considerably slower than the October 5 and November 28 events. If the CME were directed at the longitude of Ulysses (~27° in front of the west limb), then we invert Equation (3) to derive the fastest actual leading edge speed of ~510 km s^{-1} at the Sun.

Figure 6 shows the magnetic field and plasma data during the time that one or more of the events observed by SOHO from December 21-25 passed by Ulysses. The first region of interest during this interval spans January 3 through the forward wave observed late on January 8. During this time, Ulysses observed an abnormally long (6-day) interval of nearly radial field (described by *Jones et al.* [1998]) during a rarefaction of the plasma, which included decrease in the speed v (from ~700 km s^{-1} to ~460 km s^{-1}), proton density n_P, proton pressure P, and proton temperature T_P. Neither counterstreaming suprathermal electrons nor a helium abundance enhancement were observed during this time interval.

Using Equation (1), the calculated time t_C that the plasma within the rarefaction left the Sun, illustrated in Figure 6

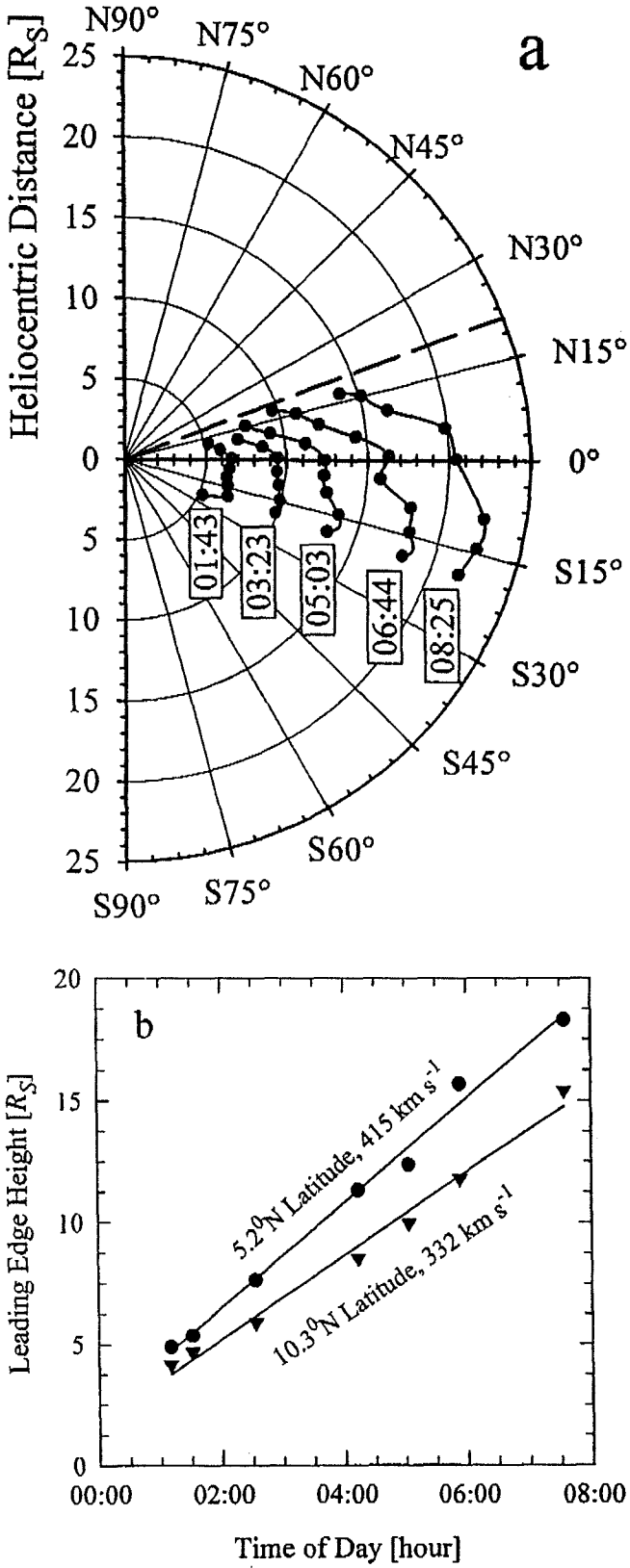

Figure 5. LASCO observations of the December 21, 1996, CME: (a) Latitude profiles of the leading edge are shown at several points in time, where the Ulysses latitude projected onto the plane of the sky (20.9°N) is shown in the dashed line. (b) The CME leading edge height is shown as a function of time at both 5.2°N and 10.3°N, and the leading edge speeds at these latitudes are 415 km s^{-1} and 332 km s^{-1}, respectively. Ulysses was apparently located at the northern edge of the CME.

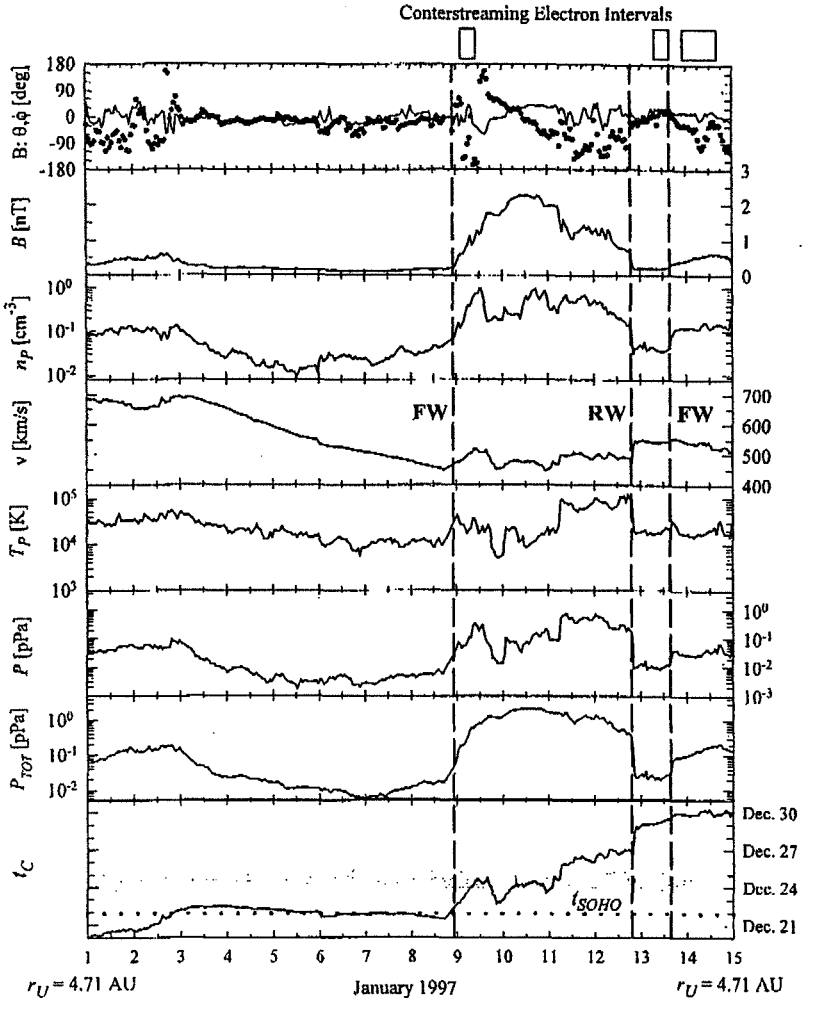

Figure 6. Magnetic field and plasma data for the time interval encompassing the December 21-25 events observed by SOHO. The dashed lines indicate a forward wave (FW) and reverse wave (RW). The interval of January 3-9 associated with the December 21 event is characterized by a radial magnetic field and a plasma rarefaction. The interval January 9-12 associated with the December 23-25 events contained a magnetic field rotation, a brief counterstreaming electron interval, and a high total (plasma + magnetic) pressure P_{TOT} and was bounded by forward and reverse waves. The bottom diagram shows the calculated time that the CME was emitted from the Sun versus the actual time of observation at Ulysses. The dotted horizontal line in the bottom diagram indicates the time that SOHO first observed the December 21 event, and the shadowed box shows the December 23-25 interval over which SOHO observed several CME events.

(bottom), lies quite close to the time t_{SOHO} that the December 21 CME was first observed by LASCO, which is shown as the lower dotted line. This suggests that the rarefaction and the CME observed by LASCO may be associated, although the flow speed within the event at Ulysses was generally much faster than the leading edge speed of the CME at the Sun, which probably was ~510 km s^{-1}.

The second region of interest in Figure 6 is an extended region of high pressure bounded by forward and reverse waves (but not shocks) on January 8 and 12, respectively. This time interval contains a mixture of possible CME signatures, including a brief episode of counterstreaming suprathermal electrons, a smooth magnetic field rotation of at least ~360° in ϕ, and a large magnetic field strength enhancement. Also observed were large increases in proton density, proton temperature, and proton pressure relative to the ambient wind in front of and behind the event. During this interval, the wind speed remained slow (450-500 km s^{-1}). Additionally, Ulysses observed two brief intervals in which the He^{++}/H^{+} ratio decreased from ~4% to ~2%.

As shown in Figure 6, the total (plasma + magnetic) pressure P_{TOT} during this interval was nearly 50 times that of the ambient wind. The bottom diagram also suggests that the plasma in this compression region departed the Sun close to the time that the series of CMEs were observed by LASCO, which is shown as the shaded band in the diagram. If the magnetic cloud was a single event that was emitted from the Sun, then its high internal pressure should have driven an expansion into the slower ambient solar wind [*Gosling et al.*, 1998]. This expansion would have produced signatures such as pressure enhancements at the leading and trailing edges, a declining speed across the event, and decreases in the temperature and pressure in the middle of the structure. However, none of these signatures were observed, so we infer that the compression region may be the result of the complex interactions of two or more of the events observed at the Sun

by SOHO during December 23-25 (see *Burlaga* [1995] for discussions of such effects).

Taken as a whole, the interval January 2-13 included a large rarefaction preceded by fast (700 km s^{-1}) ambient wind and followed by a strong compression region bounded by forward and reverse waves. *Gosling and Riley* [1996] showed that this is the characteristic signature that results when a slow CME is injected into faster ambient plasma. Both the rarefaction that forms on the leading edge of the CME and the compression that forms on the trailing edge serve to accelerate the CME to a higher wind speed while decelerating the leading and trailing ambient plasma. It is possible that the January 2-13 interval is a consequence of such processes. Persistent radial magnetic fields have been associated with declining speeds within CMEs, [*Neugebauer et al.*, 1997] although they occur at the trailing region of the CME and the longest observed duration was less than 2 days.

The addition of the LASCO observations to the Ulysses measurements clouds the interpretation of these events. Unique association of the SOHO events during December 21-25 with either the rarefaction having a radial field or the compression region bounded by forward and reverse waves is not feasible with high confidence because of several factors, including multiple events observed by SOHO over several days, possible mixing of these events during their travel to Ulysses, lack of information on the emission longitude of the events, LASCO observations suggesting the December 21 CME did not reach the Ulysses latitude, and no clear series of CMEs within the Ulysses data.

The isolation of the October 5 and November 28 events enables direct association of events observed by both SOHO and Ulysses. When several events are emitted from the Sun within a short time as in the case of the December 21-25 events, unique association of any individual event observed at the Sun by SOHO with Ulysses observations becomes difficult.

3. Summary

The location of Ulysses approximately above the northwest limb of the Sun in late 1996 and early 1997 has enabled direct association of SOHO observations of CMEs emitted at the Sun with observations of the same CMEs at Ulysses, located at a heliocentric distance of ~4.5 AU. These associations have revealed several aspects of the evolution of CMEs as they propagate into interplanetary space.

The October 5, November 28, and December 21-25 CMEs originated near Carrington longitudes of 281°, 221°, and 256°-227°, respectively. Over this time interval, no other prominent events were observed above the west limb by SOHO, indicating that these events were associated with a single band of active longitudes that was first observed in July 1996 associated with NOAA AR 7978 and persisted through December 1996. While large west limb CMEs were observed by both SOHO and Ulysses during Carrington rotations 1914 (October 5), 1915 (November 28), and 1917 (December 21-25), no events were observed at Ulysses during Carrington rotation 1916.

The CME observed by SOHO on October 5 was identified by prolonged intervals of counterstreaming suprathermal electrons, high helium abundance, and unusually low proton temperatures. The declining speed across the CME indicated that it was still expanding as it passed Ulysses (as is typical for many CMEs), and this expansion appears to have driven a forward shock. The leading edge speed of the CME at the Sun was calculated using Ulysses data to be 935 km s^{-1}, which was significantly greater than the speed of 650 km s^{-1} derived from the SOHO observations. This discrepancy was due to emission of the CME out of the plane of the sky at a longitude of 48° behind the west limb of the Sun. Between the SOHO observations, which show no deceleration of the leading edge plasma, and the time that the leading edge passed Ulysses, the leading portion of the CME was decelerated as it interacted with the ambient wind ahead.

While the November 28 event observed by SOHO was spectacular, it was identified only as a CME at Ulysses from the long interval of counterstreaming electrons. None of the other signatures common to CMEs in the solar wind were present. The CME was expanding as it passed by Ulysses, although it was not driving a large pressure wave in front because of the fast ambient wind speed ahead. Nevertheless, as with the October 5 event, the front half of the CME shows a net deceleration of plasma between the Sun and Ulysses. The CME leading edge speed near the Sun, which was calculated using combined SOHO and Ulysses observations, agreed closely with the speed derived from SOHO alone, indicating that the leading edge as observed by SOHO was located close to the plane of the sky.

During December 21-25 several CMEs were observed by LASCO. Unique association of the Ulysses observations with these events is difficult because of the numerous events departing from the Sun in a short time period. On the basis of the SOHO observations, Ulysses appeared to be located at the northern edge of the December 21 CME. The plasma that departed from the Sun during December 21-22, which was calculated using the flow speed measured by Ulysses, contained a plasma rarefaction and an abnormally long (6-day) interval of radial magnetic field, but no counterstreaming suprathermal electrons or enhanced helium abundance that would suggest a CME. Following this rarefaction, Ulysses observed a compression region with an abnormally high pressure bounded by forward and reverse waves that appeared to come from the Sun during the same time (December 23-25) that LASCO observed several CMEs departing the Sun. However, with such a large rarefaction and compression present, the plasma have been significantly accelerated, so accurately mapping the Ulysses results back to the Sun to infer a departure time of the event from the Sun is questionable. Counterstreaming electrons and a magnetic field rotation were observed within the compression region. Taken independently, this compression region was perhaps the interaction of two or more CMEs in interplanetary space. When the compression region is associated with the rarefaction, the collective Ulysses observations over January 2-13 suggest a slow CME injected into ambient high-speed solar wind. Thus, for the December 21-25 events, it is not a simple matter to relate specific features in the Ulysses observations to specific features in the SOHO events.

Acknowledgments. Work at Los Alamos was performed under the auspices of the United States Department of Energy with support from NASA.

Janet G. Luhmann thanks Daniel Berdichevsky and David F. Webb for their assistance in evaluating this paper.

References

Bame, S.J., J.R. Asbridge, W.C. Feldman, J.T. Gosling, and R.D. Zwickl, Bi-directional streaming of solar wind electrons >80 eV:

ISEE evidence for a closed-field structure within the driver gas of an interplanetary shock, *Geophys. Res. Lett., 8,* 173, 1981.

Bame, S.J., D.J. McComas, B.L. Barraclough, J.L. Phillips, K.J. Sofaly, J.C. Chavez, B.E. Goldstein, and R.K. Sakurai, The Ulysses solar wind plasma experiment, *Astron. Astrophys. Suppl. Ser., 92,* 237, 1992.

Borrini, G., J.T. Gosling, S.J. Bame, and W.C. Feldman, Helium abundance enhancements in the solar wind, *J. Geophys. Res., 87,* 7370, 1982.

Brueckner, G.E., et al., The large angle spectroscopic coronagraph (LASCO), *Sol. Phys., 162,* 357-402, 1995.

Burlaga, L. F., *Interplanetary Magnetohydrodynamics,* Oxford Univ. Press, New York, 1995.

Burlaga, L., and J.H. King, Intense interplanetary magnetic fields observed by geocentric spacecraft during 1963-1975, *J. Geophys. Res., 84,* 6633, 1979.

Burlaga, L., E. Sittler, F. Mariani, and R. Schwenn, Magnetic loop behind an interplanetary shock: Voyager, Helios, and IMP 8 observations, *J. Geophys. Res., 86,* 6673, 1981.

Cane, H. V., N. R. Sheeley, and R. A. Howard, Energetic interplanetary shocks, radio emission, and coronal mass ejections, *J. Geophys. Res., 92,* 9869, 1987.

Chen, J., and D. A. Garren, Interplanetary magnetic clouds: Topology and driving mechanism, *Geophys. Res. Lett., 20,* 2319, 1993.

Delaboudinière, J.-P., et al., EIT: Extreme-ultraviolet imaging telescope for the SOHO mission, *Sol. Phys., 162,* 291, 1996.

Dere, K.P., et al., EIT and LASCO observations of the initiation of a coronal mass ejection, *Sol. Phys., 175,* 601, 1997.

Farrugia, C. J., L. F. Burlaga, V. A. Osherovich, I. G. Richardson, M. P. Freeman, R. P. Lepping, and A. J. Lazarus, A study of an expanding interplanetary cloud and its interaction with the Earth's magnetosphere: The interplanetary aspect, *J. Geophys. Res., 98,* 7621, 1993.

Goldstein, R., M. Neugebauer, and D. Clay, A statistical study of coronal mass ejection plasma flows, *J. Geophys. Res., 103,* 4761, 1998.

Gosling, J. T., Coronal mass ejections and magnetic flux ropes in interplanetary space, in *Physics of Magnetic Flux Ropes, Geophys. Monogr. Ser., Vol. 58,* edited by C. T. Russell, E. R. Priest, and L. C. Lee, pp. 343-364, AGU, Washington, D.C., 1990.

Gosling, J. T., Corotating and transient solar wind flows in three dimensions, *Annu. Rev. Astron. Astrophys, 34,* 35, 1996.

Gosling, J.T. and P. Riley, The acceleration of slow coronal mass ejections in the high-speed solar wind, *Geophys. Res. Lett.,* 23, 2867, 1996.

Gosling, J.T., V. Pizzo, and S.J. Bame, Anomalously low proton temperatures in the solar wind following interplanetary shock waves: Evidence for magnetic bottles?, *J. Geophys. Res., 78,* 2001, 1973.

Gosling, J.T., E. Hildner, R.M. MacQueen, R.H. Munro, A.I. Poland, and C.L. Ross, Speeds of coronal mass ejection events, *Sol. Phys., 48,* 389, 1976.

Gosling, J.T., D.N. Baker, S.J. Bame, W.C. Feldman, R.D. Zwickl, and E.J. Smith, Bidirectional solar wind electron heat flux events, *J. Geophys. Res., 92,* 8519, 1987.

Gosling, J.T., D.J. McComas, J.L. Phillips, and S.J. Bame, Geomagnetic activity associated with Earth passage of interplanetary shock disturbances and coronal mass ejections, *J. Geophys. Res., 96,* 7831, 1991.

Gosling, J.T., S.J. Bame, W.C. Feldman, D.J. McComas, P. Riley, B.E. Goldstein, and M. Neugebauer, The northern edge of the band of solar wind variability: Ulysses at ~4.5 AU, *Geophys. Res. Lett.,* 24, 309, 1997.

Gosling, J. T., P. Riley, D. J. McComas, and V. J. Pizzo, Over-expanding coronal mass ejections at high heliographic latitudes: Observations and simulations, *J. Geophys. Res., 103,* 1941, 1998.

Howard, R., N.R. Sheeley, M.J. Koomen, and D.J. Michels, Coronal mass ejections: 1979-1981, *J. Geophys. Res., 90,* 8173, 1985.

Hundhausen, A.J., Sizes and locations of coronal mass ejections: SMM observations from 1980 and 1984-1989, *J. Geophys. Res. 98,* 13,177, 1993.

Hundhausen, A.J., J.T. Burkepike, and O.C. St. Cyr, Speeds of coronal mass ejections: SMM observations from 1980 and 1984-1989, *J. Geophys. Res., 99,* 6543, 1994.

Jackson, B.V., and R.A. Howard, A CME mass-distribution derived from Solwind coronagraph observations, *Sol. Phys., 148,* 359, 1993.

Jones, G.H., A. Balogh, and R.J. Forsyth, Radial heliospheric magnetic fields detected by Ulysses, *Geophys. Res. Lett., 25,* 3109, 1998.

Lepping, R.P., J.A. Jones, and L.F. Burlaga, Magnetic field structure of interplanetary magnetic clouds at 1 AU, *J. Geophys. Res., 95,* 11957, 1990.

Montgomery, M.D., J.R. Asbridge, S.J. Bame, and W.C. Feldman, Solar wind electron temperature depressions following some interplanetary shock waves: Evidence for magnetic merging?, *J. Geophys. Res., 79,* 3103, 1974.

Neugebauer, M. and R. Goldstein, Particle and field signatures of coronal mass ejections in the solar wind, in *Coronal Mass Ejections, Geophys. Monogr. Ser., Vol. 99,* edited by N. Crooker, J.A. Joselyn, and J. Feynman, pp. 245-251, AGU, Washington, D.C., 1997.

Neugebauer, M., R. Goldstein, and B.E. Goldstein, Features observed in the trailing regions of interplanetary clouds from coronal mass ejections, *J. Geophys. Res., 102,* 19,743, 1997.

Palmer, I. D., F. R. Allum, and S. Singer, Bidirectional anisotropies in solar cosmic ray events: Evidence for magnetic bottles, *J. Geophys. Res., 83,* 75, 1978.

Richardson, I. G. and D. V. Reames, Bidirectional ~1 MeV/amu ion intervals in 1973-1991 observed by the Goddard Space Flight Center instruments on IMP-8 and ISEE-3/ICE, *Astrophys. J. Suppl., 85,* 411, 1993.

Richardson, I. G., C. J. Farrugia, and D. Winterhalter, Solar activity and coronal mass ejections on the western hemisphere of the Sun in mid-August 1989: Association with interplanetary observations at the ICE and IMP 8 spacecraft, *J. Geophys. Res., 99,* 2513, 1994.

Schmieder, B., L. Van Driel-Gesztelyi, J.E. Wilk, T. Kucera, B. Thompson, C. De Forest, C. St. Cyr, and G.M. Simnett, Prominence activity related to CME observed by SOHO, Yohkoh, and ground-based observatories, in *Proceedings of the Fifth SOHO Workshop, Eur. Space Agency Spec. Publ., ESA SP-404,* 663, 1997.

Sheeley, N. R., R. A. Howard, M. J. Koomen, D. J. Michels, R. Schwenn, K.-H. Muhlhauser, and H. Rosenbauer, Coronal mass ejections and interplanetary shocks, *J. Geophys. Res., 90,* 163, 1985.

St. Cyr, O.C., and D.F. Webb, Activity associated with coronal mass ejections at solar minimum: SMM observations from 1984-1986, *Sol. Phys., 136,* 379, 1991.

Watari, S., R. Watanabe, L.W. Acton, and H.S. Hudson, Limb events observed by Yohkoh and coronal mass ejections: A filamentary soft x-ray structure on 5 October 1996, in *Proceedings of the Fifth SOHO Workshop, Eur. Space Agency Spec. Publ., ESA SP-404,* 725, 1997.

Webb, D.F., and R.A. Howard, The solar-cycle variation of coronal mass ejections and the solar wind mass flux, *J. Geophys. Res., 99,* 4201, 1994.

R. J. Forsyth, The Blacklett Laboratory, Imperial College, London, SW7 2BZ England. (rforsyth@ic.ac.uk)

H. O. Funsten and J. T. Gosling, MS D466, Los Alamos National Laboratory, Los Alamos, NM, 87545. (hfunsten@lanl.gov; jgosling@lanl.gov)

R. A. Howard, Naval Research Laboratory, Code 7660, Washington, DC, 20375. (howard@cronus.nrl.navy.mil)

P. Riley, SAIC, 10260 Campus Point Drive MS-E3X, San Diego, CA 92121-1578. (uk2@iris023.saic.com)

R. Schwenn, Max Planck Institut für Aeronomie, Katlenburg-Lindau 37189, Germany. (schwenn@linax1.mpae.gwdg.de)

O. C. St. Cyr, Computational Physics, Inc., Naval Research Laboratory, Washington DC 20375 (cst@sdac.nascom.nasa.gov)

(Received April 7, 1998; revised September 25, 1998;
accepted October 26, 1998.)

REPORT DOCUMENTATION PAGE

Form Approved
OMB No. 0704-0188

1. AGENCY USE ONLY *(Leave Blank)*	2. REPORT DATE	3. REPORT TYPE AND DATES COVERED
	02/28/01	Interim Contractor Report, 02/01/01 - 02/28/01

4. TITLE AND SUBTITLE
An Investigation of the Large Scale Evolution and Topology of Coronal Mass Ejections in the Solar Wind

5. FUNDING NUMBERS
C: NASW-98007

6. AUTHOR(S)
Dr. Peter Riley

7. PERFORMING ORGANIZATION NAME(S) AND ADDRESS(ES)
SciberNet, Inc.
5414 Oberlin Drive, Suite 251
San Diego, CA 92121

8. PERFORMING ORGANIZATION REPORT NUMBER

9. SPONSORING / MONITORING AGENCY NAME(S) AND ADDRESS(ES)
National Aeronautics and Space Administration
Goddard Space Flight Center
Greenbelt, MD 20771

10. SPONSORING / MONITORING AGENCY REPORT NUMBER

11. SUPPLEMENTARY NOTES

12a. DISTRIBUTION / AVAILABILITY STATEMENT
Unclassified-Unlimited

12b. DISTRIBUTION CODE

13. ABSTRACT

This investigation (subcontract Sci-0201-99 of contract NASW-98007) is concerned with the large-scale evolution and topology of coronal mass ejections (CME's) in the solar wind. During the course of this three-year investigation, we have undertaken a number of studies that are discussed in more detail in this report. For example, we conducted an analysis of all CME's observed by the Ulysses spacecraft during its in-ecliptic phase between 1 and 5 AU. In addition to studying the properties of the ejecta, we also analyzed the shocks that could be unambiguously associated with the fast CME's. We also analyzed a series of "density holes" observed in the solar wind that bear many similarities with CME's. To complement this analysis, we conducted a series of 1-D and 2 1/2-D fluid, MHD, and hybrid simulations to address a number of specific issues related to CME evolution in the solar wind. Foe example, we used fluid simulation to address the interpretation of negative electron temperature-density relationships often observed within CME/cloud intervals. As part of this investigation, a number of fruitful international collaborations were forged. Finally, the results of this work were presented at scientific meetings and communicated in 8 scientific, refereed papers.

14. SUBJECT TERMS
Electron, Thermalization, Solar Wind, Planetary Plasma Boundaries

15. NUMBER OF PAGES
1

16. PRICE CODE

17. SECURITY CLASSIFICATION OF REPORT	18. SECURITY CLASSIFICATION OF THIS PAGE	19. SECURITY CLASSIFICATION OF ABSTRACT	20. LIMITATION OF ABSTRACT
Unclassified	Unclassified	Unclassified	UL